CHEMICAL REVIEWS

Review

pubs.acs.org/CR

Plasma Catalysis: Synergistic Effects at the Nanoscale

Erik C. Neyts,[*,§] Kostya (Ken) Ostrikov,[†,‡] Mahendra K. Sunkara,[∥] and Annemie Bogaerts[§]

[§]Department of Chemistry, Research Group PLASMANT, Universiteit Antwerpen, Universiteitsplein 1, 2610 Wilrijk-Antwerp, Belgium

[†]Institute for Future Environments and School of Chemistry, Physics and Mechanical Engineering, Queensland University of Technology, Brisbane, Queensland 4000, Australia

[‡]Plasma Nanoscience Laboratories, Manufacturing Flagship, Commonwealth Scientific and Industrial Research Organization, P.O. Box 218, Lindfield, New South Wales 2070, Australia

[∥]Conn Center for Renewable Energy Research and Chemical Engineering, University of Louisville, Louisville, Kentucky 40292, United States

ABSTRACT: Thermal-catalytic gas processing is integral to many current industrial processes. Ever-increasing demands on conversion and energy efficiencies are a strong driving force for the development of alternative approaches. Similarly, synthesis of several functional materials (such as nanowires and nanotubes) demands special processing conditions. Plasma catalysis provides such an alternative, where the catalytic process is complemented by the use of plasmas that activate the source gas. This combination is often observed to result in a synergy between plasma and catalyst. This Review introduces the current state-of-the-art in plasma catalysis, including numerous examples where plasma catalysis has demonstrated its benefits or shows future potential, including CO_2 conversion, hydrocarbon reforming, synthesis of nanomaterials, ammonia production, and abatement of toxic waste gases. The underlying mechanisms governing these applications, as resulting from the interaction between the plasma and the catalyst, render the process highly complex, and little is known about the factors leading to the often-observed synergy. This Review critically examines the catalytic mechanisms relevant to each specific application.

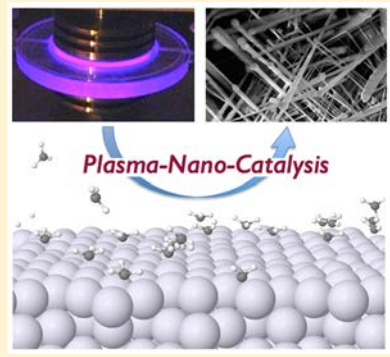

CONTENTS

Received: June 18, 2015
Published: November 30, 2015

DOI: 10.1021/acs.chemrev.5b00362
Chem. Rev. 2015, 115, 13408–13446

1. INTRODUCTION

Plasma catalysis is an emerging branch of plasma processing, at the interface of a variety of disciplines, including physical chemistry, material science, nanotechnology, plasma physics and plasma chemistry, catalysis, and others. In short, its objective is to enhance catalytic reactions by virtue of adding a plasma to the reaction cycle. As most catalysts are nanofeatured materials, the specific plasma−nanostructure interactions may lead to synergistic effects. Until now, however, very little has been understood in terms of the basic processes taking place.

1.1. Scope and Structure of the Review

This Review is concerned with gas processing by combining a plasma (partially) derived from that gas and a catalyst. The goal of such gas processing is either to convert the gas or gas mixture into another gas mixture, as, for instance, in dry reforming of CH_4, or to grow some material or structure from the precursor gas molecules, as, for instance, in plasma-enhanced catalytic growth of carbon nanotubes (CNTs). This is the realm of (mostly) low-temperature plasmas in combination with heterogeneous catalysis. Thus, we shall not be concerned with high-temperature plasmas, such as fusion plasmas, nor with homogeneous or enzymatic catalysis. Within this scope, we aim to review the current understanding in the field in terms of the basic processes taking place and provide an explanation of them based on findings in the literature, rather than collecting a large number of results.

We shall commence by reviewing a few basic general concepts, which will serve as a basis to discuss the observed plasma-catalytic processes and indicate how a low-temperature plasma and nanofeatures of the catalyst affect these concepts. Where possible, we will mostly focus on molecular-level phenomena rather than discuss observations at a phenomenological basis. Readers already familiar with catalysis (sections 2.1 and 2.2) or low-temperature plasmas (section 2.3) may skip the concerning sections.

Given the need for fundamental insight in this field, we shall not be overly concerned with more practical issues, such as the preparation of (nano)catalysts, reactor design, or performance. Moreover, as we will focus on nanoscale phenomena in catalysis, and how these are affected by the plasma, we will not provide an extensive overview of types of plasmas, plasma processes, or applications of plasmas.

As will be pointed out in sections 4 and 5, plasma catalysis is already a highly successful approach for small-scale fabrication of expensive materials, including, for instance, CNTs or inorganic nanowires. Indeed, plasma catalysis currently still is an expensive process, due to the high energy investment and capital costs involved, currently prohibiting the large-scale production of basic chemicals such as synthesis gas (a mixture of CO and H_2), ethylene epoxide, or methanol. However, reducing this energy cost is a very active field of research within the plasma community, and it is exactly the combination of plasmas with catalysis that may open perspectives for better energy efficiency, in combination with the selective production of targeted compounds. We shall return to this issue in section 4.2.

1.2. Brief Historic Perspective

Catalysis is already an old and very mature field in chemistry.[1] The first report came from Johann Wolfgang Döbereiner in 1823, stating that "finely divided platinum powder causes hydrogen gas to react with oxygen gas by mere contact to water whereby the platinum itself is not altered", a process that in 1835 was termed "catalysis" by Jöns Jacob Berzelius. Around 1900, Wilhelm Ostwald defined catalysis in terms of chemical kinetics: "A catalyst is a substance which affects the rate of a chemical reaction without being part of its end products". A few years later, in 1909, Ostwald was awarded the Nobel Prize in Chemistry for his contributions to catalysis. Some extremely important reactions also date back to that period. For instance, Fritz Haber realized the nitrogen fixation reaction $N_2 + 3H_2 \rightarrow 2NH_3$ in 1909 on an osmium catalyst (see also section 5.5), and Fischer and Tropsch reported on the conversion of synthesis gas (a mixture of CO and H_2, commonly termed syngas) in hydrocarbons in 1924 (see also section 5.4). Nowadays, some 80% of all industrial processes are based on catalysis, which amounts to a value for catalysis-produced goods of about $20 trillion yearly worldwide.[2]

What was not realized as such in the early days of catalysis is that a large surface area is crucial. This determines the number of active catalytic sites and is, thus, crucial for the overall performance of the catalyst. To quote Ertl,[1] "In fact, catalysis has been a nanotechnology long before this term was introduced." We shall elaborate on the importance of catalyst nanofeatures in section 2.2.2.

Plasma science is also an old field; the first gas discharge was created by Francis Hauksbee in 1705, essentially by charging and discharging an evacuated sphere containing a small amount of mercury. The first industrial device was a so-called silent discharge or dielectric barrier discharge used for producing ozone, in 1857 by Siemens. The term "plasma" for this kind of gas discharge was coined by Langmuir in 1927.[3] Gas discharges or low-temperature plasmas nowadays are used in a large number of applications.[4,5] Many current plasma processing and plasma applications rely on a limited number of fundamental plasma−surface interaction processes, described in section 2.3.2.

Whereas catalysis is most often conducted as a thermal process, plasma-based catalysis is gaining in interest and popularity. One of the earliest reports on plasma catalysis is the 1976 U.S. patent by Henis for NO_x removal.[6] The plasma adds a number of means to control the process, potentially allowing a more efficient process. As we will describe in detail below, the plasma enables one to modify both the feedstock (section 2.3.1), by virtue of the occurring plasma chemistry in the gas phase, and the catalyst (section 3.2), by virtue of the plasma/surface interactions. The catalytic process in plasma catalysis is thus determined by both the "bare" catalytic system and the nanofeatures of the catalyst, as well as by the modification of gas phase and catalyst by the plasma. This

DOI: 10.1021/acs.chemrev.5b00362
Chem. Rev. 2015, 115, 13408−13446

interaction between the plasma and the nanofeatures of the catalyst may lead to sometimes unexpected benefits or synergy. A variety of synergistic effects have been observed, examples of which will be described in sections 3, 4, and 5.

2. GENERAL ASPECTS OF PLASMA CATALYSIS

2.1. Chemical Bonding and Thermal Surface Processes

At the fundamental level, catalysis is determined by the precise nature of the adsorbate/catalyst interaction.[1] Moreover, on the microscopic level the catalyst is nanofeatured, i.e., it is either composed of nanoparticles, or it contains nanofeatures such as high nanoscale roughness or nanopores. It is therefore natural to consider the atomic/molecular level details of catalysis as fundamental to the process. We shall now first concentrate on these molecular-level details. First, we shall review the basics of bonding of adsorbates to metal surfaces at the molecular level (section 2.1.1) and surface reactions and kinetics (section 2.1.2), to sketch the conceptual framework relevant for many catalysis processes, followed by a short discussion on zeolites and metal oxides as used in plasma catalysis. Subsequently, in section 2.2.1, we describe basic definitions and concepts in thermal catalysis, and in section 2.2.2, we continue by reviewing the properties of nanocatalyst particles and the influence of the nanoscale features of the nanocatalyst on the catalysis process. As we will see, these concepts are of major importance for a wide variety of plasma-catalytic processes, including the growth of CNTs, graphene, and inorganic nanowires, abatement of toxic waste, CO_2 conversion, hydrocarbon reforming, ammonia production, and more, as will be described in sections 4 and 5.

2.1.1. Molecular Description of Bonding on Catalyst Surfaces. *Transition Metal Surfaces.* A large portion of active catalysts used in plasma catalysis are transition metals. The adsorbates are very often hydrocarbons or functionalized hydrocarbons, as, for instance, in CNT or graphene growth (sections 4.1 and 5.1), dry reforming of methane (DRM) (section 4.2), or volatile organic compound (VOC) abatement (section 5.3). The interaction of hydrocarbons with transition metals is determined, to a large extent, by the position of the metal in the periodic table.[7−9] In general, less noble metals interact stronger with the atoms than with undissociated molecules, which leads to molecular dissociation. More noble metals, on the other hand, show the opposite trend, which preserves the molecules intact. These features are important for catalytic action and are affected by the plasma−surface interactions. The latter will be discussed in more details in section 3. Here, we first explain the microscopic mechanisms of adsorbate−adsorbent interactions.

In the case of an atomic adsorbate, the (vertically oriented) p_z orbital of the carbon (or oxygen or nitrogen) atom interacts with symmetric surface orbitals like the d_{z^2} orbitals or symmetric combinations of s orbitals, typically leading to high coordination. The coupling of the adsorbate to the broad metal s/p states leads to a shift and broadening of the adsorbate states, which is essentially the same for all transition metals.[10,11] Additionally, the asymmetric p_x and p_y orbitals may interact with asymmetric surface orbitals like the d_{xz} or asymmetric combinations of s orbitals. This coupling is largely responsible for the difference between the different transition metals.

The coupling between the adsorbate states and the metal d states typically gives rise to bonding and antibonding states,[11] as shown in Figure 1. In more noble metals such as Cu, the

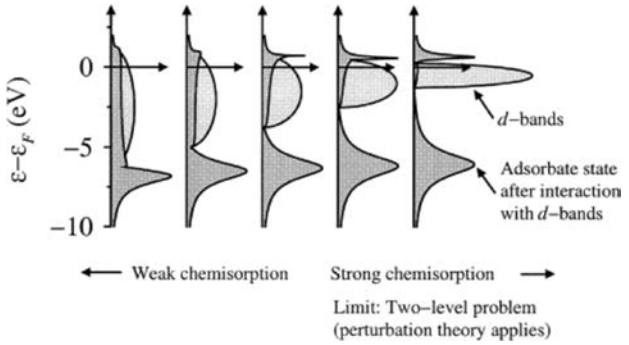

Figure 1. Local density of states projected onto an adsorbate state interacting with the d bands at a surface. The strength of the adsorbate−surface coupling matrix element V is kept fixed as the center of the d bands (ε_d) is shifted up toward the Fermi energy ($\varepsilon_F = 0$) and the width W of the d bands is decreased to keep the number of electrons in the bands constant. As ε_d shifts up, the antibonding states are emptied above ε_F and the bond becomes stronger. Reproduced with permission from ref 12. Copyright 1998 The Royal Society of Chemistry.

antibonding states are below the Fermi level and thus are occupied. This decreases the overall adsorbate−metal bonding interaction. In contrast, in less noble metals such as Ni or Fe, these antibonding states are above the Fermi level and thus are unoccupied. Bonding of adsorbates is stronger, therefore, at non-noble metals than it is at noble metals.[12,13] Therefore, the metal−adsorbate bond becomes stronger when moving to the left in the periodic table.

When considering molecular adsorbates, there are usually more adsorbate valence states to consider than in the case of atomic adsorbates, although the overall picture remains the same. Consider for instance, CO binding to a transition metal. The CO valence states to consider are the filled 5σ and the empty double degenerate $2\pi^*$ states, as shown in Figure 2. The interaction with the metallic s states merely results in a downshift and broadening of both the 5σ and $2\pi^*$ states, as was the case for atomic adsorption. Interaction with the d states, on the other hand, leads to the formation of bonding and antibonding states below and above the original states,[12] respectively, as indicated in Figure 1.

The emerging picture is that the CO−metal bond consists of electron donation from the 5σ state to the metal, as well as back-donation from the metal to the $2\pi^*$ state. The contribution of the 5σ state—electron donation—to bonding is negligible or even negative: both the bonding and antibonding orbitals will be populated, as they lie below the Fermi level. The contribution of the back-donation, in contrast, determines the bonding interaction. Before bonding, the adsorbate $2\pi^*$ states are above the Fermi level. Upon bonding, they shift partially below the Fermi level, leading to significant bonding. As we now move toward the left in the periodic table, starting from noble metals, the d-band center moves up, and more antibonding states move through the Fermi level and become empty, thus strengthening the bond. The effect, however, is weaker for molecules than it is for atoms.

DOI: 10.1021/acs.chemrev.5b00362
Chem. Rev. 2015, 115, 13408−13446

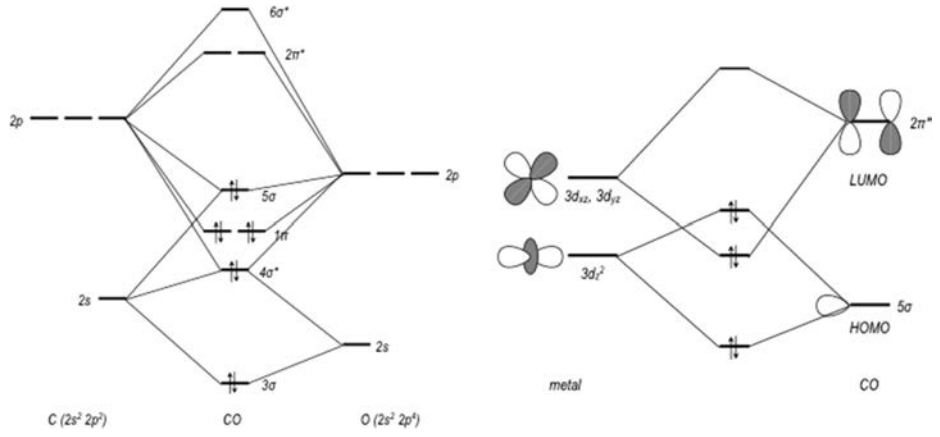

Figure 2. (a) Formation of the CO molecular orbitals from the atomic 2s and 2p oxygen and carbon atoms, showing the highest occupied molecular orbital (HOMO) 5σ and the lowest unoccupied moleculary orbital (LUMO) 2π* orbitals; (b) donation and back-donation in CO interacting with the metal d orbitals (here shown for copper).

The more noble metals, which show the weakest interactions, therefore show a stronger bonding to molecules than to the corresponding atoms (i.e., CO will bind stronger than the separate C and O atoms, such that molecular dissociation is not favored), but when moving to the left in the periodic table, the increase in metal−adsorbate bond strength is greater in the case of atomic adsorbates than in the case of molecular adsorbates, such that lesser noble metals show stronger bonding to atoms than to the corresponding molecule (i.e., separate C and O atoms will bind more strongly to the metal than the CO molecule, such that molecular dissociation is favored).

Transition Metal Oxide Surfaces. Oxides of transition metals are used for both thermal catalysis and plasma catalysis. The three most widely used metal oxide catalysts in plasma catalysis are CoO_x, MnO_x, and TiO_2. Metal oxide nanostructures are characterized by their redox and acid−base properties.[14] Some metal oxides, like TiO_2, are also widely used thanks to their photocatalytic activity. Metal oxides show a variability in both structure and oxidation state, form mixed valence compounds, and often exist as nonstoichiometric compounds, which further adds to their catalytic properties.[15−17] In plasma catalysis, metal oxides are often used as support material for active transition metal catalysts, next to other typical support materials such as carbons, SiO_2, and zeolites.[15]

The acid−base and redox properties of metal oxides are determined by their ability to accept electron density and thus to be reduced, leading to the generation of Brønsted acid sites or stabilizing the cationic transition state.[14,18] Such reduction processes are favored by low-lying LUMO orbitals, and this ability is size-dependent. Indeed, the relative acidity and basicity of a particular surface site is determined by the local coordination of the site atoms. Hence, factors such as size, geometry, and defects greatly influence the catalytic and plasma-catalytic behavior.

Metal oxides show a wide distribution in work function, from ∼2 eV for ZrO_2 to ∼7 eV for V_2O_5. As will be discussed in section 3.2.2, the plasma may affect the catalyst work function. Depending on the position of the Fermi level, and the alignment with the HOMO−LUMO gap of the adsorbent, the adsorbing molecule may either remain neutral upon adsorption or become charged.[19] Specifically, when the Fermi level lies within the HOMO−LUMO gap, the neutral molecule is thermodynamically most stable. When on the other hand the Fermi energy becomes higher than the molecules' ionization energy, the ionized form of the molecule will be more stable.[19] Also, the precise position of the Fermi level is determined by the presence of oxygen vacancies or interstitials, in addition to general factors such as strain, curvature, facetting, etc. affecting their properties. For instance, as the metal oxide domains become smaller, the electron density becomes less delocalized and the band gap increases.[18]

The essential process in metal oxide redox catalysis is the donation of surface lattice oxide ions to an adsorbed reductant, as well as the subsequent uptake of oxygen from the gas phase to reoxidize the metal oxide. This mechanism is known as the Mars and Van Krevelen mechanism. In addition to the direct oxidation by oxygen species originating from the plasma, the Mars and Van Krevelen mechanism is probably essential in catalytic oxidative degradation of VOCs.[20]

Zeolites. Zeolites are often described as solid acids, whose catalytic function is mainly determined through their surface acidity and shape selectivity.[21,22] In the context of plasma catalysis, zeolites have been used both as catalysts and as catalyst-support materials.[23−27]

A distinguishing feature of zeolites is their unique and sharply defined geometry. As a result, zeolites often exhibit shape selectivity, defined as the dependence of the heterogeneously catalyzed reaction on the pore size and/or pore architecture.[21,28] In the context of plasma catalysis, however, the importance of the micro- and nanofeatured zeolite structure is the possible ability to generate a plasma near or perhaps even inside the pores.[29,30] Because of the small dimensions, the electric field near these pores may be very high, leading to plasma-catalytic mechanisms not available in thermal catalysis. The effects and importance of catalyst-induced electric field enhancement will be discussed in section 3.3.

2.1.2. Surface Reactions and Kinetics. *Bond Breaking and Bond Formation.* Activated processes are characterized by the activation barrier E_a separating products from reactants. In a thermal process, the energy required to overcome this barrier is supplied by the thermal energy k_BT.

In plasma catalysis, the plasma itself may affect the energy barrier of the process in several ways, e.g., by altering the reactants either chemically by creating radicals, by providing

DOI: 10.1021/acs.chemrev.5b00362
Chem. Rev. 2015, 115, 13408−13446

some of the energy required for overcoming the activation barrier by excitation (see sections 3.2.3 and 3.4.1), or by modifying the size, structure, and morphology of the catalyst, thereby also changing its properties and thus its activity. These factors will be described in more detail in section 3.2. Note that besides the kinetics of the reaction also the thermodynamics of the process are modified by both the nanofeatures of the catalyst and the plasma.[31]

Early and Late Barriers. The bond formation and bond breaking may be understood in generally the same terms as those used to describe adsorption and desorption.[11,32,33] Conceptually, there are two types of surface reaction barriers (Figure 3): so-called early-barrier reactions and late-barrier

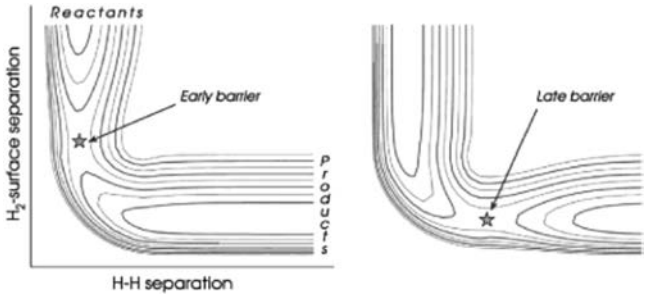

Figure 3. Calculated position of the transition state for H_2 dissociation on metallic substrates: (left) early barrier; (right) late barrier. Reprinted with permission from ref 34. Copyright 2003 Elsevier.

reactions. In early-barrier reactions, the transition state resembles the initial configuration of the reactants, whereas in a late-barrier reaction, the transition state resembles the final configuration, resembling the products.

A typical example of an early-barrier reaction is dissociative adsorption of H_2 on transition metal surfaces.[34] Early-barrier reactions are usually enhanced by translational energy instead of vibrational excitation. In this case, the barrier is encountered before the bond has noticeably elongated. Typical examples of late-barrier reactions are the dissociative adsorption of H_2 on noble metals or the catalytic dissociation of CH_4 on transition metal surfaces.[35−37] The latter process is of interest in plasma-catalytic dry reforming. In this case, one of the hydrogen atoms nearly completely separates from the methane molecule at the transition state, which resembles the final products in which both the hydrogen atom and the CH_3 radical are bonded to the metal surface.

We may now also understand the difference in reactivity from one metal to another. As described above, the higher the d-band center (i.e., moving toward the left in the periodic table), the more bonding orbitals will be below the Fermi level, the stronger the bonds will be between adsorbate and the metal, and the more prone the adsorbate will be to dissociation. Hence, the lesser noble metals show a higher reactivity and, correspondingly, a lower activation barrier. This determines the reactivity in early-barrier reactions. In late-barrier reactions, the transition state resembles the products. The differences in transition state energies thus also closely follow the differences in adsorbed products.

2.2. Catalysis

2.2.1. Definitions and Concepts in Catalysis. Catalysis is defined as the process in which the rate of a reaction is increased without changing the overall standard Gibbs energy change. This rate increase is brought about by the use of a catalyst, which itself is regenerated after each reaction cycle.

A number of measures are used to determine the catalyst performance and activity. The overall catalyst activity is measured by the conversion, which is the number of moles of reactant converted into products divided by the number of moles of reactant fed. The selectivity for a given product is defined as the conversion of the reactant(s) into the desired product divided by the total conversion of the reactant(s). It is thus roughly equal to the ratio of the reaction rate forming that product over the total rate. Also, for a given set of reaction conditions, the selectivity is often found to be dependent on the conversion.[38−40] The selectivity is determined by the mechanisms of the competing reactions and by the surface state of the catalyst, as will be explained later. The yield is defined as the number of moles of product divided by the number of moles of reactant fed, or, equivalently, the product of the total conversion and the average selectivity. Finally, another measure for the activity is the turnaround frequency, or TOF, and is defined as the number of times that the overall catalytic reaction takes place per catalytic site and per unit of time for a fixed set of reaction conditions.

A central concept in catalysis is the Sabatier principle, which states that optimum activity is obtained for an optimum interaction energy between the adsorbates and the catalyst. When the reactants reach the surface, they need to adsorb and bind sufficiently strongly to the catalyst such that they do not immediately desorb into the gas phase again. Their probability to react is related to their lifetime. After all required elementary reactions have taken place, the formed products need to desorb from the surface. Thus, these products may not be bound too strongly to the surface, as this would prevent them from desorbing. The optimum reactant adsorption is reflected by so-called volcano plots, an example of which is shown in Figure 4.[41]

Consider, for instance, the adsorption of CO on three typical metal surfaces: Co, Ni, and Cu. This is a critical step in, e.g., plasma DRM. The largest heat of adsorption for CO is found on Co, i.e., 110 kJ/mol. Of these three metals, Cu has the lowest d-band center, and Co has the highest. Thus, Co is most reactive and shows the strongest binding, both

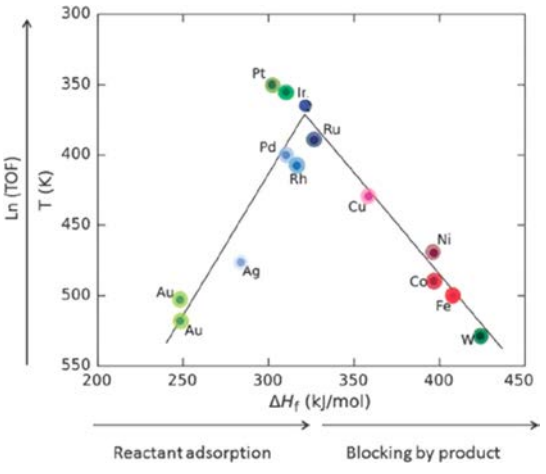

Figure 4. Typical volcano plot, here shown for formic acid formation. Reproduced with permission from ref 41. Copyright 2014 The Royal Society of Chemistry.

DOI: 10.1021/acs.chemrev.5b00362
Chem. Rev. 2015, 115, 13408−13446

toward the molecule and toward the separate atoms (see section 2.1). As the molecular binding energy of CO on Cu is less than the CO bond energy, CO will not dissociate on Cu. The heat of adsorption of CO on Ni is ∼95 kJ/mol, and on Cu it is 80 kJ/mol. This small difference in adsorption energy between Ni and Cu is magnified when the molecule dissociates, because after dissociation the valence electrons of the CO molecule are no longer tied to molecular orbitals but are freely available. Consequently, the dissociation process is exothermic on Co, thermoneutral on Ni, and endothermic on Cu. Such simple arguments explain, for instance, the difference in selectivity between these metals for the conversion of synthesis gas: while Cu is an active component for methanol synthesis catalysts, Co is a Fischer−Tropsch catalyst producing higher hydrocarbons.

The Sabatier principle and the typical volcano curves are a direct result of the above.[11] Indeed, moving toward the left in the periodic table gives a lower activation barrier and higher reactivity but also stronger bonding to the surface and, thus, less free active surface and less desorption. What is less clearly emphasized in the literature is that volcano plots are also dependent on the catalyst size, as adsorbate−catalyst interactions are indeed size-dependent. Therefore, we shall now briefly review nanocatalyst properties.

2.2.2. Properties of Nanocatalysts. The nanoscale feature dimensions of catalysts are responsible for the very different properties of nanocatalysts compared to their bulk counterparts and, in fact, for their actual use as catalysts. Let us discuss the properties of nanocatalysts that are most relevant to plasma nanocatalysis. A nanoparticle is defined as a particle containing fewer than $\sim 10^6$ atoms, as above this number the properties resemble those of the bulk. This number corresponds to a diameter of less than ∼100 nm.[42,43]

The activity of nanoparticles is determined, to a large extent, by their size, composition, morphology, and interaction with the support. The origin of this dependence resides in the size-dependence of their geometrical and electronic structure.[44] Given that the surface-to-volume ratio increases with decreasing particle size, and that the chemical reactivity of a heterogeneous catalyst is proportional to this ratio, small nanoparticles are generally the more-efficient catalysts.[45] Detailed investigations have revealed, however, that the relationship between size and reactivity is not always monotonic. A clear example is the size-dependence of adsorption energies on nanoparticles. This size-dependence of the nanocatalyst chemical reactivity has been demonstrated experimentally by Campbell et al. (as shown in Figure 5a)[46,47] and theoretically by Yudanov et al. (Figure 5b).[48] It was shown by density functional theory (DFT) calculations that the CO adsorption on Pd-nanoclusters is weakest (lowest adsorption energy) for clusters containing 30−50 atoms. Below and above this size range, the CO adsorption is stronger. Below this size range, the interaction is stronger because of the decreasing energy gap between the $2\pi^*$ lowest unoccupied molecular orbital (LUMO) of the CO molecule and the energies of the d levels of the metal. Above this size, on the other hand, the interaction energy increases due to a decrease in lattice contraction with increasing particle size. As a result of these size-dependent interactions, volcano plots are also size-dependent.

The electronic structure of nanoparticles is not composed of complete bands as in the case of macroscale solids but is intermediate between atoms and molecules on the one hand and solids on the other hand. Schematically, this may be represented as shown in Figure 6.[49] Indeed, for nanoparticles smaller than ∼10 nm, the electronic, optical, and magnetic properties of the material change due to quantum mechanical effects. Specifically, when the de Broglie wavelength of the electrons becomes comparable to the system size, the particles electronically behave as zero-dimensional.[45] The de Broglie wavelength of a 1 eV electron with rest mass energy of 0.511 MeV is 1.23 nm, which is a typical nanocatalyst particle size.

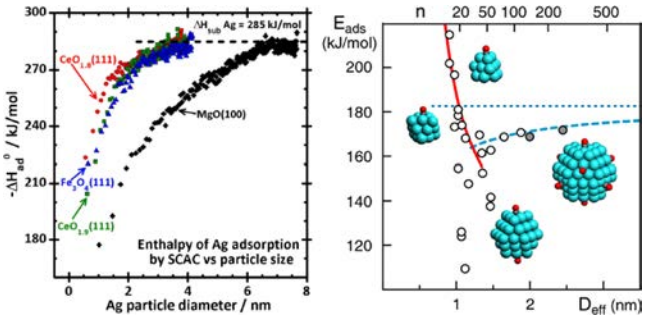

Figure 5. (a) Size dependence of the heat of adsorption of Ag on Ag. Reprinted with permission from ref 47. Copyright 2013 American Chemical Society. (b) Size dependenceof the heat of adsorption of CO on Pd. Reprinted with permission from ref 48. Copyright 2011 American Chemical Society.

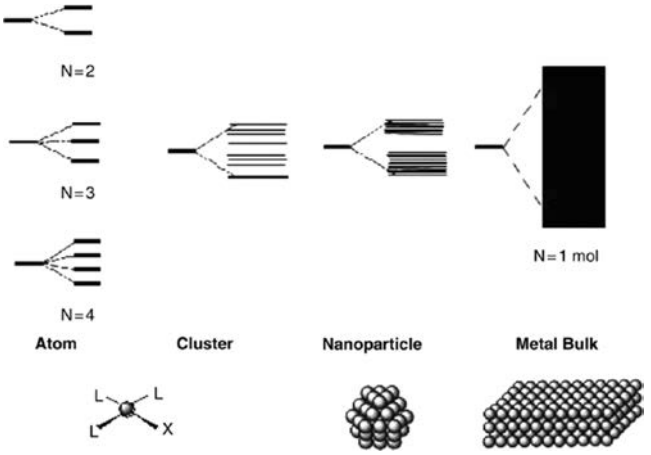

Figure 6. Electron levels of atom, cluster, nanoparticle, and bulk metal. Reproduced with permission from ref 49. Copyright 2013 John Wiley and Sons.

Nanofeatures of catalysts typically show a wide variety of surface structures, possibly containing various crystal facets, amorphous local surfaces, and defects. This is especially important because both the interaction energy and the reaction mechanism are determined by the coordination number of the atoms involved. Generally, lower-coordinated surfaces are more reactive than densely packed surfaces, and hence catalysts usually come in the form of nanoparticles.

The melting point of nanoparticles is another well-known size-dependent property of nanocatalysts, affecting their catalytic behavior. Melting of nanoparticles is described by the Gibbs−Thomson equation,

$$\Delta T = \frac{2T_M\sigma_{SL}}{\rho_S \Delta H r} \quad (1)$$

DOI: 10.1021/acs.chemrev.5b00362
Chem. Rev. 2015, 115, 13408−13446

expressing the depression of the melting temperature of small particles relative to the bulk material, where T_M is the bulk melting temperature, σ_{SL} is the solid−liquid interfacial energy, ρ_S is the density of the solid, ΔH is the melting enthalpy, and r is the radius of the particle. A variety of experimental[50−52] and theoretical works[53−57] have indeed demonstrated this melting-point depression. This is especially important for processes taking place at elevated temperatures close to the size-dependent melting temperature, as is the case in CNT growth, for instance. Depending on the exact process conditions, the nanocatalyst may exist in either the solid or the liquid state, and consequently, a small change in temperature may induce a change in process mechanism. This has been observed in metal-catalyzed CNT growth, where carbon transport may occur either by surface diffusion at low temperature (solid nanocatalyst) or by bulk diffusion at higher temperature (liquid nanocatalyst).

The most important effect on the catalytic behavior of a material seems to be the occurrence and availability of undercoordinated surface atoms, including face atoms (terrace atoms), corner atoms, edge atoms, and kink atoms.[58,59] Other effects, including the interaction with the support and charge transfer, also contribute but to a lesser extent. DFT calculations point out that changes in metal coordination lead to significant changes in catalytic behavior.[60]

To summarize, the catalytic activity of nanoparticles is determined by their size, facetting, presence of steps, defects and other "special sites", strain, oxidation state, and support material used. In plasma catalysis, all of these factors are influenced by the plasma, thus affecting the catalytic process.[31]

2.3. Low-Temperature Plasmas

2.3.1. Basic Properties. A plasma or gas discharge is a partially ionized gas, consisting of electrons, various ions, and neutral species (molecules, radicals, and excited species), which can all interact with each other, giving rise to a "rich" and reactive plasma environment. A key characteristic of such plasmas is their far-from-equilibrium state at relatively low temperatures, typically in the range 300−1000 K. This combination of reactivity, far-from-equilibrium state, and low-temperature operation enables plasmas to be used for many complex applications, including catalysis. Plasma reactivity in turn increases reactivity at surfaces in contact with the plasma. As a result, low-temperature plasmas show superior characteristics that allow the production of structures and induce processes at surfaces more efficiently and with more control than is possible with traditional thermal methods. Here we introduce the various aspects of low-temperature plasmas and plasma−surface interactions of particular relevance to plasma nanocatalysis.

Low-temperature plasmas used in plasma catalysis are characterized by the occurrence of various temperature scales and energy distributions for neutrals, ions, and electrons, a high chemical reactivity, and their lack of selectivity in terms of product formation. Depending on how the power is coupled into the plasma, a variety of different plasmas may be obtained, including direct current (dc), capacitively coupled radio frequency (RF), and inductively coupled RF sources, microwave discharges, dielectric barrier discharges, gliding arcs, plasma jets and plasma torches, etc.[4,5]

Structure of the Plasma. When an electric field of sufficient magnitude is applied to a gas, the gas will (partially) break down in ions and electrons. Because of the much higher mobility of electrons compared to the ions, all exposed surfaces will attain a negative charge, which sets up an electric field, slowing down the electrons and accelerating the positive ions. This in turn establishes a dynamic equilibrium, with equal fluxes of electrons and ions. As a result, a region in front of the surface develops that is characterized by an excess positive charge. This region is called the sheath. The sheath is extremely important in plasma-processing applications, as it determines the fluxes and energies of the (charged) species reaching the surface. Also the neutral gas is affected in the sheath, as the modified energy distributions of the electrons and ions influence the reactions taking place. Thus, the plasma−surface interactions are determined, to a large extent, by the electric-field distribution in the plasma and especially in the sheath, as well as to closely related plasma characteristics such as the power coupled into the plasma, the gas pressure, and the chemical composition of the plasma.

Energy Distributions in Plasmas and Reactivity. The chemical composition of the plasma is determined by the occurring reactions, which are in turn determined to a large extent by the energies of the electrons, ions, and neutrals. The electron energy distribution function (EEDF) is strongly dependent on the precise electric field distribution and gas composition, as well as on the discharge type.

The EEDF might be a simple Maxwellian distribution or might show a more complex behavior such as the bi-Maxwellian distribution or Druyvenstein distribution. The ion energy distribution function (IEDF) is typically not far from Maxwellian,[5] as the ions are typically too heavy to be strongly accelerated by the electric field. The neutral species are typically showing a simple Maxwellian distribution, as they are not (directly) influenced by the electric field. Gas heating, however, may occur through collisions with (mainly) the energetic ions.

Vibrationally excited species are of special importance in plasma catalysis, because they may strongly influence the occurring plasma−surface interactions (see section 3.4.1). Moreover, the energetic electrons induce reactions creating highly reactive radicals, which can react further into new molecules. Hence, even reactions that are strongly endothermic and that require high temperatures to proceed under thermal reaction conditions can occur in a plasma at sufficiently high rates at room temperature.

2.3.2. Plasma−Surface Interactions. Because of their peculiar properties, plasmas interact with surfaces differently from neutral gases. These interactions are determined by the fluxes and energies of all species involved, and they induce processes such as sputtering, etching, heating and formation of hot spots, charging, deposition, implantation, and photon irradiation.[61] These processes affect the plasma-catalytic process and are briefly discussed here.

Etching and Sputtering. Etching is the chemical removal of surface material by formation of volatile compounds upon impinging particles reacting at the surface. A typical example in plasma catalysis is etching of amorphous carbon with hydrogen in plasma-catalytic growth of carbon nanotubes and other nanocarbons.[62−64]

Sputtering is the physical removal of surface material by impact of energetic particles, typically ions. The impact of the ion on the surface results in a collision cascade in the top surface layers, leading to the ejection of material. It has been shown both theoretically[65,66] and experimentally[67−70] that

DOI: 10.1021/acs.chemrev.5b00362
Chem. Rev. 2015, 115, 13408−13446

sputtering can be a crucial factor in plasma-catalytic growth of CNTs.

Heating. Plasmas can heat up surfaces they are in contact with by the impact of charge carriers, photons, metastable and excited neutrals, and fast ground-state neutrals, as well as through exothermic surface reactions. Locally intense electric fields induced by the strong local curvature of the nanoparticles contribute to the heating. The heating effect depends on the power coupled into the plasma and may lead to the formation of so-called "hot spots" that influence catalytic processes.[71−74] Plasma heating may reduce or even eliminate the required external heating. When catalyst nanoparticles or nanofeatures are subjected to this heating, they can melt because of the Gibbs−Thomson effect (see section 2.2.2), resulting in, e.g., a different solubility.[56,75,76] Moreover, the plasma heating is a localized effect where energy is predominantly delivered to the topmost atomic layers of catalyst nanoparticles (CNPs), where nanoscale plasma−surface interactions are most intense. This effect is of great importance for, e.g., plasma-enhanced metal-catalyzed CNT growth, where ion bombardment stimulates the nanotube nucleation process.[65,66] This will be further elaborated in section 4.1.3.

Charging and Charge Transfer. Continuous electron and ion deposition leads to surface charging, which affects the catalytic function, especially in the case of nanocatalysts. Indeed, charging is a size-dependent effect, and single-electron-transfer and charge fluctuations come into play at small nanoparticle sizes. Therefore, charge transfer to and from the plasma affects the charge on catalyst nanoparticle surfaces, which is determined by the dynamic balance between the electron and ion currents onto the surface. The dynamically varying electric charge in turn affects the catalytic function of nanocatalysts. An example of charge transfer in plasma-catalytic growth of CNTs is provided in section 4.1.3.

Deposition and Implantation. Plasmas are typically very reactive, due to the effective creation of radicals that effectively stick to the surface, thus making plasmas particularly suitable for deposition of nanomaterials such as graphene, CNTs, or inorganic metal oxide nanowires as discussed later (see sections 5.1, 4.1, and 5.2, respectively). Neutral nonradical molecules created in the plasma also contribute to the deposition process. However, the sticking coefficients that quantify their attachment to the surface are typically lower compared to the radical species.

Ions with sufficient energies may penetrate the surface of the substrate and become implanted. This effect may change the surface condition and electronic structure of the catalyst, thereby affecting its catalytic performance. For instance, atomic-scale simulations predict that the CNT growth mode may be modified by allowing energetic ions to impinge on the growing structure.[77,78] On the other hand, experiments show that ion bombardment modifies the catalyst dispersion.[79]

Photon Irradiation. Gas discharges create a significant number of electronically excited species, which may decay to a lower-energy state by emitting photons. These photons may be advantageous in plasma catalysis, as they may activate photocatalysts, such as anatase TiO_2 (see section 5.3).

However, the photon flux generated by low-temperature plasmas should be sufficiently high to play a significant role in photocatalytic processes.[80,81] The arising opportunities are presently underexplored, and we will return to this issue in section 3.4.

3. PLASMA−CATALYST INTERACTIONS AND SYNERGIES AT THE NANOSCALE

When the effects of nanoscale features described above are combined with the presence of a plasma, interesting interactions appear, yielding improved process results in terms of efficiency, rate, yield, or selectivity. This phenomenon is often termed synergy. We shall now describe the origins of this synergistic effect.

3.1. What is Synergy?

In the context of plasma catalysis, we can define synergy as the surplus effect of combining the plasma with a catalyst, i.e., the effect of combining the plasma with the catalyst is greater than the sum of their individual effects. Synergism in plasma catalysis is a complex phenomenon, originating from the interplay between the various plasma−catalyst interaction processes.[61,82−85] Conceptually, we can break down the interaction in two parts. First, both the plasma and the catalyst, independent from each other, affect the surface processes. The plasma does so by establishing an electric field and by modifying the gas composition, resulting in the delivery of a variety of reactive species, ions, electrons, and photons to the surface where the plasma−catalyst interactions take place. The catalyst will also affect the surface reactions, by lowering the activation barrier for certain reactions. Second, the plasma and catalyst show some interdependence, as the plasma affects the catalyst properties and the catalyst affects the plasma properties. For instance, the plasma can modify the catalyst morphology or work function, modifying the catalyst operation. Vice versa, catalyst properties such as the dielectric constant or its morphology affect plasma properties near the surface such as the electric-field distribution and the electron-energy distribution. This complex interdependence is graphically represented in Figure 7.

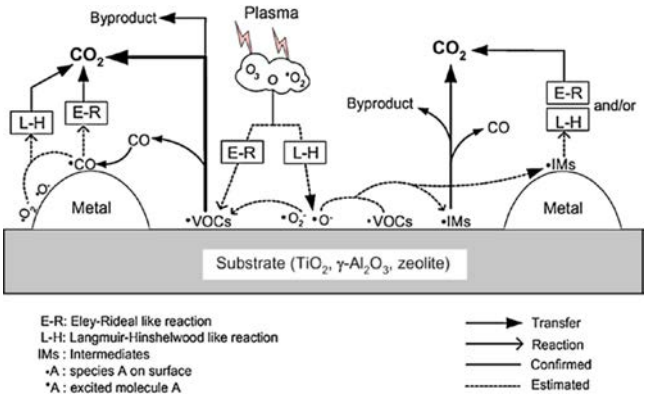

Figure 7. Complex interdependence of effects of plasma on catalyst and catalyst on plasma. Reprinted with permission from ref 85. Copyright 2011 Elsevier.

An important parameter in plasma catalysis, often differentiating the operating conditions from thermal catalysis, is the system pressure. Thermal catalysis operates in a wide range of pressures, including reduced pressures for, e.g., the growth of nanomaterials such as CNTs or graphene and high pressures, as in the case of, e.g., ammonia production. The current tendency in plasma catalysis, in contrast, is to work at atmospheric pressure. Relative to a low-pressure setup, this eliminates the requirement of using expensive vacuum

DOI: 10.1021/acs.chemrev.5b00362
Chem. Rev. 2015, 115, 13408−13446

equipment and it reduces the influence of damaging ion bombardment. High pressures (i.e., above atmospheric pressure) at near-room temperature, on the other hand, are not feasible in plasma catalysis, because the high-frequency gas-phase collisions would thermalize all species, extinguishing the plasma.

3.2. Plasma–Catalyst Interactions and Synergy 1: Effects of the Plasma on the Catalyst

A significant number of effects of the plasma on the catalyst have been reported and are discussed in this section. Importantly, these effects and induced changes are closely related. For instance, a change in morphological properties typically leads to a modification of the electronic properties of the catalyst, which in turn leads to a change in its chemical properties. The division among the various listed effects is, therefore, somewhat arbitrary.

3.2.1. Plasma-Induced Morphological Changes in the Catalyst. The application of plasma has been observed to lead to a higher catalyst dispersion and, hence, to a larger active surface area.[86−88] This can be attributed in part to the lower process temperatures that can be employed in plasma-catalysis systems, leading to less agglomeration and sintering of catalyst particles and, hence, to a higher dispersion. Moreover, bombardment of the catalyst surface by charged particles may contribute to an enhanced dispersion. Shang et al., for instance, demonstrated that the dispersion of the Ni/γ-Al_2O_3 catalyst more than doubled from 14.7% when prepared thermally to 30.6% when prepared by a plasma-enhanced method.[79]

Application of the plasma may also lead to significant changes in surface structure and morphology, due to the fact that the catalyst surface is subject to large fluxes of plasma species, including energetic ions, radicals, and electrons, which may induce a change in surface facetting and oxidation state and, hence, stability and structure of the surface. For instance, Guo et al. demonstrated a change in morphology of their manganese oxide catalyst when exposed to a dielectric barrier discharge (DBD) plasma.[89] It was found that the granularity of the catalyst features decreased upon plasma exposure, along with an increase in catalyst dispersion. Hence, the specific area of the catalyst was enlarged and the number of special sites (such as vacancies, corner atoms, edges, etc.) at the catalyst surface increased, leading to a plasma-enhanced reactivity.[89]

3.2.2. Chemical and Electronic Changes in the Catalyst. *Change in Oxidation State.* Upon exposure of the catalyst to the plasma, the oxidation state of the catalyst may change. For instance, the change in catalyst morphology observed by Guo et al., as described earlier,[89] was accompanied by a decrease in oxidation state of the manganese from Mn(III) to Mn(II,III). Similarly, the reduction of NiO to metallic Ni was observed by Gallon et al.,[90] Tu et al.,[91] and others[79,92] upon plasma exposure, in the context of plasma DRM.

In contrast, an increase in the oxidation state of a manganese oxide catalyst from Mn(IV) to Mn(V) was found by Demidyuk and Whitehead, during plasma-catalytic decomposition of toluene.[93] This increase in oxidation state was attributed to the interaction with plasma-generated O atoms.

Change in Catalyst Work Function. The work function of a catalyst is highly sensitive to its precise surface condition, including, for instance, its morphology, the occurrence of contaminations, and surface reactions. Because the plasma strongly affects the catalyst surface condition, it is clear that the catalyst work function will be influenced. Additionally, the presence of a voltage or current may alter the work function. Hence, the catalytic activity and selectivity is governed in part by the plasma-induced modification of the catalyst work function.

3.2.3. Changes in Surface Processes. *Reduced Coke Formation and Poisoning.* An important issue in catalysis is preventing or limiting catalyst poisoning and coke formation. This may be achieved by combining the catalyst with a plasma. An interesting example of such a plasma/catalyst synergism is the NH_3 decomposition for fuel cell applications.[94] Whereas NH_3 conversion was only 7.4% and 7.8% in the case of Fe-catalyst alone and DBD plasma alone, respectively, a conversion of 99.9% was obtained when combining both. This spectacular conversion increase was attributed to plasma-induced prevention of nitrogen poisoning, by N_2 desorption initiated by surface-adsorbed N atoms recombining with activated plasma species such as metastable NH_3 molecules and NH radicals. However, we note that the reactor was operated using an excessive input power of about 3600 J/L, which would cause too high an energy cost from the practical point of view.

Modification of the Reaction Pathways. Besides preventing catalyst poisoning and coke formation, the application of the plasma also entails a modification of the reaction pathways. As is clear from the above, the interaction between plasmas and. In the thermal process, Wang et al. found that desorbing N_2 molecules are formed by surface recombination of two N atoms, i.e., following a Langmuir−Hinshelwood mechanism.[94] This process thus inevitably leads to significant surface coverage by N atoms. In the plasma-catalytic setup, on the other hand, surface-adsorbed N atoms react with excited NH_3* molecules and with NH· radicals, thereby forming N_2, which can desorb from the surface. In the plasma-catalytic process, the reaction thus proceeds through an Eley−Rideal mechanism.[94]

Lower Activation Barriers and Higher Pre-exponential Factors. Further, the modification of the reaction pathways may also lead to a change in activation barrier and pre-exponential factor. Nozaki and Okazaki investigated steam reforming of methane and found through Arrhenius-plot analysis an activation barrier of ∼100 kJ/mol in the reaction-limited regime, for a setup combining both plasma and catalyst and catalyst alone.[95] The pre-exponential factor, however, was found to increase by a factor of 50 in the case of plasma catalysis. The same observation was made in the diffusion-limited regime, albeit in this case the increase in pre-exponential factor was only a factor 7. The increase in pre-exponential factor can be ascribed to the significantly increased dissociative adsorption of vibrationally excited CH_4 at the catalyst surface compared to vibrationally ground-state CH_4. This conclusion quantifies the contribution of the vibrationally excited plasma species in the plasma-enhanced catalytic processes, which proceed quite differently compared to common thermally activated processes.

Next to increasing the pre-exponential factor, igniting a plasma in contact with the catalyst may also lower the activation barrier. A convincing example was shown for destruction of toluene on Ag_2O/Al_2O_3.[93] Through Arrhenius-plot analysis, a drop in overall activation energy from 63.2 to 49 kJ/mol, i.e., by >20%, was observed. This drop was

DOI: 10.1021/acs.chemrev.5b00362
Chem. Rev. 2015, 115, 13408−13446

attributed to the generation of surface oxygen radicals. In contrast, no such change in activation energy was observed in the case of a MnO_2/Al_2O_3 catalyst. Instead, an increase in pre-exponential factor was found, signifying an increase in active catalytic centers, which was related to a change in oxidation state of the Mn-oxide, as described above. Note, however, that the use of the Arrhenius equation is limited, in principle, to thermal processes, and its application is not straightforward for plasma processes. Hence, while the synergy demonstrated in these experiments is clear, the quantitative values should be treated with care.

3.3. Plasma–Catalyst Interactions and Synergy 2: Effects of the Catalyst on the Plasma

Some effects of the catalyst on the plasma have been reported as well: an enhancement of the electric field due to catalyst nanofeatures, formation of microdischarges in porous catalysts, and changes in discharge type, all of which are closely related.

Probably the most often described effect of the catalyst on the plasma is the enhancement of the electric field near the catalyst surface. This enhancement may occur both in the case of a nanostructured catalyst film and for catalyst-coated dielectric packing in the form of pellets, granulates, or fibers. The field enhancement results from the high local curvature of the surface, in addition to the possible accumulation of charges and polarization effects in the case of dielectric materials. While the field enhancement does not directly modify the chemical properties of the catalyst material, it does modify the electron energy distribution—which in turn determines the plasma composition and, hence, the relative fluxes of plasma species reaching the catalyst. For instance, Tu et al. demonstrated a clear increase in the high-energy tail of the electron energy distribution upon packing their DBD with TiO_2 pellets. Especially zeolites and certain ferromagnetic materials with a high dielectric constant such as $BaTiO_3$ have often been demonstrated to be effective materials in plasma-catalytic destruction of VOCs.[96−99] Although not specified in the original works, the strong field enhancement may be related to the strong nonuniformity of the electric field lines near the nanopore openings in zeolites and microscopic-scale polarizability of $BaTiO_3$.

Upon partially filling the plasma reactor with packing material, e.g., dielectric beads or catalyst-coated pellets, the typical discharge mode is the formation of filamentary microdischarges.[100] However, when fully packing the reactor, the discharge volume is strongly reduced, leading to a modification of discharge mode from filamentary discharges to predominantly surface discharges,[101] which in turn may lead to a decrease in CH_4 and CO_2 conversion in plasma-catalytic DRM.

Moreover, partially or completely filling the discharge volume will also locally modify the electric field. The strongest manifestation of this is seen when using zeolites or ceramic foams. Indeed, in this case, the electric field inside the pores is very strong, which modifies the discharge characteristics. Hensel et al. demonstrated the effect of the pore sizes on the discharge formation and its characteristics. When pores with a size beyond 15 μm were used, a stable discharge could be maintained inside the pores.[30,102] It is possible that, below this size, the surface recombination rates exceed the rates of plasma species generation, thus causing the discharge to become unstable or even extinguish.

3.4. What Possible Synergies Are Currently Unexplored?

As is clear from the above, the interaction between plasmas and catalyst is complex, and often the net result of combining both cannot be attributed to a specific single process. Whereas some factors may prevail, such as the influence of the packing in DBDs on the resulting electric-field distribution and the resulting net effect on the plasma-catalytic process, other factors have not been considered in much detail yet. We describe here a number of such factors that may have a significant effect on the process.

3.4.1. Vibrationally Excited Species. As discussed in section 2.1.2, the Polanyi rules state that translational energy is more efficient than vibrational energy in activating early activation barriers whereas the reverse is true for late activation barriers. Vibrational excitation is particularly important in some plasmas, such as microwave discharges and gliding arcs. In these plasmas, the amount of energy that is deposited in vibrational excitations can be tuned to some extent. As far as the kinetics of plasma–surface reactions is concerned, this has two important consequences, as shown in Figure 8.[35,36] First, some of the vibrational energy may be

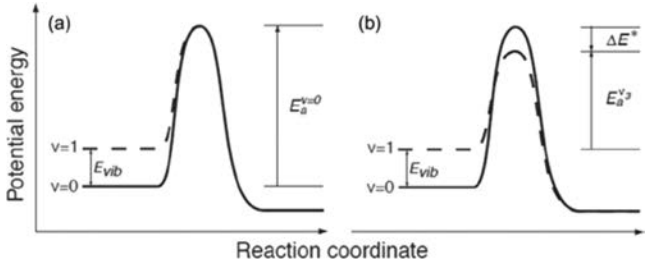

Figure 8. Effect of vibrational excitation of CH_4 on the activation barrier for adsorption on methane. Vibrational excitation may decrease the effective activation barrier by increasing the energy of the reactants by an amount E_{vib} (a) but also by allowing access to an otherwise inaccessible part of phase space, thus lowering the activation barrier further by an amount ΔE^*. Reprinted with permission from ref 35. Copyright 2004 AAAS.

used to decrease the energy barrier to be surmounted, by increasing the reactant energy by an amount E_{vib}, as shown in Figure 8a. In this case, the barrier for the back reaction remains unaltered. Note that not all vibrational energy contributes to this, as the vibrational coordinate in general does not fully map onto the reaction coordinate. Second, vibrationally excited species may also experience a lower activation barrier than ground-state species, as ground-state species may not have access to the portion of phase space containing the lowest transition barrier. This is shown in Figure 8b, where the amount of lowering of the activation barrier due to this second effect is denoted by ΔE^*. In this case, the activation barrier for the back reaction is decreased as well. The resulting energy barrier due the combination of both effects is $E_a^{v_3}$, which is lower by an amount $E_{vib} + \Delta E^*$ relative to the energy barrier $E_a^{v=0}$ experienced by ground-state species.

Clearly, the interplay between catalyst and vibrationally excited species is very complex. To the best of our knowledge, only a few studies have focused on this interaction in the context of plasma catalysis, and especially in the field of DRM.[95] We expect to see an increased research focus on the effects associated with vibrationally excited species in plasma

DOI: 10.1021/acs.chemrev.5b00362
Chem. Rev. 2015, 115, 13408−13446

catalysis in the near future, and we shall return to this issue in section 5.4.

3.4.2. Plasma Photocatalysis. A plasma is generally a source of both photons and electrons, both of which may induce electronic excitations, which in turn may initiate catalytic surface reactions. In the cases of metal and metal oxide catalysts, irradiation of the catalyst surface by photons may enhance the catalytic activity.

While the lifetime of electronic excitations at metal surfaces is very short (in fact, much shorter than the time scale for nuclear motion),[103] this is (in part) compensated by the high photon absorption probability in the near-surface region of the metal. The photon absorption leads to photoexcitation of the electrons. These electrons then relax through scattering events, which in turn leads to a time-dependent electron energy distribution (see left-hand side of Figure 9). These so-called hot electrons may attach to empty adsorbate states, thus leading to the formation of an excited adsorbate complex (see right-hand side of Figure 9, showing the transition from the ground-state potential to an excited state). If this excited state is repulsive, the adsorbate may accumulate sufficient kinetic energy to induce bond breaking while returning to the ground state.

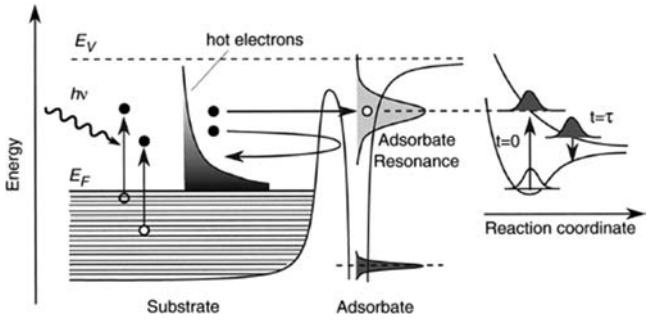

Figure 9. Energy diagram for an adsorbate-covered metal surface under the influence of light absorption. E_V and E_F denote the vacuum level and the Fermi level, respectively. Reprinted with permission from ref 103. Copyright 2000 Elsevier.

In the context of plasma catalysis, however, the possibility for plasma-induced catalytic reactions has been considered mostly for metal oxides such as TiO_2—a well-known photocatalyst. It has been proposed that intense irradiation of the catalyst by plasma-generated photons may be responsible for the TiO_2 catalytic activity in VOC abatement.[71,104,105] In this case, a photon energy of minimum 3.2 eV is required to excite an electron from the anatase TiO_2 valence band to the conduction band. In contrast to metals, the recombination of these charge carriers is relatively slow. The electron in the conduction band can reduce an acceptor molecule, while the photoinduced hole in the valence band can oxidize a donor molecule. This donor molecule may be, for instance, water or O_2, leading to the formation of an OH radical and the superoxide O_2^- anion. Both species are highly reactive and able to oxidize VOCs. However, some reports indicated that the flux of (plasma-generated) photons in a typical discharge is insufficient to induce an appreciable photocatalytic effect.[80,81,106,107] In contrast, photocatalyst activation was only found to occur under additional UV-irradiation. Therefore, unambiguous proof of plasma-induced photocatalysis has not been reported as yet, and it is clear that substantial research is needed in this area.

3.4.3. Collision-Induced Surface Chemistry. The energy required to overcome the surface reaction barrier typically comes from the adsorbate and/or adsorbent thermal fluctuations. As discussed above, this energy or part of this energy may be delivered through vibrational excitation, or by impinging photons or electrons. Yet another energy delivery channel is through the kinetic energy of impinging inert atoms and/or ions. The first observations of this process were on Ar-impact induced CH_4 dissociation on a Ni(111) surface.[103,108,109]

This process may be resolved in two steps. First, the impinging atom transfers a fraction of its energy to the adsorbed CH_4 molecule. The amount of energy transferred depends on the position and direction of the impact. The transferred energy may then be used to dissociate the molecule in the second step. Thus, the adsorbed molecule is accelerated toward the surface, which may or may not lead to dissociation, depending on the precise geometry of the adsorbate/adsorbent system. If the molecule does not dissociate, it may desorb from the surface. In fact, it was found that the probability of collision-induced desorption is significantly higher than that of collision-induced dissociation.[108]

In the context of plasma catalysis, this principle has been proposed as the mechanism underlying ion-induced network healing in plasma-catalytic growth of carbon nanotubes.[65] It was found that, in a narrow energy window of 15−25 eV, impinging Ar ions transfer sufficient energy to the growing network to reorganize itself, leading to the formation of a more crystalline and less amorphous structure, but they do not transfer enough energy to break up the network and destroy the structure. Hence, by fine-tuning the surface bias and, hence, the ion kinetic energy, specific processes requiring well-defined energies may be promoted through this mechanism.

4. CONTRASTING CATALYTIC, PLASMA, AND PLASMA-CATALYTIC PROCESSING: CNT GROWTH AND CO_2 CONVERSION

4.1. Carbon Nanotube Growth

The first case study to illustrate synergy in plasma catalysis is the growth of one-dimensional (1D) carbon nanostructures on solid surfaces exposed to either a hydrocarbon source gas or a low-temperature nonequilibrium plasma. These examples include single- and multiwalled carbon nanotubes (SWCNTs and MWCNTs, respectively) and carbon nanofibers (CNFs).

Although the SWCNT thickness may vary from 0.5 to 10 nm or even more, the most typical thickness is of the order of 1−2 nm. MWCNTs and CNFs broadly vary in size, and their typical thickness is of the order of tens of nm. The thickness of these structures is usually limited by the catalyst nanoparticles (CNPs) or catalyst-surface features (CSFs), which support nucleation and growth of the nanostructures.[110] In the case of SWCNTs, however, there is no unique correlation between the CNP diameter and the tube diameter. Indeed, two distinctive tangential and perpendicular nucleation and growth modes are possible.[111] In the tangential mode the tube diameter is close to the CNP diameter, whereas in the perpendicular mode the tube diameter is smaller than the CNP diameter. Both modes were shown to occur independently of CNP size.[111]

DOI: 10.1021/acs.chemrev.5b00362
Chem. Rev. 2015, 115, 13408−13446

The growth requires a source of carbon atoms, which can be delivered to the CNP or CSF surfaces by the chemical vapor deposition of hydrocarbon precursor gases such as methane (CH_4), acetylene (C_2H_2), ethylene (C_2H_4), and others.[112−114] Most often, a hydrogen-based etching carrier gas, such as H_2 or NH_3, is added to remove amorphous carbon deposit. The precursors need to be decomposed (dissociated) to release carbon atoms that can then nucleate and give rise to the initial nuclei that eventually develop into the 1D nanostructures. Dissociation of hydrocarbon precursors has a specific energy barrier that needs to be overcome, which depends on the geometrical and electronic properties of the nanostructure (see section 2.2.2). Apart from heating the precursor gas flow in the reaction chamber, the common means of supplying energy required for the nucleation and growth is by heating the deposition substrate. The exact amount of energy required is determined by the surface material and topography. Moreover, besides determining the specific mechanisms and activation energy of hydrocarbon precursor dissociation, they also govern the capturing and directing of carbon atoms into the sites of nucleation and incorporation into the developing nanostructures.

The pressure in both thermal-catalytic and plasma-based CNT growth can vary from the sub-Torr range up to atmospheric pressure.[63] Traditionally, plasma processing makes use of reduced pressures, allowing easy plasma ignition and the formation of a homogeneous discharge. Atmospheric pressure setups, however, do not require expensive vacuum pumps, which is advantageous in an industrial setting. Moreover, ion bombardment at reduced pressure may damage the growing structure. In contrast, because of the much higher collision rates, ion-induced damage is strongly reduced in atmospheric pressure growth systems. Hence, we envisage atmospheric pressure sources as the current and future systems of choice for CNT growth.

The outcomes in terms of nanostructure growth are the results of interaction of the neutral precursor gases in thermal chemical vapor deposition (CVD) or partially ionized gases in plasma-enhanced CVD (PECVD) with the surfaces. They also depend on the way the surface texture is formed.

The two most common ways to form such features is by either depositing (or forming otherwise) nanoparticles or surface texturing. The particles and the textures made of different materials exhibit very different solubilities of carbon atoms. Generally, nanometer-sized CNPs or CSFs catalytically facilitate precursor gas dissociation and help capture the as-produced carbon atoms to direct them to the nanostructure nucleation sites. These nucleation sites are random and, hence, poorly controllable on smooth surfaces. Importantly, nanostructure nucleation on smooth surfaces may not even be possible. In this case the CNPs or CSFs are the decisive enabling factors in 1D nanostructure nucleation and growth.

Let us now consider the difference between metal-catalyzed CVD, PECVD without catalyst, and metal-catalyzed PECVD, focusing specifically on the synergistic plasma-specific effects that arise.

4.1.1. Thermal Growth with a Catalyst. CNTs are most often grown by thermal metal-catalyzed CVD. The growth process is commonly accepted to follow the vapor−liquid−solid (VLS) mechanism, as shown schematically in Figure 10.[63]

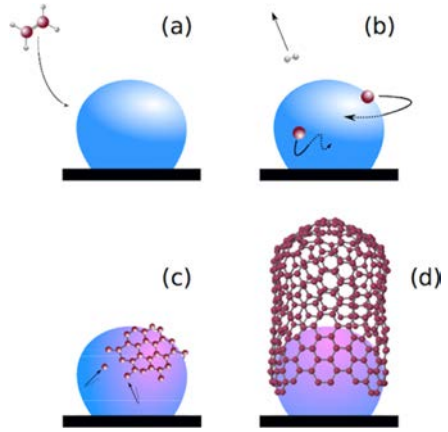

Figure 10. VLS model applied to CNT growth. (a) Adsorption of gas-phase hydrocarbon species on the nanocatalyst particle; (b) catalytic decomposition into carbon atoms and dissolution in the liquid bulk; (c) surface carbon segregation with the formation of a solid precipitate; (d) formation of a solid crystalline structure. Reprinted with permission from ref 63. Copyright 2012 American Vacuum Society.

In this mechanism, originally proposed in 1964 for the growth of Si-whiskers[115] and subsequently applied to the growth of carbon nanofibers,[116] the gas-phase hydrocarbon precursor molecules are catalytically decomposed on the surface of the catalyst nanoparticle. The catalyst is assumed to be liquid, allowing the carbon to easily diffuse through the bulk of the particle. After supersaturation, carbon starts to segregate in order to form a bent graphene patch partially covering the nanoparticle. By continuous addition of carbon from the bulk of the particle, which is delivered through a continuous influx of hydrocarbon precursor molecules, a solid CNT eventually emerges.

The assumption that the catalytic particle is liquid is indeed justified by the typically used growth temperatures, in the order of 1000 K, in combination with the Gibbs−Thomson effect, as discussed in section 2.2.2. Indeed, often used metals such as Fe, Co, and Ni show melting temperatures in the order of or slightly below that value.[55−57] Moreover, atomistic simulations pointed out that the activation energy for metal−metal and metal−carbon bond switching decreases with increasing carbon concentration in the nanoparticles. This leads, in turn, to an increasing amorphization of the nanoparticles, thus rendering them liquid at an even lower temperature than would be expected based solely on the Gibbs−Thomson effect for the pure metallic nanoparticles.[117]

The catalyst nanoparticle may be located both at the top or the bottom of the 1D nanostructure as shown in Figure 11.[118] The first case is more common for MWCNTs and CNFs whereas the second case is more relevant to SWCNTs. The interface between the CNP and the nanostructure is accepted as the point of incorporation of carbon atoms into the developing structure. The only significant difference between the CNT and CNF cases is the wall shape resembling straight coaxial cylindrical walls for CNTs and a bamboo-like structure for CNFs.

4.1.2. Plasma Growth without a Catalyst. Although CNT growth usually requires a catalyst, both SWCNTs and MWCNTs can also be grown without a catalyst, provided some other curved seed particle is available allowing for cap formation and continued growth.[119−121] In this case, the

DOI: 10.1021/acs.chemrev.5b00362
Chem. Rev. 2015, 115, 13408−13446

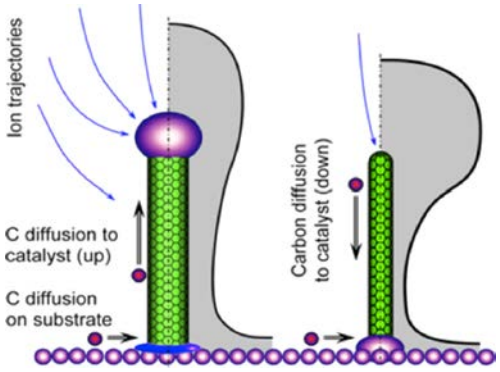

Figure 11. Two common locations of metal catalyst nanoparticles in the growth of MWCNT (left) and SWCNT (right) nanostructures. Reprinted with permission from ref 118. Copyright 2008 John Wiley and Sons.

plasma may facilitate the growth process. One possibility is to grow MWCNTs directly on an oxide-free Si surface in methane-based microwave plasmas without any external heating, as shown in Figure 12.[122]

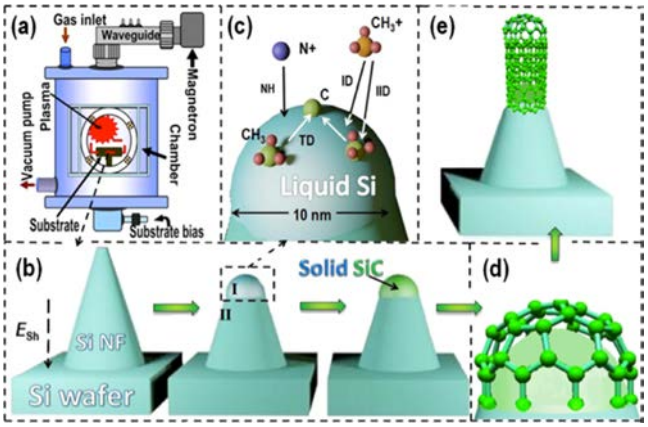

Figure 12. Schematic of the microwave plasma CVD system (a); melting of the topmost part of the Si nanofeature (NF) and formation of a solid SiC hemispherical tip (b); elementary surface processes involved in the heating of the Si NF and generation of C atoms (c); formation of the graphene cap (d); and growth of the vertically aligned nanotubes (e). The important surface processes sketched in (c) are ion-induced dissociation (IID), ion decomposition (ID), nitrogen ion heating (NH), and thermal dissociation of hydrocarbon radicals (TD). Reproduced with permission from ref 122. Copyright 2013 John Wiley and Sons.

According to the Si/C phase diagram,[123] bulk Si has only a limited maximum carbon solubility of 9×10^{-4} at% at 1674 K due to the formation of β-SiC precipitates and, hence, does not catalyze CNT growth in the way that is common for metal CNPs discussed earlier. In this case, the extent of contact of the plasma with the surface plays the key role.[122] When the Si surface was smooth, both CVD and PECVD failed to produce CNTs. When arbitrary small scratches and dots were made on the Si surface, only direct plasma contact with the surface produced the nanotubes. Importantly, both thermal CVD and remote plasmas failed to produce the MWCNTs.

Surface microscopy revealed that microscopic Si nanofeatures with tip sizes of the order of 10 nm were produced upon scratching. As mentioned in section 2.3.2, the plasma can provide heating necessary for the nucleation and growth of carbon nanotubes or nanofibers. The surface temperature at the discharge power that produced the nanotubes matched the melting temperature of a Si nanoparticle of a ~10 nm size.[122] Once molten, Si easily forms a carbide phase when exposed to a flux of carbon atoms. SiC particles are known to catalyze CNT growth,[124,125] and this was a likely reason for the formation of MWCNTs only on Si NFs and only upon direct contact with the plasma.

This manifests a synergistic effect: the process only works when both the Si nanofeatures and the plasma are present. Exposing a smooth Si surface to a plasma or Si nanofeatures to a neutral gas of the equivalent CVD process both did not work.[122]

4.1.3. Plasma-Catalytic Growth. Plasma-catalytic growth is rather common for SWCNTs, MWCNTs, and CNFs, and many works reported on the beneficial effects of combining the catalyst with the plasma.[61−63,126] Compared to thermal growth, a large variety of active species may contribute to the growth process, including atoms, molecules, excited metastable species and radicals, ions and electrons, and photons, as shown in Figure 13. Typically, electric fields are also present, further modifying the growth conditions relative to thermal metal-catalyzed growth.[61,63]

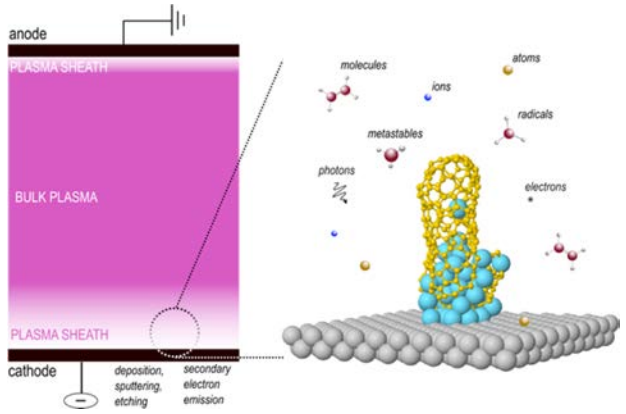

Figure 13. Factors affecting the growth of CNTs in a PECVD process. Electromagnetic fields are not shown. Reprinted with permission from ref 63. Copyright 2012 American Vacuum Society.

In a plasma-catalytic process, the nonequilibrium reactive plasma chemistry leads to the effective precursor conversion in the gas phase, as described in section 2.3.1, and also to an accelerated carbon species production at the catalyst surface. Moreover, these carbon species can be delivered to the growth surface faster in the plasma, for example, through the ion fluxes. The contributions of these fluxes can be very significant, even in comparison to the contributions of neutral radical species due to their typically high sticking coefficients. This will lead to larger amounts of carbon atoms on the surface or dissolved within CNPs, which may on the one hand lead to lower diffusion barriers and higher bond switching rates.[117] On the other hand, CNP supersaturation may occur faster, thereby shortening the lead time before the nucleation (incubation time).[127] However, increased C-fluxes may also cause CNP poisoning or even complete encapsulation of the catalyst by amorphous carbon.

DOI: 10.1021/acs.chemrev.5b00362
Chem. Rev. 2015, 115, 13408−13446

Ion bombardment may play an important role in plasma-enhanced catalytic CNT growth. During the SWCNT cap nucleation in particular, ion bombardment leads to the top-down energy transfer from the plasma to the C-network. This makes it possible first to improve the structural quality of the C-network,[65,66] as shown in Figure 14. Moreover, the ion

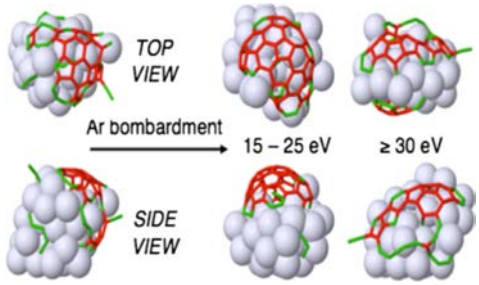

Figure 14. Ion-induced improvement of structural quality of a SWCNT cap on a Ni CNP in the ion energy range of 15−25 eV. Reprinted with permission from ref 65. Copyright 2013 American Physical Society.

bombardment may also provide the additional "bending energy" (see Figure 15) to lift up the initial as-nucleated

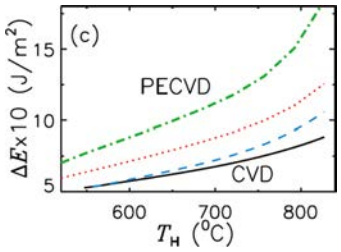

Figure 15. Bending energy ΔE as a function of the substrate holder temperature T_H for PECVD and thermal CVD processes. Reprinted with permission from ref 128. Copyright 2011 American Chemical Society.

graphene monolayer off the CNP surface to form a SWCNT cap.[128] Ion bombardment may change the growth mechanism, as has recently been shown by atomic-scale simulations.[77,78] However, ion bombardment may be detrimental for CNT growth, leading to etching and sputtering.[67−70,129] A discussion of the beneficial and detrimental effects of ion bombardment during CNT growth can be found elsewhere.[130]

The local temperature of the CNPs can also increase due to the effects of ions and other plasma species (see section 2.2.2). In the case of plasma-catalytic CNT growth, this effect may lead to nanostructure nucleation using reduced substrate heating.[131] In this way, the nanostructure growth rates can be substantially increased.[132]

The importance of both ion bombardment and plasma-induced heating is highlighted by numerical simulations on CNF growth. Figure 16 shows a range of reactions that take place on the surface of a Ni CNP located on top of a CNF, exposed to low-temperature nonequilibrium plasma.

Most of these processes and factors (e.g., adsorption, desorption, activation energies, etc.) are similar for both CVD and PECVD. However, the presence of ion-induced reactions and localized plasma heating makes a major difference between these two processes, including the rates of similar processes. Indeed, the relative importance of carbon atoms

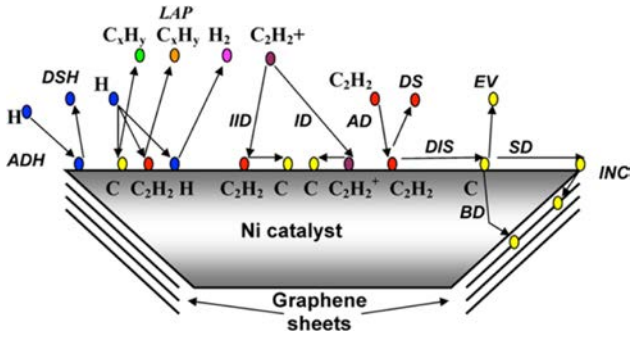

Figure 16. Range of plasma-affected elementary processes on the surface and bulk of a Ni CNP in PECVD of carbon nanofibers. The following processes are sketched: AD = adsorption of C_2H_2, DS = desorption of C_2H_2, DIS = dissociation, EV = evaporation, SD = surface diffusion, INC = incorporation into a graphene sheet, BD = bulk diffusion, ADH = adsorption of H atoms, DSH = desorption of H atoms, LAP = loss of adsorbed particles at interaction with atomic hydrogen, IID = ion-induced dissociation of C_2H_2, and ID = ion decomposition. Reprinted with permission from ref 134. Copyright 2007 AIP Publishing LLC.

diffusing over the surface or through the bulk of the CNP (termed surface (SD) and bulk (BD) diffusion in Figure 16, respectively) is very different between CVD and PECVD and in different temperature ranges.

Both experiments[133] and numerical modeling[134] of CNF growth in the plasma suggest that surface diffusion dominates in low-temperature growth of CNFs in the plasma whereas bulk diffusion is the main mechanism in thermal CVD of CNFs at higher temperatures. This is shown in Figure 17. Indeed, Figure 17 shows the growth rates, H_s and H_v, corresponding to the surface diffusion and bulk diffusion channels, respectively, taken separately. In Figure 17b, the blue curve corresponding to the surface diffusion channel fits to the experimental curve.[135] This fit is particularly clear in the lower temperature range where the purely thermal CVD growth is not even possible ($1000/T_s > 1.4$, where T_s is the surface temperature). On the other hand, the bulk diffusion mechanism quantifies the thermal CVD growth in the higher temperature range where $1000/T_s < 1.4$. We find this numerical result to be in good quantitative agreement with the available experimental data.[136]

Therefore, one of the synergistic effects of the plasma and the Ni CNPs where purely thermal CVD growth is in redirecting carbon atoms to the nanofiber incorporation sites through the catalyst surface at lower temperatures when their diffusion through the bulk becomes ineffective. This leads to the growth of CNFs in the temperature range below 714 K (yet above 400 K) where purely thermal CVD growth is impossible.

When only plasmas are used without catalyst nanoparticles, 1D nanostructures do not nucleate on smooth surfaces with low carbon solubility, as described above. When CNPs are exposed to the plasma, the growth rates are usually higher at the same external heating temperatures compared to thermal CVD using the same precursor gas under the same conditions. Alternatively, the same growth rates can be achieved in PECVD at much lower external heating temperatures than in CVD.

We emphasize that in several cases reported in the literature the external heating may even become completely redundant as was the case for the MWCNT growth described

DOI: 10.1021/acs.chemrev.5b00362
Chem. Rev. 2015, 115, 13408−13446

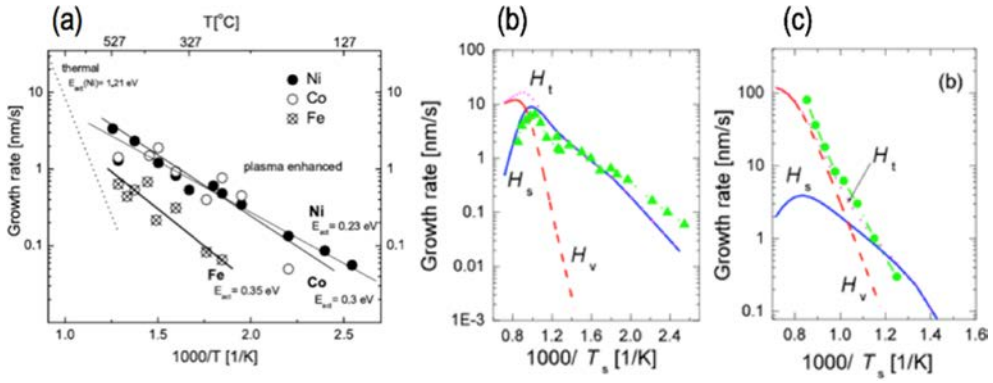

Figure 17. (a) Arrhenius plots for CNF growth rates on Ni, Co, and Fe catalysts in NH_3-diluted C_2H_2 in thermal (dotted line) and plasma-enhanced CVD. Reprinted with permission from ref 133. Copyright 2005 American Physical Society. (b, c) Growth rates H_s, H_v, and $H_t = H_s + H_v$ as functions of the surface temperature for PECVD (b) and CVD (c). The triangles and circles represent the experimental points.[135,136] Reprinted with permission from ref 134. Copyright 2007 AIP Publishing LLC.

in section 4.1.2. This indicates the constructive, synergistic interaction between the plasma and the CNPs, which leads to the reduced amounts of external heating required to nucleate and grow the nanostructures and to increase the nanostructure growth rates.

Another clearly synergistic effect of the plasma and CNPs is vertical alignment along the direction of the applied electric field in the plasma sheath near the substrate surface. Whereas thermal CVD processes usually produce tangled, twisted CNTs with random orientations and growth directions unless dense crowding effects guide CNTs growth vertically, PECVD produces vertically aligned, free-standing single-walled CNTs.[137−140]

This common observation clearly shows the synergistic effect defined in section 3. Indeed, just using plasmas and very smooth surfaces usually produces (e.g., amorphous) carbon films rather than localized CNTs. Therefore, plasma requires surface features or catalyst to produce CNTs. When catalyst particles are used in conjunction with thermally dissociated flow of gas precursor (thermal CVD), the nucleation/growth temperatures are notably higher (at least a couple of hundred degrees Celsius) than when the plasma is used. In this case the nanotubes are thicker, the chirality distribution is broader, and the orientation is random. When both plasma and catalyst are used, the growth temperatures are notably lower, alignment is vertical, the tubes are thinner, and the chirality distribution can also be narrower.[141,142] This observation may in part be attributed to the combination of the electric field and ion bombardment, allowing for nucleation at lower external heating, with smaller radii, and with predetermined vertical orientation.

It is thus quite clear that the various plasma-specific factors may enhance the growth, also in the case of catalyst materials with low solubility of carbon atoms, such as Au. This suggests that if plasma enables growth of 1D (and 2D as we will see in section 5.1) nanostructures at low temperatures and surface diffusion is the dominant mechanism, then there is no real need to use catalysts with high carbon solubility in this low-temperature range. Because plasmas also increase the rates of generation and delivery of precursor species to the growth surfaces, the nanotubes can be grown very quickly. A striking example is the possibility to grow short single-walled nanotubes using Au catalyst nanoparticles, as demonstrated by both experiments and simulations.[128,141,143] Specifically, SWCNTs (an example is shown in Figure 18) were detected even after only 2−15 s of the plasma-discharge operation.

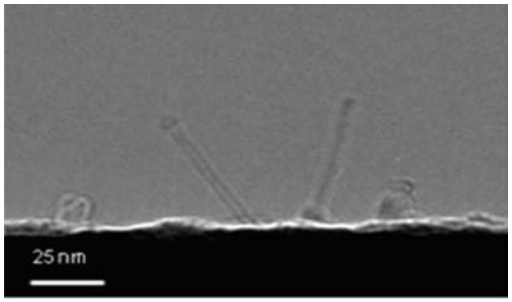

Figure 18. Single-walled carbon nanotubes grown using Au catalyst nanoparticles. Plasma-assisted CVD enables very fast growth at significantly reduced temperatures. Reprinted with permission from ref 143. Copyright 2010 American Chemical Society.

Thin SWCNTs with a relatively narrow chirality distribution were produced at temperatures 580−640 °C, inaccessible by thermal CVD for the given catalyst nanoparticle size range. For SWCNTs with (8,6) chirality, the difference between the nucleation temperatures in thermal and plasma CVD is ∼200 degrees.

In addition to the previously mentioned vertical-alignment effect, the electric field generated in the plasma sheath (see section 2.3.1) also plays a major role at the nucleation stage of CNTs. As shown by atomic-scale numerical simulations,[138] the electric field should be sufficiently strong to play a significant role in the nanotube growth. First, these electric fields ensure the vertical growth direction and SWCNT alignment, in agreement with experimental results.[137] Second, the graphitic network shows a better ordering compared to the cases when there is no electric field or when the electric field is weak. Third, similar to the CNF and MWCNT cases (as well as other nanostructures such as Si nanowires), the growth rates of SWCNTs are increased by the application of the electric field.

The electric field increases the degree of directionality of carbon atom movement along the CNP surfaces as opposed to the completely random motions in all directions without the electric field. Because the direction of the electric field in the plasma is normal to the surface, it guides polarized (see explanation below) carbon atoms upward, toward the top of

DOI: 10.1021/acs.chemrev.5b00362
Chem. Rev. 2015, 115, 13408−13446

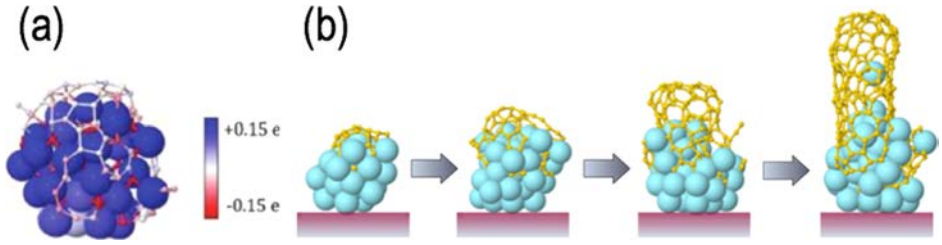

Figure 19. (a) Charge transfer in the nucleation of SWCNT cap on a Ni CNP; (b) effect of the electric field on the continued CNT growth, leading to vertical alignment. (a) Reproduced with permission from ref 138. Copyright 2012 American Chemical Society.

the CNPs, eventually giving rise to the nucleation of SWCNT caps at the summit of the catalyst nanoparticle. This is very different from common thermal CVD cases where nucleation of CNT caps occurs randomly, leading to disordered, misaligned growth, which is often referred to as a "spaghetti-type" growth.[144,145]

Importantly, this phenomenon arises through the combined effects of the plasma and the catalyst nanoparticle. Without CNP, the carbon atoms are charge-neutral. However, direct contact with a Ni nanoparticle during the SWCNT cap nucleation stage leads to charge transfer in the C−Ni system, as shown in Figure 19.[138] Carbon atoms acquire a small negative charge while Ni atoms become slightly positively charged. The plasma electric field can then act on this polarization to induce directed growth. Note that polarization of carbon atoms on noncatalytic surfaces is weaker or absent compared to the case of the Ni−C system. This demonstrates synergistic effects of the plasma-produced electric field and Ni catalyst nanoparticles, which then lead to better growth directionality with higher rates and improved quality of the graphitic network.

In combination with other plasma effects (higher supersaturation of carbon within CNPs and higher local temperatures on their surfaces, in addition to nonthermal surface activation), the synergistic effects of the CNPs and electric field are further amplified by allowing for the nucleation of thinner nanotubes at lower temperatures of external heating with predetermined base positions (at the CNP summits), and also possibly with narrower chirality distributions, in addition to the common vertically oriented growth. This shows clear synergistic effects in plasma-catalytic nucleation and growth of CNTs. We emphasize that quite similar synergistic effects may be applicable to other related 1D nanostructures. This opens an interesting opportunity for future research.

4.2. CO_2 Conversion

The second case study to illustrate the synergy of plasma catalysis is for gas conversion. This includes air pollution control (e.g., destruction of volatile organic compounds, VOCs), CO_2 conversion into value-added chemicals, hydrocarbon reforming, ammonia production, etc. Several examples will be given in section 6. Here, we describe greenhouse gas (i.e., CO_2 and CH_4) conversion into value-added chemicals or new fuels, such as syngas (a mixture of CO and H_2), methanol, formaldehyde, and other hydrocarbons or oxygenates. This process is gaining increasing interest worldwide, because of the global climate change and the increasing energy consumption. Indeed, these greenhouse gases could constitute an alternative for petroleum, which will become less available and therefore more expensive in the future. The conversion of these greenhouse gases is therefore considered as one of the main challenges for the 21st century.[146,147] Moreover, as this process aims to convert waste (i.e., greenhouse gases) into a new feedstock (raw materials for the chemical industry), it can be considered to fit the "cradle-to-cradle" concept.[148] However, the conversion process of CO_2 and CH_4 is not straightforward, because both molecules are thermodynamically stable, and their dissociation requires significant amounts of energy. Here, we will critically examine the state of the art and current challenges for the conversion of CO_2 (and CH_4), based on thermal-catalytic processing, plasma conversion without catalyst, and plasma catalysis.

4.2.1. Thermal-Catalytic Conversion. Splitting CO_2 into CO and O_2 is an endothermic process with a reaction enthalpy of 283 kJ/mol or 2.9 eV per molecule, at 298 K:[149]

$$CO_2 \rightarrow CO + 1/2O_2 \quad (2)$$

The equilibrium of this reaction lies strongly to the left,[149] such that the equilibrium yield of CO and O_2 varies from about (or less than) 1% at T < 2000 K up to ∼60% at temperatures between 3000 and 3500 K.[150] The equilibrium constant as a function of temperature can be found in the work of Wagman et al.[149]

Active removal of one (or both) products increases the conversion, following Le Châtelier's principle. This may be accomplished by the use of zirconia membranes, as demonstrated by Nigara and Cales[151] and Itoh et al.[152] By using a calcia-stabilized zirconia membrane and CO as sweep gas, Nigara and Cales reached conversions of 21.5% at 1954 K in the most reducing conditions, to be compared to a conversion of CO_2 of no more than 1.2% at this temperature in thermal splitting. The overall conversion, however, was much lower and in line with the overall thermodynamic equilibrium conversion, due to permeation of O_2 through the membrane reacting with the CO sweep gas, thereby forming CO_2.[150,151]

Approximately 92 kJ/mol is needed to heat 1 mol of CO_2 from 300 to 2000 K, while the reaction enthalpy is equal to 245 kJ/mol at 2000 K. On the basis of a conversion of 1.2%, the energy cost for total conversion is ∼7.9 MJ/mol, yielding an energy efficiency of 3.6% with respect to the reaction enthalpy of 283 kJ/mol at 300 K. To heat 1 mol of CO_2 to 3500 K, on the other hand, ∼184 kJ/mol is needed, while at this temperature the reaction enthalpy is equal to 206 kJ/mol. On the basis of a conversion of 60%, the energy cost of total conversion is then only ∼513 kJ/mol, yielding an energy efficiency of 55% with respect to the reaction enthalpy of 283 kJ/mol at 300 K.

Hence, it is clear that thermal CO_2 splitting is thermodynamically and energetically only favorable at very high temperatures,[149,150] while alternative approaches at lower temperatures have not yet realized comparable conversions

DOI: 10.1021/acs.chemrev.5b00362
Chem. Rev. 2015, 115, 13408−13446

and energy efficiencies.[150−152] Because thermal-catalytic CO_2 splitting is very energy consuming, the only practical way of thermal CO_2 conversion is dry reforming of methane, i.e., the simultaneous conversion of CO_2 with CH_4, yielding the production of syngas:

$$CH_4(g) + CO_2(g) \rightarrow 2CO(g) + 2H_2(g) \quad (3)$$

Following Le Châtelier's principle, increasing the pressure of the reactants will drive the reaction backward, and hence the reaction is commonly carried out at atmospheric pressure. Just like direct CO_2 splitting, this is also an endothermic reaction, with a standard reaction enthalpy of 247.3 kJ/mol or 2.56 eV per converted molecule. Therefore, it needs to be carried out at high temperatures (600−900 °C), by means of a catalyst, typically containing Ni, Co, precious metals, or Mo_2C as the active phase. Substantial research efforts are devoted to the search of the optimum catalyst materials,[153,154] as the process suffers from significant carbon deposition at the catalyst material, giving rise to catalyst poisoning.[155] On the industrial scale, the process is most efficient at 700 °C, reaching thermodynamic equilibrium conversions of CH_4 and CO_2 of 72% and 82%, respectively. As the reaction between 1 kmol of CH_4 and 1 kmol of CO_2 at 700 °C requires 260 MJ energy, and at least an additional 70 MJ is required to bring the gas flow to this temperature, at least about 330 MJ energy is required for this process, resulting in an energy input of at least ca. 3.42 eV per molecule and a corresponding maximum theoretical energy efficiency of 58%. It is crucial to realize that this is the theoretical energy efficiency. We emphasize that, to estimate the overall energy efficiency, one also has to account for the thermal efficiency of the heaters, which depends on the type of heater, the type of fuel, and the use of heat-recovery systems.

4.2.2. Plasma Conversion without a Catalyst. In recent years, there has been an increasing interest in the use of plasma technology for CO_2 conversion. Experiments are carried out in several types of plasmas. The most common types reported in the literature are DBDs,[156−158] microwave,[159,160] and gliding arc discharges.[161,162] The first type is a nonequilibrium or cold plasma, where the gas is more or less at room temperature, and the electrons are heated to temperatures of 2−3 eV by the strong electric field in the plasma. The microwave and gliding arc plasmas are considered to represent the so-called warm plasmas, an intermediate case between thermal and nonthermal (cold) plasmas. The gas can reach temperatures up to 1000 K and more, and the electron temperature is typically ∼1 eV. This temperature is ideal for populating the vibrational levels of CO_2, and because the CO_2 splitting is most energy-efficient when it proceeds through the vibrational levels,[5,163] warm plasmas are more advantageous in terms of energy efficiency of the process. Indeed, the highest energy efficiency for pure CO_2 splitting reported for a microwave reactor is 90%.[5] However, we emphasize that this result was obtained at reduced pressure (∼100−200 Torr), and increasing the process pressure to atmospheric pressure, desirable for industrial applications, dramatically reduces the energy efficiency. The highest energy efficiency for CO_2 splitting in a gliding arc plasma, operating at atmospheric pressure, is reported to be 43%, at a conversion of 18%.[161] For DRM, a conversion of 8−16% was reported, with a corresponding energy efficiency of 60%.[162]

While the energy efficiency reached with DBDs is considerably lower, i.e., in the order of 4−8% for both pure CO_2 splitting and for DRM,[164,165] a DBD reactor has a very simple design, which is beneficial for upscaling, and operates at atmospheric pressure, making it suitable for practical applications. It can also easily be combined with a (catalytic) packing, as will be elaborated in the next section, which is important for the selective production of targeted compounds.

The important point, which to some extent has been overlooked in the literature, is the substantial lack of selectivity when plasmas are used. Indeed, the reactive species, created by the electrons, easily recombine, and a large number of different products can be formed. In pure CO_2 splitting, this is not an issue, as CO and O_2 are the main components.[165] However, in DRM, typical products formed are syngas, higher hydrocarbons (C_2H_6, C_2H_4, C_2H_2, C_3H_8, ...), as well as oxygenates, such as methanol, ethanol, formaldehyde, acetaldehyde, and carboxylic acids.[164,166] Combination with catalysis will then be highly desirable, if some specific compounds are targeted.

4.2.3. Plasma-Catalytic Conversion. The selectivity and energy efficiency of plasma-based CO_2 conversion can be improved by combining the plasma with a catalyst. Plasma-catalytic CO_2 conversion usually takes place in a DBD reactor, which typically operates at atmospheric pressure. It is important to distinguish between the physical and chemical effects of introducing a catalyst in the plasma. In simple terms, the chemical effects are the basis for the improved selectivity toward the targeted products, while the physical effects are mainly responsible for the better energy efficiency. In the case of pure CO_2 splitting, mainly CO and O_2 are formed, so the primary added value of the catalyst is to increase the energy efficiency, although the conversion can also be improved by chemical effects such as enhanced dissociative chemisorption due to catalyst acid/basic sites. In the case of DRM, or other reactions involving CO_2 and a coreactant (e.g., H_2O, H_2), the selectivity toward targeted products can be tuned (see below). We will first elaborate on the physical effects, before showing some examples of the chemical effects, although it needs to be realized that both effects are interrelated and cannot always be separated.

The local electric field in the plasma can be enhanced due to sharp edges of the nanostructured catalyst (see section 3.3), or simply at the contact points of the catalyst pellets. It should be stressed that this effect also occurs when introducing a simple dielectric packing in the plasma, because of polarization of the dielectric beads. This enhanced electric field, for the same applied power, yields higher electron energies, increasing the ionization and dissocation efficiency of the gas molecules, leading to more energy-efficient conversion.

The packing or catalyst loading in the reactor is of prime importance in plasma catalysis for CO_2 conversion. For instance, DRM was investigated in a single-stage reactor system comprising a coaxial dielectric barrier discharge (DBD) reactor combined with Ni/γ-Al_2O_3 catalysts as a function of the packing method.[100] Three packing methods were employed: full packing, partial packing (axial), and partial packing (radial). Unlike the full packing method where the gas discharge is limited due to the suppression of the filamentary microdischarges as a result of low discharge volume, the partial packing method (radial or axial) shows a strong filamentary discharge due to the large void fraction in the discharge gap. This improves the physicochemical

DOI: 10.1021/acs.chemrev.5b00362
Chem. Rev. 2015, 115, 13408−13446

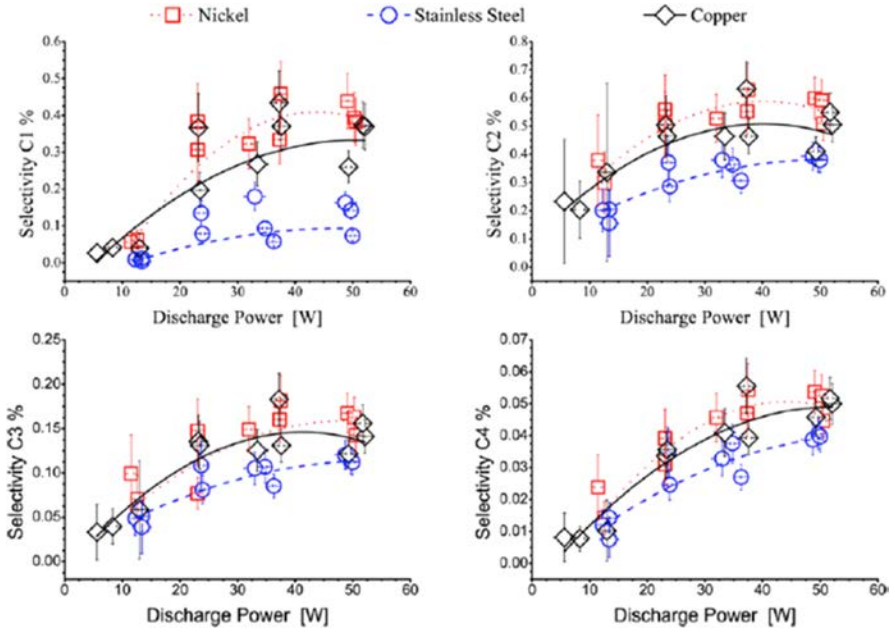

Figure 20. Selectivity for the formation of formic acid (C1), acetic acid (C2), propionic acid (C3), and butyric + 2-methylpropionic acid (C4), in the case of DRM in a DBD plasma, using nickel, stainless steel, or copper electrodes. Reproduced with permission from ref 170. Copyright 2014 John Wiley and Sons.

interactions between the plasma and the catalyst, leading to high methane conversion (56.4%) and significant hydrogen yield (17.5%).

The use of ceramic foams may yield higher conversion efficiencies, as demonstrated, e.g., by Kraus et al. in a DBD used for DRM.[167] This conversion improvement was explained by the higher electron energies, arising from the smaller discharge volumes in the pores of the ceramic foams. Tu and colleagues demonstrated a change in the discharge behavior (i.e., less filaments and more surface discharges) in the case of a TiO_2 packing (see section 3.3).[101] It was noted that this change affects the electron energy distribution function (EEDF), yielding more electrons in the high-energy tail. Similar results were also obtained for nonconductive (Al_2O_3, zeolite 3A, NiO/Al_2O_3) and conductive (reduced Ni/Al_2O_3) packings. However, strong filaments were still observed for porous quartz wool or small catalyst flakes, where the effect is quite similar to nonpacked DBD, presumably due to the high porosity of the material. Thus, one can conclude that the relative contributions of filamentary versus surface discharges depends on the particle size, shape, packing location, and, hence, the void fraction.[101] The same group reported a higher CH_4 conversion and H_2 yield for quartz wool in the case of DRM, due to changes in the physical properties (i.e., more intense filaments), whereas in the case of γ-Al_2O_3 and zeolite 3A, a lower discharge intensity was obtained, yielding lower CH_4 and CO_2 conversions.[168]

Importantly, these results indicate that a catalyst does not always lead to better performance of the plasma conversion. Nevertheless, the zeolite 3A catalyst still yielded a better selectivity toward H_2 and light hydrocarbons, while the formation of liquid hydrocarbons was inhibited, due to the shape-selectivity determined by the zeolite pore diameter.

Dielectric materials such as glass and ferroelectric materials such as $BaTiO_3$ may induce a shift in discharge mode. Recently, Mei et al. demonstrated that, in plasma-assisted conversion of CO_2, the typical filamentary discharge changes into a combination of filamentary discharge and surface discharge, upon adding the packing. The added packing in turn gives rise to an enhanced average electric field and mean electron energy due to polarization effects (i.e., by a factor 2 for $BaTiO_3$), resulting in a higher CO_2 conversion, CO yield, and energy efficiency.[168] It is obvious that the plasma is modified significantly by the catalyst. However, it presently remains unclear how the modified plasma properties affect the catalytic process.

Even when the discharge mode is not altered by the packing, the packing material still has a profound impact on the overall plasma characteristics and on the CO_2 decomposition. Yu et al. studied how different packings (i.e., silica gel, quartz, γ-Al_2O_3, α-Al_2O_3, and $CaTiO_3$), with different dielectric constants, pore sizes, and therefore BET surface areas,[169] affect the EEDF in a packed-bed DBD for CO_2 conversion (see section 2.3.1). The CO_2 decomposition in the case of quartz was higher than that for silica gel, although both materials are chemically inert and have the same dielectric constant. This different performance could be attributed to the different pellet morphology, i.e., the quartz pellets had rigid edges whereas the silica gel pellets were spherical. The sharp edges lead to an electric field enhancement near the contact points and hence to more high-energy electrons. Besides the physical properties, the acid−base properties of the packing material also were reported to affect the reaction, through chemisorption of CO_2 on the basic sites. Indeed, CO_2 will preferentially chemisorb on γ-Al_2O_3, which is an amphoteric oxide, and will almost not adsorb on α-Al_2O_3, which is chemically inert.[169]

Whereas the physical effects of introducing a catalyst in the plasma seem to be quite straightfoward, i.e., change in discharge behavior, local electric field enhancement, effect on the EEDF, and yielding higher energy efficiencies, the chemical effects of plasma catalysis are clearly less understood. One of the reasons is that the physical and chemical effects are often correlated, as the catalysts are mostly introduced in

DOI: 10.1021/acs.chemrev.5b00362
Chem. Rev. 2015, 115, 13408−13446

a packed bed, so it is not easy to distinguish between the two effects.

An enhanced selectivity toward desired products can in part be obtained by judiciously selecting the catalyst material. Scapinello et al. demonstrated an improved selectivity toward the production of carboxylic acids in the case of DRM, when using copper or nickel electrodes instead of stainless steel.[170] This effect may be attributed to a pure chemical catalytic effect of these metals, as no packing was involved. This is illustrated in Figure 20 for the formation of formic acid (C1), acetic acid (C2), propionic acid (C3), and butyric + 2-methylpropionic acid (C4). The effect is most pronounced for formic acid, where the selectivity in the case of nickel is four times higher than when using stainless steel. These results taken together indicate that, besides gas-phase reactions, surface reactions, and more specifically hydrogenation of chemisorbed CO_2, play a key role in the synthesis of these carboxylic acids.

Another reason why the chemical effects of plasma catalysis for CO_2 conversion are not yet fully understood is that a wide variety of catalyst materials are being explored, including metals (Au, Pd, Pt, Rh, Cu),[171] zeolites (NaY, NaOH-treated Y, HY, Na, NaX, Na-ZSM-5, and Linde-type 5A zeolite),[23,172] La_2O_3/γ-Al_2O_3, CeO_2/γ-Al_2O_3,[173] n-type oxide semiconductors (ZnO, CuO), and Al_2O_3 foams with Ni, Rh, or Ca catalysts.[174] Commercial Ni/Al_2O_3 catalysts, which are also used in thermal catalysis, are probably the most popular catalysts for DRM, but they are not necessarily the most suitable ones under plasma conditions.

These discussions suggest that there is still a lack of insight into which catalysts should perform best in a plasma environment, and more systematic studies on both the physical effects (of the structural packing and the support materials, including, e.g., their dielectric constant, acid/base properties, and porosity) and the chemical effects of the catalyst material (including type and coordination of the active element) are highly needed.

A highly important synergistic effect of plasma catalysis is promotion of catalyst activity at reduced temperatures and, hence, a significant reduction in the energy cost for activating the catalyst. Wang et al.,[175,176] for instance, illustrated such synergy for the single-stage plasma catalysis of DRM with Ni/Al_2O_3 catalyst but did not observe this synergy in two-stage plasma catalysis or when the catalyst was only placed at the end of the plasma zone. Moreover, the synergy was a bit more pronounced in a fluidized bed than a packed bed, because the fluidized bed reactor favors the interaction between the plasma and the catalyst material. Typical synergistic effect factors of 1.25−1.5 were obtained, i.e., the conversion in the plasma-catalysis system was up to 50% higher than the sum of the conversions in the pure plasma and thermal-catalysis cases. A maximum in the synergistic effect factor was obtained at ∼700 K, because at higher temperatures thermal catalysis becomes gradually equally efficient. It was thus concluded that the plasma promotes the catalyst activity at lower temperature. We stress that the above conclusion is very similar to the case of plasma-based SWCNT nucleation and growth on metal catalyst nanoparticles, as discussed in section 4.1, indicating the closely related nature of these catalytic processes.

Similar observations as earlier mentioned were also made by Eliasson et al.[177] Figure 21 shows the methanol yield as a function of temperature in the range from 50 to 250 °C at a pressure of 8 bar for the hydrogenation of CO_2 to methanol in the case of pure thermal catalysis, plasma (DBD) only, and plasma catalysis, using $CuO/ZnO/Al_2O_3$ catalytic pellets. Note that the high pressure was needed to favor methanol formation against methanation, which is the main competitive reaction. The methanol yield was only ∼0.1% in the plasma-only case, as well as in the catalysis case at low temperature (∼100 °C). A maximum methanol yield of 2% was obtained in the case of thermal catalysis at a temperature of 220 °C. In the case of plasma catalysis, a maximum methanol yield of 1% was reached at a temperature of 100 °C. This means that the plasma can shift the region of maximum catalyst activity to lower temperatures by >100 °C, which corresponds to a significant reduction in the energy cost for activating the catalyst.

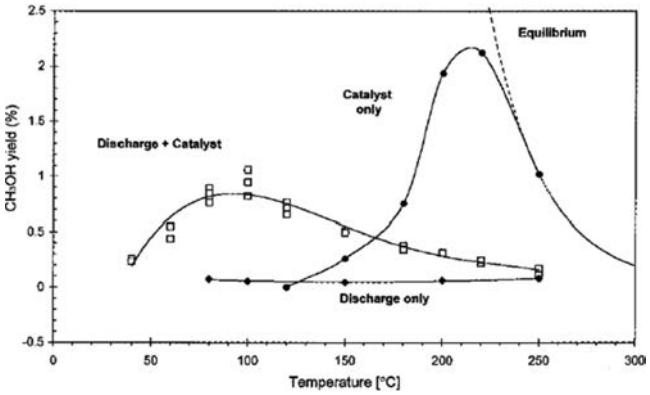

Figure 21. Methanol yield as a function of catalyst/wall temperature, in the case of plasma (DBD discharge) only, catalyst only, and plasma catalysis, at a pressure of 8 bar, a plasma power of 500 W (no power in the case of catalyst only), a flow rate of 0.5 L/min, and a H_2/CO_2 gas mixing ratio of 3:1. Reprinted with permission from ref 177. Copyright 1998 American Chemical Society.

Very convincing results on the plasma/catalyst synergy in the case of DRM were presented by Zhang et al., using different $Cu-Ni/\gamma$-Al_2O_3 catalysts (see Figure 22).[178] The CH_4 conversion in the case of plasma-only and thermal catalysis was 13% and 10%, respectively, whereas the maximum conversion in the case of plasma catalysis was 69%. Similarly, the CO_2 conversions in the cases of plasma,

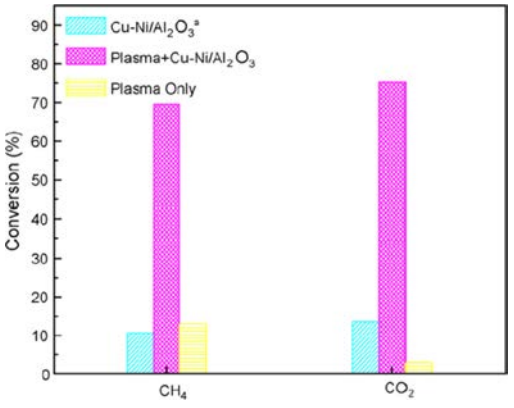

Figure 22. Maximum CH_4 and CO_2 conversion in the case of plasma-only, thermal catalysis, and plasma catalysis, clearly illustrating the synergy of plasma catalysis, in the case of DRM. Reprinted with permission from ref 178. Copyright 2010 Elsevier.

DOI: 10.1021/acs.chemrev.5b00362
Chem. Rev. 2015, 115, 13408−13446

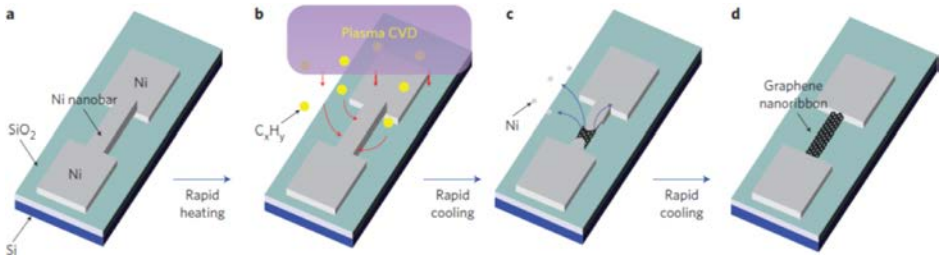

Figure 23. Interaction of the plasma and Ni catalyst during the direct conversion of a Ni nanobar to a graphene nanoribbon. Reprinted with permission from ref 185. Copyright 2012 Macmillan Publishers Ltd.

thermal catalysis, and plasma catalysis amounted to 2.5%, 13%, and 75%, respectively. Furthermore, the selectivities toward H_2 and CO were much better in the plasma-catalysis case. A reaction mechanism was put forward, based on the adsorption of reactive plasma species (CH_x radicals, O and H atoms) on the catalyst surface, followed by recombination of the adsorbed species. Furthermore, it was suggested that the plasma will heat the catalyst surface and, therefore, enhance the desorption of the surface species. The proposed mechanisms align well with the discussions of relevant processes in the previous sections of this review.

Note, however, that synergy in plasma catalysis is not always observed for CO_2 conversion or DRM. For instance, Tu et al.[179] showed a conversion of CH_4 and CO_2 with a Ni/Al_2O_3 catalyst slightly lower than that without a packing. Similar trends were observed by Sentek et al.[180] for the conversion of CH_4 with a Pd/Al_2O_3 catalyst. The changes in the product selectivities, on the other hand, were considerable, pointing out at least some chemical effects of the catalyst.

In general, the enhanced performance of plasma catalysis can in part be attributed to (vibrational) excitation of CO_2 (and the coreactants CH_4 and H_2) in the plasma, which enables easier dissociation at low temperature on the catalyst. This was also suggested by Amouroux et al.,[174] who claimed that another effect is the expelling of water from the catalyst surface by supplying electrons from the plasma (so-called electropolarization). This gives a higher methanol yield in plasma catalysis. Indeed, the plasma electrons affect the catalyst properties (chemical composition or catalytic structure). Furthermore, it was stated that short-lived plasma species (e.g., excited O atoms) are formed inside the catalyst pores. Thus, a catalyst with high dielectric constant should be desirable, as this gives more pronounced polarization of the pellets and thus higher electric fields, favoring the dissociation of species inside the catalyst. It was indeed demonstrated that CaSrTi oxides, which are characterized by high permittivities, give much better CO_2 conversion than Al_2O_3 and SiO_2.[174] These conclusions are consistent with our discussion of the electric field and polarization effects of zeolite and $BaTiO_3$ catalysts in section 4.2.3.

It is worth mentioning that all these examples are based on a DBD plasma. Up to now, there are indeed only a limited number of efforts for combining a catalyst with a microwave[181] or gliding arc plasma,[182−184] with the latter example being for CH_4 reforming. The reason might be that it is less straightforward to introduce a catalyst material in these plasma types, to ensure enough contact time between gas and catalyst, and to avoid too much unused volume, as well as to guarantee that the catalyst remains stable under higher temperatures. It is our opinion that catalysis with warm plasmas could be very promising, as the catalyst surface can be activated by the somewhat elevated temperature, characteristic for warm plasmas (see earlier), possibly leading to extra synergies.

5. OTHER CURRENT AND FUTURE APPLICATIONS OF NANOCATALYST-BASED PLASMA CATALYSIS

Besides plasma-enhanced nanoparticle catalyzed CNT growth and CO_2 conversion, a variety of other processes also show synergistic effects when the plasma and catalytic effects are combined. Below we critically discuss nonexhaustive examples of some of the most interesting effects.

5.1. Catalytic Synthesis of Graphene and Related Nanostructures

In this section we again consider low and high solubilities of carbon atoms in catalyst materials, similar to the CNT growth of section 4.1. We will also consider an interesting case when plasma-assisted dissolution and diffusion through a nanocatalyst helps to form graphene films on silica surfaces.

The first example shows the possibility to grow thin graphene nanoribbons under reduced pressure using nickel nanobars as growth catalysts, connected to transistor terminals.[185] The thickness of the Ni nanobars was in the ∼23−105 nm range, height 35−85 nm, and length 200 nm−5 μm (see Figure 23). RF plasmas of methane and hydrogen mixtures were used during the rapid (5−60 s) plasma exposure of preheated Ni nanobars. During this exposure the Ni nanobars only melted partially and plasma-produced species were dissolved in Ni. During rapid cooling, graphene nanoribbons nucleated and eventually covered the nanobars as shown in Figure 23. The Ni nanobars nearly completely evaporated, leaving graphene nanoribbons connecting the Ni terminals. For sufficiently high Ni nanobars (e.g., >60 nm), interesting graphene nanobridge structures formed while the Ni beneath them evaporated.

Rapid heating, delivery of species to Ni nanobars, and then rapid cooling appear to be critical. The nanobars themselves are also essential because they provide spatial localization for carbon deposition and nanoribbon formation. Purely thermal processes at similar conditions failed, mostly because Ni nanobars evaporated faster than graphene nanoribbons were able to connect the Ni transistor terminals.

This example suggests that both nanobar-shaped catalysts and plasma were essential to enable these unique graphene nanoribbon structures. The graphene could be grown directly in the device location, without damaging the electrode structure, which is a common problem in nanoelectronics. Importantly, the nanoribbons showed excellent performance, such as the clear transport gap (present in nanoribbons and absent in large-area graphene) of 58.5 meV and high on/off

DOI: 10.1021/acs.chemrev.5b00362
Chem. Rev. 2015, 115, 13408−13446

ratio (>10^4) of transistor devices. This process is scalable and is promising for integration with Si micro/nanofabrication technology.

Synergistic interactions between the plasma and carbon-dissolving Ni catalyst also lead to other interesting effects, such as the possibility to grow graphene films on SiO_2 surface, which is quite challenging by using thermal CVD or other methods. Figure 24 shows that it is possible to accomplish

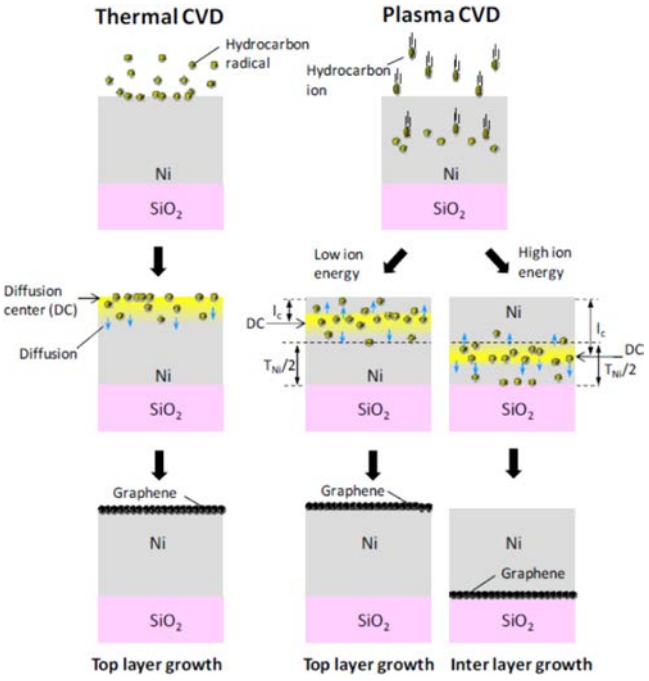

Figure 24. Mechanisms of graphene growth on top of Ni catalyst and at the interface between the Ni catalyst and SiO_2 substrate. Reprinted with permission from ref 186. Copyright 2012 American Chemical Society.

that by depositing a Ni nanofilm (~55 nm) on SiO_2 and then using plasma exposure to "push" carbon atoms through the Ni film to enable nucleation of graphene films at the interface between the Ni film and the SiO_2 substrate.[186] Thermal CVD under similar conditions fails, leading to fast evaporation of Ni films. The interlayer growth of graphene films only occurs when the fluxes of delivered hydrocarbon precursors are low and the energy of the plasma ions is relatively high.

Under plasma CVD conditions, using a low flux of carbon species, and high ion energy, carbon species are able to diffuse through the Ni layer much faster and reach the Ni–SiO_2 interface well before the Ni film evaporates, as sketched in Figure 24. Next to the thermodynamics, pertinent to the nucleation in both the thermal-catalytic and the plasma-catalytic growth processes,[187] it was suggested that the selectivity of nucleation of graphene at different surfaces/interfaces (or both) also critically depends on the diffusion length of carbon ions (l_c in Figure 24). When the ion energy is higher, l_c is larger, and when it becomes larger than approximately half of the thickness of the Ni film (T_{Ni} in Figure 24), nucleation of carbon atoms at the bottom interface becomes possible. The mechanisms of these plasma–catalyst interactions still need to be understood and quantified. For example, the qualitative criterion that compares the diffusion length with the film thickness needs to be refined to account for the variation of l_c with the plasma process (e.g., operating pressure) conditions. Nonetheless, it is clear that both Ni film and plasma exposure are essential to enable nucleation of graphene at the interface between Ni and SiO_2, thus evidencing the plasma–catalyst synergistic effect.

Graphene growth is possible in another extreme case when carbon atoms are not or are hardly dissolved in the catalyst. The most typical example is growth of graphene on Cu films. This method has become very popular because of the possibility to grow high-quality, large-area graphene films,[188] and also because of its scalability to roll-to-roll production and transfer to other substrates for the envisaged applications.[189,190] In thermal CVD, such growth typically requires very high temperatures of at least 800–900 °C or even higher[191] and the growth process typically lasts at least a few tens of minutes. Furthermore, preheating and postprocess cooling are required, costing additional process time and energy. When the thermal CVD process is carried out in common thermal furnaces, the combined pressure of the carbon source and carrier gases is maintained close to atmospheric pressure. Plasma-based methods have emerged as a viable alternative because they allow for the growth at substantially lower temperatures, while the working pressure is typically in the order of a few tens to a few hundred mTorr.[192−194] Moreover, common CVD processes usually require postgrowth etching of the Cu catalyst to enable graphene transfer, which leads not only to the loss of catalyst but also to the need of hazardous chemicals, which raises further environmental issues upon disposal.

Lower growth temperatures and faster growth processes can be regarded as manifestations of synergistic effects of the plasma and the Cu catalyst. When the rates of delivery of carbon species are low, the density of the nucleation centers can be reduced, eventually leading to larger graphene grain sizes. It is noteworthy that this is quite difficult to control in the plasma because plasmas typically provide high rates of material delivery to the surface, as is presently well acknowledged in the literature. To avoid this, it was recently proposed to use very low amounts of carbon atoms contained as impurities in Cu foils (and elsewhere in the growth reactor) as carbon source for the graphene growth.[195]

Another interesting example of synergistic interaction of Cu catalyst and plasmas is in the enabling water-based transfer of graphene microwell (GMW) structures.[194] The GMWs are hybrid structures made of interconnected layers of horizontal and vertical graphenes, as sketched in Figure 25a. A relatively short treatment of polycrystalline Cu foil with H_2/Ar plasmas at a very low temperature of 190 °C has led to significant modifications of the crystal expression on the Cu surface—such as the appearance of (101) and (111) domains in addition to the (100) domain, which was prevailing before the plasma treatment.

This plasma-induced modification of the catalyst not only enables the growth (because higher-index (101) and (111) facets are believed to favor graphene nucleation because of better lattice matching) but also changes the contrast in surface energies and consequently water contact angles of the bottom surface of the GMWs and the top surface of the catalyst. After the plasma treatment, the Cu foil is hydrophilic, while the graphene surface is hydrophobic (see Figure 25b). This allows intercalating water molecules to adhere to the Cu catalyst and repel the GMW, leading to the observed interesting effect of water-based GMW film separation.

DOI: 10.1021/acs.chemrev.5b00362
Chem. Rev. 2015, 115, 13408–13446

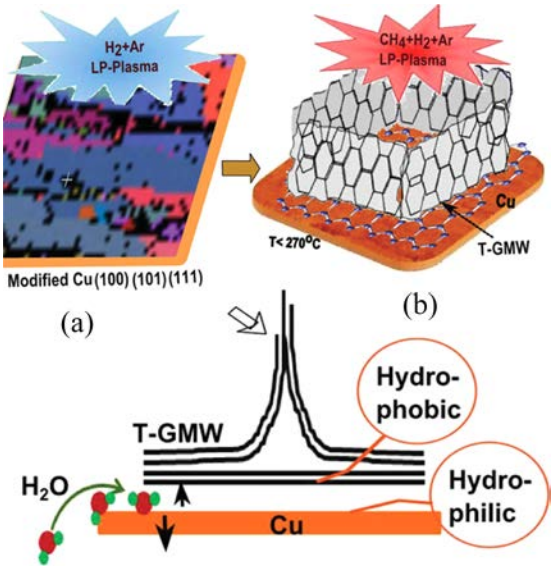

Figure 25. Growth process of graphene microwells in the plasma. Modification of facet expression on the catalyst surface enables not only the growth (a) but also water-based film transfer (b). Reproduced with permission from ref 194. Copyright 2014 John Wiley and Sons.

The discussed examples of synergistic interactions of the plasma and catalysts are representative and nonexhaustive. The interesting manifestations of their positive practical effects suggest that this area should definitely be explored further in both breadth and depth.

5.2. Catalytic Growth of Inorganic Nanowires

Metal nanocatalysts are used not only to grow CNTs but also for growth of other inorganic one-dimensional materials both at micrometer and nanoscales. In this case, the growth is typically enabled by the vapor−liquid−solid mechanism.[115] The synthesis is typically performed well above the eutectic temperatures to enable rapid mixing and diffusion through the molten catalyst. Various catalytic materials have been successfully used, including Au,[196−200] Ni,[201] Fe,[202] Cu,[203] Ag,[204] and Co.[205] The typical catalytic metals and synthesis temperatures for VLS growth of inorganic nanowires (NWs) are summarized in Table 1. The pressure may range from very low pressures up to atmospheric pressure.

As shown in Figure 26, Si nanowires are grown by allowing $SiCl_4$ and H_2 precursor gases to react on the gold

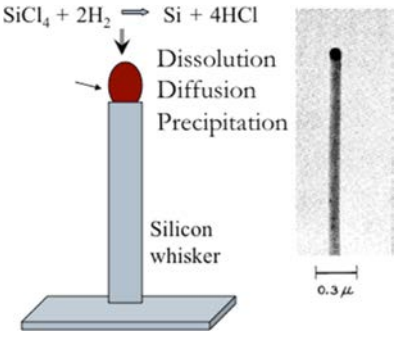

Figure 26. Schematic of silicon nanowire growth using catalyst metal clusters and vapor-phase source for precursors and transmission electron microscopy (TEM) image of silicon nanowire grown using gold clusters through the vapor−liquid−solid (VLS) mechanism. TEM image reprinted with permission from ref 115. Copyright 1964 AIP Publishing LLC.

nanoparticle, leading to selective dissolution of silicon into the molten gold nanoparticle. The alloying of silicon with gold leads to gold−silicon alloys whose melting point (eutectic temperature) is much less than those of both silicon and gold. The subsequent precipitation from the gold−silicon alloy leads to one-dimensional growth of silicon NWs. Typically, the synthesis temperature for crystalline silicon nanowires on Au tends to be in the range from 550 to 900 °C, well above its eutectic temperature.

The use of plasma activation of gas phase over traditional catalytic metal nanoparticles reduces the synthesis temperatures,[206−209] often to near the eutectic temperature. For example, this was demonstrated for Au catalyst,[210] where the synthesis temperature has been reduced to 380 °C by using PECVD. We emphasize that, similar to one-dimensional carbon nanotubes described in section 4.1, plasma-catalytic growth significantly increases the growth rates of inorganic nanowires.[211]

An interesting feature of the plasma-assisted processes is that the temperature of the metallic nanoparticle alloy during growth can be much higher than that of the substrate holder due to heating by radical recombination and ion impact dissociation reactions.[212] Such effects allow for growth at

Table 1. State-of-the-art Catalytic Metals and Synthesis Temperatures for VLS-Grown Inorganic Nanowires; T_E is the Eutectic Temperature, $T_{synth,trad}$ is the Temperature in Traditional Synthesis, and $T_{synth,plasma}$ is the Temperature in Plasma-Based Synthesis

material system	metallic catalyst	reactor class	T_E (°C)	$T_{synth,trad}$ (°C)	$T_{synth,plasma}$ (°C)
Si	Au	PECVD	363	550−1000[196,199]	380[210]
GaN	Au	DBD,[206,208] hot filament PECVD[207]	461.3,[a] 55% at. Ga	960[200]	900,[206,208] 850[207]
$In_xGa_{1-x}N$	Au	PECVD			700−750[216]
SiO_xN_y	Ni	RF-plasma	963,[b] Si−Ni eutectic		300[217]
GaN	Ni	plasma-assisted molecular beam epitaxy	895, Ni−Ga liquid phase	900[201]	730[209]
Si	Fe	arc plasma	1200[c]	1000[202]	
GaN	Co		∼910	800−1050[205]	
Si	Ag		836[204]	490−500[204]	

[a]Elliott, R. P.; Shunk, F. A. The Au−Ga (Gold−Gallium) System. *Bull. Alloy Phase Diagrams* **1981**, 2, 356−358. [b]Murray, J.; Massalski, T. In *Binary alloy phase diagrams*; American Society for Metals: Metals Park, OH, 1986; p 173. [c]Wang, Z. L.; Liu, Y.; Zhang, Z. In *Handbook of Nanophase and Nanostructured Materials: Synthesis/Characterization/Materials Systems and Applications I/Materials Systems and Applications II*; Springer: New York, 2003; Vol. 3.

DOI: 10.1021/acs.chemrev.5b00362
Chem. Rev. 2015, 115, 13408−13446

much lower substrate temperatures. In addition, plasma activation enables the growth of thinner nanowires than in thermal CVD (Figure 27).

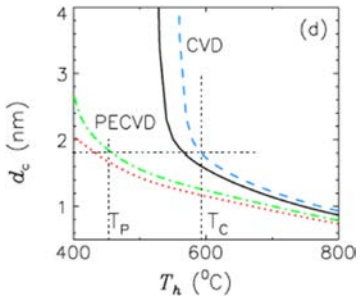

Figure 27. Critical diameter of catalyst nanoparticle as a function of the substrate holder temperature for CVD (solid and dashed curves) and PECVD (dotted and dash–dotted curves) for a pressure p = 50 mTorr and a gas composition $Ar/SiH_4/H_2$ = 70:20:10. Reproduced with permission from ref 212. Copyright 2011 IOP Publishing. All rights reserved.

Importantly, under plasma exposure the supersaturation can be higher at much lower temperatures owing to the Gibbs–Thomson effect discussed in section 2.2.2. This allows one to produce nanowires at temperatures below 600 °C and reduce their lowest possible thickness (size limit), in part due to the enhanced flux of vapor-phase species through the plasma sheath and more effective dissolution.[212] Figure 27 shows that the critical diameters of Si nanowires for thermal CVD are larger than those for PECVD. Similar observations have been made by other research groups.[210,213]

The key attributes for plasma activation of nanowire synthesis include effective dissociation of the precursor gas phase to produce radicals and local heating temperature via radical recombination, which makes the catalyst temperature higher than the average substrate temperature.[214] It has been proposed that electron–ion recombination and other surface chemical reactions may lead to considerable nanoparticle heating.[215] The combined use of gold nanocatalyst and plasmas for the growth of silicon nanowires results in the growth of 1D nanostructures at lower temperatures and higher growth rates than in conventional neutral gas-based processes.[210]

For the plasma-catalytic growth of GaN nanowires, nitrogen can be used as a precursor instead of ammonia, which is traditionally used in thermal catalysis. This is mainly due to the fact that the active nitrogen species created by the plasma allow the growth to happen.[208] Indeed, effective dissociation of nitrogen molecules requires energies that are much higher than typical energies of thermal activation; this becomes possible to achieve in plasmas through electron-impact reactions. The resulting GaN nanowires are single-crystalline and of high quality.

Furthermore, the combined use of Au NPs and plasmas has been shown to result in high-quality single-crystal InGaN nanowires.[216] Plasma activation of the gas phase has been shown to be critical for producing SiO_xN_y compound nanowires. In the absence of plasma, one can only synthesize a-SiO_xH NWs, regardless of the type of catalyst used.[217] The

Table 2. Summary Listing Nontraditional Catalysts and the Synthesis Temperatures Used for Nanowire Growth under Plasma Activation; No Nanowire Growth Is Observed without Using Plasma Activation

material system	metallic catalyst	metal vapor pressure range (bar), 100–800 °C	minimum synthesis temperature reported (°C)	eutectic temperature (°C)	eutectic solubility (at. %)	ref
Si	In	~1×10^{-28}–1×10^{-6}	240	156	1×10^{-8}	*a*
Si	In		500			*b*
Si	In		400			*c*
GaN	In		730			217
Si	Sn	~1×10^{-36}–1×10^{-9}	240	232	1×10^{-7}	*a*
Si	Sn		380			*d*
Si	Ga	~1×10^{-40}– $\times 10^{-8}$	400			219
Ge	Ga; In		300	30; 156.6	5×10^{-5}; 7×10^{-3}	219,220
Ga_2O_3	Ga		450		3×10^{-5} @230C	221
SiO_x	Ga		450			*e*
Si_xN_yH	Ga		450			*e*
Si_xGe_{1-x}	Ga		500			*f*
Si	Ga		220	30	5×10^{-8}	219,224
Si	Ga; Au-Ga		200			*g*
Si	Ga		500			*h*

[a]Yu, L.; O'Donnell, B.; Alet, P.-J.; Conesa-Boj, S.; Peiro, F.; Arbiol, J.; Roca i Cabarrocas, P. Plasma-Enhanced Low Temperature Growth of Silicon Nanowires and Hierarchical Structures by Using Tin and Indium Catalysts. *Nanotechnology* **2009**, *20*, 225604. [b]Zardo, I.; Conesa-Boj, S.; Estradé, S.; Yu, L.; Peiro, F ; Roca i Cabarrocas, P.; Morante, J.; Arbiol, J.; Fontcuberta i Morral, A. Growth Study of Indium-Catalyzed Silicon Nanowires by Plasma Enhanced Chemical Vapor Deposition. *Appl. Phys. A* **2010**, *100*, 287–296. [c]Xie, X.; Zeng, X.; Yang, P.; Wang, C.; Wang, Q. In Situ Formation of Indium Catalysts To Synthesize Crystalline Silicon Nanowires on Flexible Stainless Steel Substrates by PECVD. *J. Cryst. Growth* **2012**, *347*, 7–10. [d]Ball, J.; Bowen, L.; Mendis, B. G.; Reehal, H. Low Pressure Plasma Assisted Silicon Nanowire Growth from Self Organized Tin Catalyst Particles. *CrystEngComm* **2013**, *15*, 3808–3815. [e]Sunkara, Z. K.; Sharma, S.; Chandrasekaran, H.; Talbott, M.; Krogman, K.; Bhimarasetti, G. Bulk Synthesis of a-Si_xN_yH and a-Si_xO_y Straight and Coiled Nanowires. *J. Mater. Chem.* **2004**, *14*, 590–594. [f]Meduri, P.; Sumanasekera, G.U.; Chen, Z.; Sunkara, M. K. Composition controlled synthesis and Raman analysis of Ge-rich Si_xGe_{1-x} alloy nanowires. *J. Nanosci. and Nanotech.* **2008**, *8*, 3153–3157. [g]Carreon. M. Plasma-Catalysis Using Low-Melting Metals. Ph.D Dissertation, University of Louisville, December 2015. [h]Zardo, I.; Yu, L.; Conesa-Boj, S.; Estradé, S.; Alet, P. J.; Rössler, J.; Frimmer, M.; i Cabarrocas, P. R.; Peiro, F.; Arbiol, J. Gallium Assisted Plasma Enhanced Chemical Vapor Deposition Of Silicon Nanowires. *Nanotechnology* **2009**, *20*, 155602.I.

DOI: 10.1021/acs.chemrev.5b00362
Chem. Rev. 2015, 115, 13408–13446

radical species such as hydrogen and nitrogen are essential for the synthesis of a-SiO_xN_y nanowires. In this process, hydrogen radicals keep the catalyst in the reduced form (avoiding excessive oxidation) while the nitrogen radicals allow for nitrogen incorporation into the synthesized nanowires.

In the case of traditional catalyst metals, the use of plasma activation has been mainly to enhance the growth process in terms of growth kinetics, lowering the growth temperature, reducing the size limit, and using different precursors. The use of plasmas has been shown to be critical for growth of one-dimensional materials using nontraditional catalytic metals and systems. Specifically, metals such as Ga, In, and Sn work effectively as catalysts for the synthesis of silicon,[218,219] germanium,[220] and other compound nanowires[221] through the vapor−liquid−solid mechanism under the plasma activation. This is particularly important as many of these metals form eutectic alloys with Si and/or Ge at much lower temperatures than catalytic metals such as Au and Fe. Specifically, Ga forms the eutectic alloy with Si at ∼30 °C, and it has a very low solubility (∼1×10^{-8} at %) in Si at the eutectic temperature. A peculiarity of these metals is that they are noncatalytic by nature and do not facilitate the growth of 1D materials at any temperature and pressure. Importantly, several groups have observed (without specific mention) the synergistic effects between plasma and normally noncatalytic metals in inorganic nanowire growth. Table 2 summarizes various experiments involving both nontraditional catalysts and plasmas.

For the case of GaN nanowire growth with indium catalyst and plasmas, it has been observed that the much-enhanced Ga diffusion suppresses the formation of the undesired GaN 2D layer and dramatically reduces surface contamination.[222] Diffusion studies on the growth of GaN nanowires using Au catalyst and plasmas have shown an interesting interaction between Ga and hydrogen plasmas.[208] It has been observed that, when hydrogen is introduced in the chamber, Ga desorbs easily from the surface by reacting with hydrogen. While not acknowledged by the authors,[208] this interaction limits Ga precipitation on the surface (e.g., prevents the formation of the undesired 2D layers mentioned above), in a manner quite similar to hydrogen etching of amorphous carbon in the CNT/graphene growth examined in sections 4.1 and 5.1.

Of all low-melting-point metals, Ga has the lowest eutectic temperature with many materials, including Si, and also has the lowest vapor pressure. However, low-melting-point metals such as Ga, In, and Sn do not allow molecular adsorption for selective dissolution.[219] It has been shown that silicon nanowire growth using gallium can be realized in the presence of a high density of hydrogen radicals.[223] The selective dissolution of Si derived from the vapor-phase precursors through the plasma activation can be understood by considering the various possible surface reactions. The plasma-generated silyl and hydrogen radicals were found to effectively interact with molten metal nanoparticles of traditionally noncatalytic metals such as Ga.

Importantly, effective generation of atomic hydrogen in the plasma enables the synergistic interaction between the normally noncatalytic Ga nanoparticles and plasmas in the Si nanowire growth. Specifically, in the presence of plasmas, otherwise noncatalytic Ga behaves as a hydrogen sink, leading to the formation of Ga−H species that mediate the dissolution of the precursors,[224] as shown in Figure 28. It needs to be articulated that the mild plasma exposure leads to

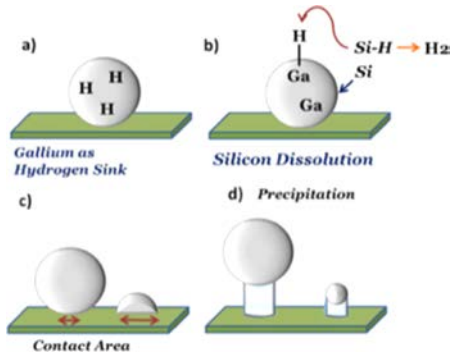

Figure 28. Synergistic interactions between plasma and Ga catalyst in the growth of silicon nanowires. Reproduced with permission from ref 224. Copyright IOP Publishing. All rights reserved.

the activation of the vapor−liquid−solid mechanism of inorganic nanowire growth and enables the otherwise ineffective catalytic effects in Ga nanoparticles. This is another clear example of synergistic effects in plasma nanocatalysis.

The synergistic effect of plasma activation can also be observed in nitrogen dissolution into low-melting metals. Molecular nitrogen is usually a nonreactive gas under mild temperature and pressure conditions in neutral gas processes. Typically, one requires a pressure of ∼20 atm and a temperature of ∼2000 K for dissolving nitrogen into Ga melts using molecular nitrogen according to reaction 4. Using plasma activation of nitrogen, the dissolution into Ga melts is favored at subatmospheric pressures and temperatures as low as 850 °C according to reaction 5.[225]

$$Ga(l) + 1/2N_2(g) \rightleftharpoons GaN(s) \quad (4)$$

$$Ga(l) + N(g) \rightleftharpoons GaN(s) \quad (5)$$

It was concluded that the recombination of N to form N_2 is sufficiently slow to allow the formation of GaN.[225] Such interactions have been exploited to grow GaN nanowires under self-catalyzed conditions using plasmas of nitrogen or nitrogen and hydrogen mixtures.

As discussed above, the hydrogen radicals resulting from the plasma can interact with and dissolve into molten metals. Similarly, plasma activation of the gas phase enables dissolution of both oxygen and nitrogen radicals into molten metals. In this case, the direct exposure of molten metals to the plasma-excited gas can result in oxide, nitride, and oxynitride nanowires. The role of plasma activation here is to enable rapid dissolution of solutes such as oxygen and nitrogen and keeping the surface of molten metals clean. This concept has been successfully exploited for synthesizing oxide nanowires of zinc, gallium, indium, aluminum, and nitrides of gallium, indium, etc.[226]

In addition to oxidation or nitridation of low-melting metals, it is also possible to use plasmas for producing oxide nanowires from surfaces of high-melting-temperature metals.[227] This method is based on exposing a thin metal foil to reactive oxygen plasmas.[228−230] In this case, plasma−surface interaction is the critical step that enables the nanowire growth without any external (e.g., through gas feed) supply of precursor material. The role of plasmas in this synthesis is to generate oxygen atoms in the gas phase mostly through electron impact, and to provide localized surface heating

DOI: 10.1021/acs.chemrev.5b00362
Chem. Rev. 2015, 115, 13408−13446

through recombination of the dissociated oxygen atoms, as well as ion bombardment and neutralization.

Another method involving plasma oxidation of metals or metal oxides in the presence of alkali salts results in nanowires even after a very short exposure of <1 min.[231] A schematic of plasma oxidation of metals in the presence of alkali salts for nanowire growth is shown in Figure 29. The resulting alloys

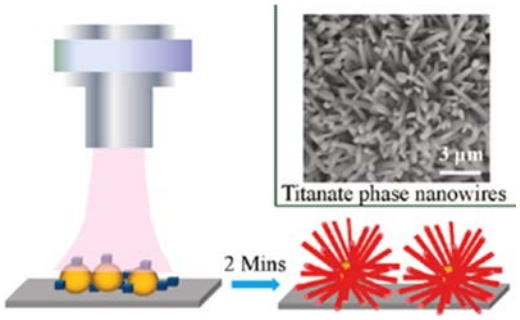

Figure 29. Rapid plasma oxidation of metals in the presence of alkali salts for producing nanowires. Reprinted with permission from ref 231. Copyright 2011 American Chemical Society.

melt at lower temperatures and enable nucleation and growth of high-density nanowires. This technique is similar to hydrothermal growth except that the use of plasmas reduces the time scales from several days to several minutes or even shorter. An overview of the time scales involved is shown in Figure 30, indicating that plasma-based techniques feature short reaction times, making them potentially amenable for high-yield, industrial-scale production.[232]

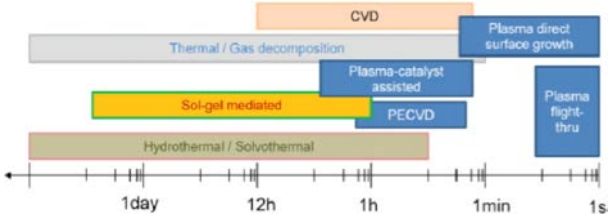

Figure 30. Time scales for the plasma-based techniques for scalable production of inorganic nanowires. Reproduced with permission from ref 232. Copyright IOP Publishing. All rights reserved.

5.3. Abatement of Toxic Waste and Air Pollution Control

The synergy of plasma and catalyst in toxic waste abatement is clearly demonstrated in Figure 31. This figure shows the destruction efficiency of 500 ppm toluene in air, by means of plasma, thermal catalysis (using a Ag/Al_2O_3 catalyst), and the sum of both individual processes, as well as plasma catalysis.[233,234] The sum of the two separate processes is only 20%, whereas the plasma-catalytic destruction efficiency is 65%, hence indicating a synergistic gain of more than a factor of 3.

Many other papers have shown such a synergy for plasma catalysis in air pollution control, and several review papers overview the type of catalysts used, the pollutant treated, the discharge conditions used, etc.[80,83,85,235,236] Given the nature of the problem, the pressure in these experiments is invariably atmospheric pressure. The most widely used catalyst supports are TiO_2 and γ-Al_2O_3. Moreover, a variety of other metal oxides (e.g., MnOx, V_2O_5, Fe_2O_3,CuO, WO_3, ...) as well as

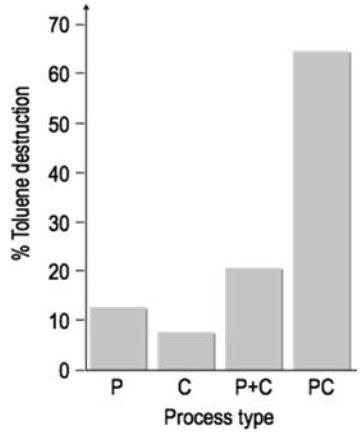

Figure 31. Destruction efficiency of 500 ppm toluene in air at 25 °C, by means of DBD plasma (P), thermal catalysis with Ag/Al_2O_3 catalyst (C), and the sum of both individual processes (P+C), as well as plasma catalysis (PC), illustrating the synergistic effect of the plasma catalysis. Data adopted from ref 233.

metals (e.g., Ag, Ni, Pt, Cu, ...) have been loaded as active elements on these supports.[83,236] It is difficult or impossible to draw a definite conclusion on the most suitable catalyst, based on all the studies available in literature. Likewise, the underlying reasons for the synergistic effects are not yet completely understood. Several review papers try to explain the performance enhancement of plasma catalysis, based on the effects of the plasma on the catalyst, and vice versa, summarizing the many studies presented in literature.[80,83,85,236] Similar explanations, but more from a fundamental perspective, were also given in sections 3 and 4.

For photocatalysts, like TiO_2, some papers state that UV light from the plasma can create electron−hole pairs.[81,237] Sano et al. demonstrated that, while UV light was produced in the absence of TiO_2, no emission was detected when TiO_2 was present, suggesting that the UV light is effectively absorbed by the catalyst.[81] On the other hand, several other papers claim that the intensity of UV light from the plasma is not high enough.[80,238,239] Indeed, the UV dose in typical photocatalytic processes should be in the order of several mW/cm^2, whereas in typical (air) plasmas it is only in the order of $\mu W/cm^2$.[80] However, it is very possible that photocatalysts are activated by other (energetic) plasma species, like ions, metastables, or electrons with suitable energy. Indeed, TiO_2 photocatalysts have a typical bandgap of 3.2 eV; hence, electrons in the plasma with energies of ∼3−4 eV should be able to excite electrons to the conduction band and to create electron−hole pairs in a similar way as produced by UV light.[239] The same mechanism was also recently suggested for $BaTiO_3$ photocatalysts.[168] Similarly, Van Durme et al. explained the activation of a TiO_2 catalyst surface by the adsorption of metastable N_2, having an energy of 6.17 eV.[83] Hence, we may conclude that the plasma might directly affect carrier generation in (photo)catalysts, and this might explain the synergy in plasma catalysis when using photocatalysts.

Finally, as mentioned in section 4.2.3, it is important to make a distinction between the physical and chemical effects in plasma catalysis. The physical effects even can be due to nonreactive materials packed in the plasma reactor to support the catalyst. For example, it has been demonstrated that a packed-bed DBD, even with noncatalytic dielectric beads, can increase the energy efficiency up to a factor of 12, depending

DOI: 10.1021/acs.chemrev.5b00362
Chem. Rev. 2015, 115, 13408−13446

on the type of pollutant being treated, the reactor geometry, and the packing pellets, compared to a nonpacked DBD reactor.[235] Moreover, the shape of nanosized particles can enhance the plasma catalysis (see sections 2.2.2 and 3.3). Kim and co-workers have demonstrated the physical role of nm-sized metal particles (Ag, Zr, Cu) for discharge generation over the surface of zeolites.[240] The plasma expansion occurred over a wide surface area, whereas with bare zeolites the plasma generation was limited to the edges of the zeolites. This enhanced plasma expansion was correlated to a better VOC decomposition.[240]

5.4. Hydrocarbon Reforming

Hydrocarbon reforming has been receiving immense attention globally because it is poised to become a major source of hydrogen, a product that has the potential of emission-free alternative fuel. Currently, almost 90% of the H_2 is produced via high-temperature steam reforming of natural gas or the light oil fraction.[241] Although not widely used today as a transportation fuel, researchers are working toward the goal of clean, economical, and safe hydrogen production and fuel-cell electric vehicles.

Even though catalytic hydrocarbon reforming has about seven decades of history, there are still some inherent challenges such as moderate thermodynamic efficiency; fouling/coking on catalyst surface and eventual deactivation; poisoning of a certain catalyst as a result of sulfur impurities in hydrocarbon feedstock; and high temperature requirements of the reforming reaction (a condition that reduces the energy efficiency of the process). The reaction pathways in the reforming process generally depend on the oxidant used. For the wet reforming process, steam oxidizes CH_4 to CO (eq 6). Equation 7 is the water gas shift (WGS) reaction, oxidizing CO further to CO_2. The overall reaction is represented by eq 8. Clearly, the energy requirement (endothermic, 165 kJ/mol) of the overall process is high, which makes the wet reforming a less favorable route.

$$CH_4 + H_2O \rightleftharpoons CO + 3H_2,\ \Delta H_{298} = 206\ \text{kJ·mol}^{-1} \quad (6)$$

$$CO + H_2O \rightleftharpoons CO_2 + H_2,\ \Delta H_{298} = -41\ \text{kJ·mol}^{-1} \quad (7)$$

$$CH_4 + 2H_2O \rightleftharpoons CO_2 + 4H_2,\ \Delta H_{298} = 165\ \text{kJ·mol}^{-1} \quad (8)$$

Plasma reforming has a number of advantages over traditional reforming,[242] viz. (1) compactness, (2) high conversion efficiency, (3) reasonable cost, (4) short residence time, and (5) suitability for a broad range of hydrocarbons, including heavy oil, raw biofuel, and other difficult-to-use fuels. Most often, a DBD reactor at atmospheric pressure is used, as was the case in plasma-catalytic DRM (see section 4.2.3). Plasma reforming of methane is an energy-efficient process with significant potential for industrial applications. Bromberg et al. reported a hydrogen yield of 100% corresponding to a methane conversion of 80%.[242] This result was achieved through heat regeneration and efficient use of heat exchangers and further optimization.

The effect of initial water content on steam reforming of aliphatic hydrocarbons with nonthermal plasma was analyzed in terms of hydrocarbon conversion, carbon recovery, and product selectivity.[243] It was found that water addition increased the CO_2 yield, despite a decrease in hydrocarbon conversion. The number of carbon atoms in the hydrocarbon affected the effect of water addition due to the insufficient supply of oxygen atoms from water.

Futamura et al. used a ferroelectric packed-bed reactor as a standard reactor in the plasma reforming of methane, propane, and neopentane with both H_2O and CO_2.[244] Methane and propane were found to be more suitable for reforming. Achieving a constant composition of syngas by controlling the ratio of initial concentrations of hydrocarbon and oxidant is possible. We stress that in this case the plasma-catalytic effect is predominantly physical because no clear chemical pathways have been activated through the plasma exposure.

Nozaki et al. clearly demonstrated a synergistic effect for plasma-catalytic CH_4 steam reforming with a Ni/SiO_2 catalyst, as shown in Figure 32.[245] The conversion in the DBD plasma without catalyst (blue solid line) was ~22% independent of temperature, but above 400 °C, solid carbon (or soot) was gradually accumulated and a stable plasma could not be maintained. The catalytic conversion without plasma (green line) was negligible at temperatures below 400 °C but increased at higher temperatures, especially above 600 °C. Finally, the conversion in the plasma-catalysis setup (red line) was already near 25% at 200 °C and increased to almost 90% at 700 °C.

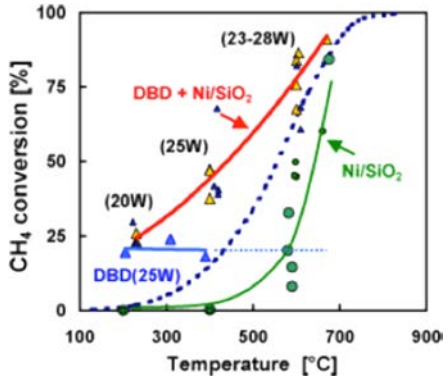

Figure 32. CH_4 conversion in a DBD (blue solid line), Ni/SiO_2 catalyst (green line), and combined DBD with Ni/SiO_2 catalyst (red line); the blue dashed line indicates the equilibrium conversion at the given temperature. Reprinted with permission from ref 245. Copyright 2004 Elsevier.

Note that the plasma-catalytic CH_4 conversion largely exceeds the equilibrium conversion (indicated by the blue dashed line). The most pronounced synergistic effects between plasma and Ni/SiO_2 catalyst take place between 400 and 600 °C. Furthermore, the CH_4 conversion curve shifts to a lower temperature by ~200 °C in the plasma-catalytic setup compared to the thermal-catalysis case (cf. red and green curves). Hence, the plasma significantly reduces the activation temperature of the catalyst, which is beneficial in terms of energy efficiency. Indeed, the energy efficiency claimed in this process was 69%.[245]

This synergy may be attributed to the presence of vibrationally excited CH_4 molecules (see section 3.4), produced in the plasma.[73,95] In plasmas without catalyst, these vibrationally excited CH_4 molecules are ineffective in hydrocarbon reforming, because of their short lifetimes (order of ns) and low threshold energy (below 2 eV, whereas the bonding energy for most hydrocarbons is between 3 and 6 eV). Hence, the energy residing in the vibrationally excited

DOI: 10.1021/acs.chemrev.5b00362
Chem. Rev. 2015, 115, 13408−13446

Table 3. Performance of Selected Plasma and Plasma + Catalyst Reforming Processes

hydrocarbon	reforming type	reactor	H_2 yield (%)	T (°C)	plasma power (kW)	ref
CH_4	steam	plasma only	44	20	0.025	244
$CH_3C(CH_3)_2CH_3$	CO_2	plasma only	17	20	0.025	244
CH_4	O_2	plasma only	32	400	0.033	248
iso-octane	O_2	plasma only	0	400	0.008	*a*
C_2H_5OH	steam	plasma only	63.9	350	0.009	*b*
CH_4 (biogas)	CO_2	plasma/catalyst (NiO/Al_2O_3)	59	700	2.4	*c*
C_2H_5OH	steam	plasma/catalyst (Pt/TiO_2)	73.5	300	0.009	*b*
CH_4	O_2	plasma/catalyst	89.9	750	0.0324	250
CH_4	O_2	plasma/catalyst (NiO/α-Al_2O_3)	72	400	0.033	248
CH_4	CO_2	plasma/catalyst (Ni/γ-Al_2O_3)	9.6	230	0.06	100
iso-octane	O_2	plasma/catalyst	9	800	0.0038	*a*

[a]Sobacchi, M. G.; Saveliev, A. V.; Fridman, A. A.; Kennedy, L. A.; Ahmed, S.; Krause, T. Experimental Assessment of a Combined Plasma/Catalytic System for Hydrogen Production via Partial Oxidation of Hydrocarbon Fuels. *Int. J. Hydrogen Energy* **2002**, *27*, 635−642. [b]Zhu, X.; Hoang, T.; Lobban, L. L.; Mallinson, R. G. Low CO Content Hydrogen Production from Bio-Ethanol Using a Combined Plasma Reforming−Catalytic Water Gas Shift Reactor. *Appl. Catal., B* **2010**, *94*, 311−317. [c]Chun, Y.N.; Yang, Y. C.; Yoshikawa, K. Hydrogen Generation From Biogas Reforming Using A Gliding Arc Plasma-Catalyst Reformer. *Catal. Today* **2009**, *148*, 283−289.

states is not efficiently used in this case; it was claimed that 40% of the plasma power is wasted in this way.[73,95]

Although the vibrationally excited CH_4 molecules are not reactive in the plasma, they appear to be much more reactive at a Ni surface than ground-state CH_4 molecules.[246] For instance, eigenstate-resolved measurements demonstrated that the antisymmetric ν_3 C−H stretch vibration yields a CH_4 reactivity on a clean Ni(100) surface 1600 times higher compared to the molecule in the ground vibrational state.[36,37] Indeed, in the case of plasma catalysis, vibrational excitation improves dissociative chemisorption of CH_4 molecules on a catalyst surface at low temperatures (see Figure 8),[82] leading to a significant process enhancement. In other words, the CH_4 conversion largely exceeds the equilibrium conversion at the given temperature. Note, however, that the subsequent chemical reactions occur at the catalyst surface, independent of the plasma; hence, the product selectivity does follow chemical equilibrium.[73] Finally, physical effects of the plasma, i.e., streamer impact, are claimed to be beneficial, as they may heat the catalyst bed.[73]

A similar synergy also holds for CH_4 steam reforming with commercial 12 wt % Ni/γ-Al_2O_3 catalyst in a packed-bed DBD.[95,247] Besides the vibrationally excited CH_4 molecules (see above), the heat produced by the DBD plasma enhances the catalytic conversion of CH_4. Furthermore, kinetic analysis revealed that the rate-determining step of the process is the dissociative adsorption of methane (see section 2.1.1). Arrhenius plots for the catalytic reaction with and without DBD suggest that the activation energy is very similar in both cases. The pre-exponential factor, however, indicative for the collision frequency (or number of active sites available), was 50 times higher (in the reaction-limited regime) in the case of the plasma-catalytic conversion. Indeed, to maximize the CH_4 conversion in steam reforming, dehydrogenation of CH_4 and chemisorption of H_2O molecules should be promoted simultaneously. In this way, one can oxidize C intermediates and thus prevent blocking of the catalytically active sites. Hence, the excited H_2O molecules play a vital role, as they increase the concentration of chemisorbed O and OH radicals. These radicals are needed for oxidation (and desorption) of the chemisorbed C intermediates, thereby leaving sufficient active sites available for CH_4 dehydrogenation.[95,247]

Some other examples suggest synergistic enhancement of hydrocarbon reforming by a factor 1.1−2.4 through plasma catalysis.[82] This enhancement is likely to be related to vibrational excitation of CH_4 molecules in the case of plasma-catalytic hydrocarbon reforming. Indeed, pure plasma-based hydrocarbon reforming, without catalysis, is energy-intensive, as the conversion needs to proceed through dissociation and ionization of the molecules. As discussed earlier, vibrationally excited molecules have a low energy and short lifetime to play any significant role in the gas-phase conversion. The minimum threshold for dissociation and ionization of CH_4 is ∼9 eV. Therefore, the energy cost for plasma-based (steam) CH_4 reforming is ∼10−100 eV.[82] This is much higher than what is needed for thermal catalysis, i.e., the energy needed to increase the CH_4 gas temperature from 25 °C to the typical working temperature of 700−900 °C is ∼0.38−0.53 eV.

However, in plasma catalysis the energy can be channeled into vibrationally excited molecules, thereby enhancing their reactivity and the overall catalytic effects. While it was concluded that hydrocarbon reforming in plasma is predominantly thermal catalysis, the plasma assists in providing the internal energy of the reactants (i.e., so-called "plasma-assisted catalysis" instead of "catalysis-assisted plasma conversion").[82] It should be realized, however, that the efficiency of vibrational excitation in enhancing the dissociation is not independent of the catalyst, and this division is probably not a correct assumption.

The extent of vibrational excitation also varies among the gas discharges. As was mentioned in section 4.2.2, DBD plasmas produce only limited vibrational excitation. Note that in warm (i.e., microwave or gliding arc) plasmas vibrational excitation is more prominent, but the combination with catalysis is still rather unexplored. However, vibrational excitation in DBDs can be promoted by using alternating high-voltage and dc pulses.[82] Furthermore, as the lifetime of the vibrationally excited molecules is only in the order of ns, these excited molecules must be delivered to the surface as quickly as possible. An improved design of the plasma-catalytic DBD reactor based on perforated electrodes coated with catalysts improves the interaction of the gas flow with the catalyst by both increasing the surface contact areas and aligning the catalyst surface perpendicular to the direction of the gas flow.[82]

DOI: 10.1021/acs.chemrev.5b00362
Chem. Rev. 2015, 115, 13408−13446

Another example was presented by Pietruszka and Heintze,[248] where the DBD reactor was employed for the steam reforming of methane at temperatures below 400 °C. When the discharge was used solely, only methane and oxygen were converted. However, by combining the DBD and a Ni catalyst, the conversion of methane was not improved but complete oxygen conversion was achieved. At a sufficient temperature to maintain the Ni catalytically active, the product selectivity changed significantly. The effect of the steam led to enhanced hydrogen yield, provided that oxygen was fully converted. A selectivity for H_2 production of ~70% over NiO/Al_2O_3 was achieved. It was found that plasma only activates the reagents and thus accelerates the adsorption−desorption processes, whereas the oxidation state of the catalyst is responsible for the surface reactions. The performance of more combined plasma/catalyst reforming systems is summarized in Table 3.

Partial oxidation of methane

$$CH_4 + 0.5O_2 \rightleftharpoons CO_2 + 2H_2,\ \Delta H_{298} = -35.7\ \text{kJ·mol}^{-1} \quad (9)$$

is suggested as a suitable alternative to alleviate the energy cost.[249] Chao et al. reported hydrogen production through partial oxidation of methane by combining the arc plasma with catalysts.[250] Because the partial oxidation reaction is highly exothermic, no additional energy was needed to maintain the temperature of the catalyst bed. Therefore, the energy of the exothermic reforming combined with the energy from the hot thermal plasma is sufficient to sustain the process, leading to a remarkable energy efficiency of 1.21 MJ/kg of hydrogen, a hydrogen yield of 89.9%, and a methane conversion in excess of 90%.

Rico et al. presented convincing results on the performance enhancement due to the plasma, in plasma-catalytic methanol reforming.[251] The authors used a $BaTiO_3$ ferroelectric packing and a Cu/Mn oxide catalyst (mainly consisting of $Cu_{1.5}Mn_{1.5}O_4$ spinel structure with cubic symmetry and a minority phase of Mn_2O_3), which was mixed with the $BaTiO_3$ packing for a uniform distribution. The temperature was kept between 115 and 180 °C to avoid condensation of methanol (or H_2O, in the case of steam reforming). An ac voltage of 800 V was applied, yielding a power of 4−12 W in the packed-bed DBD. Note that, without packing, an applied voltage of 3 kV was needed, yielding 60 W power, demonstrating again that a packing can reduce the voltage to sustain the plasma and, hence, yield better energy efficiency. As illustrated in Figure 33, no methanol conversion was detected in the case of the $BaTiO_3$ packing without plasma. Likewise, the $BaTiO_3$ packing with Cu/Mn oxide catalyst, but without plasma, yielded a conversion of only 2%. The formed products were formic acid, formaldehyde, and water.[251]

However, after plasma addition, the methanol conversion increased drastically. A maximum conversion of 92% was obtained in the case of the $BaTiO_3$ packing with plasma, producing only syngas (CO + H_2). This clearly indicates that the methanol conversion at a temperature of 115 °C is purely plasma-induced. The intended application of this process is H_2 production for fuel cell applications.

As the CO can poison the Pt electrode, it should be avoided, and this could be realized by adding the Cu/Mn oxide catalyst for the selective oxidation of CO into CO_2. In the combined plasma-catalysis system with $BaTiO_3$ packing,

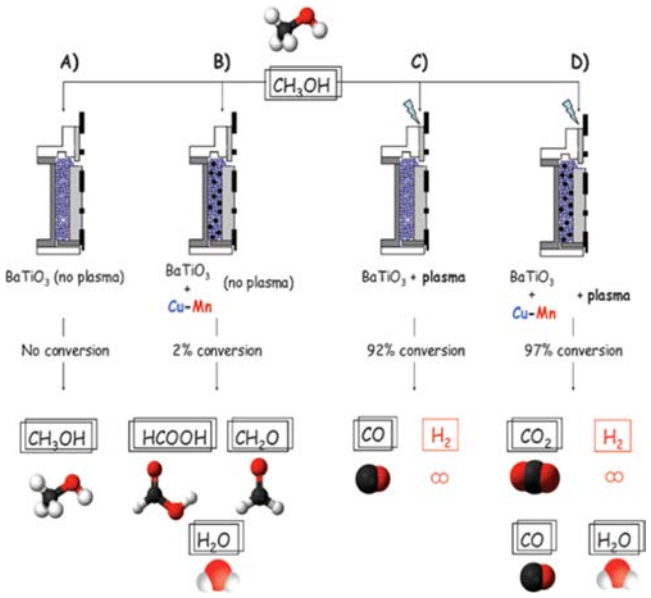

Figure 33. Schematic of the methanol conversion by $BaTiO_3$ packing without plasma (A), $BaTiO_3$ + Cu/Mn oxide without plasma (B), $BaTiO_3$ packing with plasma (C), and $BaTiO_3$ + Cu/Mn oxide with plasma (D). The obtained conversions and products formed are also illustrated. Adopted with permission from ref 251. Copyright 2009 The Royal Society of Chemistry.

Cu/Mn oxide catalyst, and DBD plasma, a maximum conversion of 97% could be reached, producing CO, H_2, CO_2, and H_2O (see Figure 33). The CO selectivity was reduced to 36%, while a H_2 selectivity as high as 80% was achieved. At higher flow rates, the conversion decreases while the selectivity remains unchanged.[251]

5.5. Ammonia Production

The current industrial ammonia synthesis uses the thermal Haber-Bosh technology developed over 100 years ago.[252] This process (eq 10) takes place at temperatures around 500 °C and pressures of 300 bar. Nitrogen is drawn from the atmosphere by using cryogenic air separation while hydrogen is mostly sourced from natural gas.

$$3H_2 + N_2 \rightleftharpoons 2NH_3,\ \Delta H_{298} = -92.22\ \text{kJ·mol}^{-1},\ \Delta S_{298} = -198.76\ \text{J·K}^{-1}\text{·mol}^{-1} \quad (10)$$

Since the reaction is exothermic, eq 10 shows that, due to the entropy change, the reaction will only proceed spontaneously at sufficiently low temperatures. However, the nitrogen dissociative adsorption presents a high activation barrier (dissociation energy of 911 kJ/mol of the triple nitrogen bond). On the other hand, the rates of ammonia synthesis increase with increasing temperature until a maximum is reached. A further temperature increase results in the ammonia decomposition, lowering the equilibrium concentration of ammonia.[253] Hence, the process temperature and pressure can be balanced to maximize the ammonia yield. In a practical process, multiple reduced Fe_3O_4 catalyst beds are placed in series, leading to an energy consumption of 9500 kWh per ton of NH_3 if H_2 is generated from steam reforming of methane.

At the molecular level, the ammonia synthesis follows a Langmuir−Hinshelwood mechanism (briefly discussed in section 3.2.3), where the reactants undergo a dissociative

DOI: 10.1021/acs.chemrev.5b00362
Chem. Rev. 2015, 115, 13408−13446

adsorption on the catalyst surface before any reaction between them. The various elemental reactions and the corresponding energy diagram are presented in Figure 34.[254]

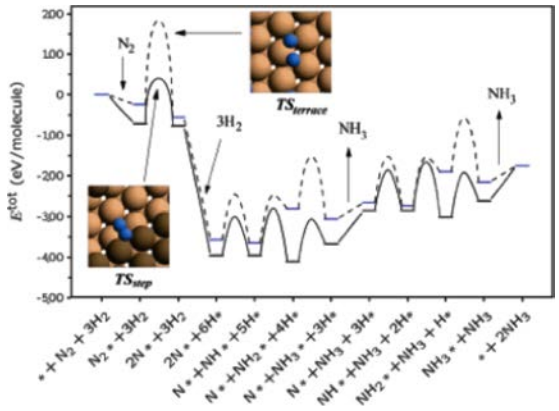

Figure 34. Reaction steps of the catalytic ammonia synthesis and calculated reaction pathways for ammonia synthesis over flat (dashed line) and stepped (solid line) Ru surfaces. Empty catalyst surface sites are represented as *, and X* is the X species adsorbed. Reprinted with permission from ref 254. Copyright 2006 American Chemical Society.

Plasma-catalytic methods are pursued as promising techniques for ammonia synthesis because they provide active nitrogen species at relatively low temperatures. A summary of recent results is given in Table 4. Note that, in contrast to the high pressures used in traditional thermal ammonia production, plasma-catalytic studies have employed pressures in the range from 20 Pa to 1 atm.

The active nitrogen species may interact on the catalyst surface, overcoming the energy barrier associated with nitrogen dissociative adsorption.[255,256] Nonequilibrium plasma is capable of generating NH radicals from a N_2−H_2 mixture in order to obtain ammonia. Besides, the metals placed in the plasma region enhance the ammonia yield, clearly indicating a synergistic effect of the plasma and the catalyst.[256]

Mindong et al. reported the use of a microgap dielectric discharge operating at ambient pressure for ammonia synthesis.[257] The maximum yield of ammonia reported reached 12 500 ppm (1.25%). A later study showed that the ammonia production can be maximized by optimizing the composition of gas mixtures and sequential inlet of specific gases into the reactor chamber directly into the reaction zone of discharge afterglow.[258]

Species formation in an electron cyclotron resonance (ECR) plasma and at a catalyst surface was also investigated.[259] The nature of the catalytic surface affected the production and surface adsorption of the plasma-activated species of diatomic nitrogen, ionized diatomic nitrogen, and NH_x. Once the species are adsorbed on the catalyst, hydrogen reacts with them to form NH_x, which leads to ammonia desorption.[259] Uyama et al. have demonstrated a synergistic enhancement in ammonia synthesis when Fe wires are used as catalyst in the presence of plasma. Ammonia production with plasma catalysis is doubled over a period of 3 h under 5 Torr of pressure and 620 ± 50 K. The plasma catalysis results in 2 orders of magnitude higher yields than the process without the discharge.[260]

When the plasma is rich in radicals, especially NH (e.g., under microwave excitation), NH_3 is predominantly formed. This can be explained by noting that mostly nitrogen atom and/or metal−nitrogen bonds are formed on the catalyst surface. When ionic species are abundant (e.g., by RF excitation), both ammonia and hydrazine are formed. This can be explained by the fact that in this case hydrogenated nitrogen species are detected more abundantly on the catalyst surface than nitrogen atoms and/or metal−nitrogen bonds.[261]

Van Helden et al. demonstrated a strong correlation between ammonia formation and the fluxes of atomic N and H radicals to the surface.[262] Moreover, catalyst played little effect under strong radical flux conditions, which further supports the importance of radical generation in the gas phase of the plasma.

Using a membrane-like catalyst reactor, Mizushima et al. studied the effects of input voltage, hydrogen-to-nitrogen molar ratio, plasma composition, and metal loading on an alumina support.[263] The latter consisted of Ru, Pt, Ni, and Fe, and among these tested metals, Ru showed the highest activity in the plasma-catalytic synthesis of ammonia. Figure 35 illustrates the synergistic effects of plasma catalysis reported by Mizushima et al.[263]

From their findings, they suggest that the nitrogen is adsorbed onto the alumina surface by dissociative adsorption or diatomic plasma excited diatomic molecules attaching to the alumina surface. Meanwhile, plasma-generated H atoms and diatomic excited hydrogen can react directly with nitrogen atoms that are adsorbed on an alumina surface or

Table 4. Reports on Plasma-Activated Catalysis for Ammonia Synthesis; RT Stands for Room Temperature

reactor	T (K)	P	N_2/H_2	production	ref
microwave discharge/Fe wires − Mo wires	620 K	650 Pa			*a*
ECR plasma/steel	RT	600 Pa	1:3		259
RF discharge/Fe wires	620 K	5 Torr	1:4		260
RF discharge − microwave discharge/Fe wires − Mo wires	620 K	5 Torr	1:4		261
expanding thermal plasma/stainless steel−SiN_x		20 Pa		11% of outlet	262
thermal plasma/stainless steel	600 K	20 Pa		2% of outlet	*b*
electric field discharge/MgO	ambient	10^5 Pa	1:4	5000 ppm	*c*
DBD/alumina (Ru)	RT	1 atm	1:3	1.6×10^{-5} mol·min^{-1} (2.4% conversion)	256
DBD/alumina (Ru, Pt, Ni, Fe)	ambient	ambient	1:3	3×10^{-5} mol·min^{-1}	263

[a]Matsumoto, O. Plasma Catalytic Reaction in Ammonia Synthesis in the Microwave Discharge. *J. Phys. IV France* **1998**, *08*, Pr7−411 and Pr417−420. [b]Vankan, P.; Rutten, T.; Mazouffre, S.; Schram, D. C.; Engeln, R. Absolute Density Measurements of Ammonia Produced via Plasma-Activated Catalysis. *Appl. Phys. Lett.* **2002**, *81*, 418. [c]Mingdong, B.; Xiyao, B.; Zhitao, Z.; Mindi, B. Synthesis of Ammonia in a Strong Electric Field Discharge at Ambient Pressure. *Plasma Chem. Plasma Process.* **2000**, *20*, 511−520.

DOI: 10.1021/acs.chemrev.5b00362
Chem. Rev. 2015, 115, 13408−13446

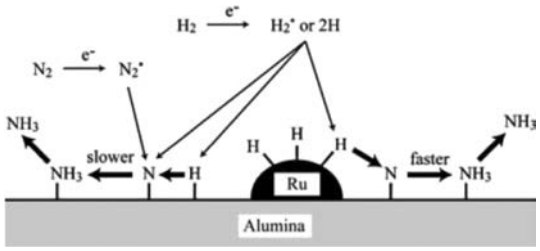

Figure 35. NH_3 formation pathway on Ru-membrane alumina in N_2/H_2 plasma. Reproduced with permission from ref 263. Copyright 2007 Springer Science and Business Media.

go through an absorption step first and then react. As for the role of Ru atoms, Mizushima et al. propose that hydrogen is absorbed on these active sites and the Ru−H species react relatively faster with adsorbed nitrogen on alumina, and therefore, a higher ammonia yield is obtained, again demonstrating the plasma-catalytic effect.[263]

6. CONCLUSIONS AND OUTLOOK

The recent advances in the areas discussed in this review suggest that plasma catalysis is a rapidly developing research field, which promises not only many exciting scientific discoveries but also the development of new technologies and industrial applications. Chemical catalysis that relies on catalytic effects of nanoparticles and other nanomaterials has many established applications, ranging from natural gas reforming into syngas, the growth of inorganic nanowires and nanotubes, and ammonia production, to name but a few.

As many examples in this review suggest, the interaction between catalysts and low-temperature nonequilibrium plasma may lead to synergistic effects. These effects may improve the process outcomes, for example, in the conversion and energy efficiency and selectivity of the process, and may potentially lead to outcomes that are normally not achievable using traditional catalytic or plasma-only approaches separately.

The outcomes may improve existing catalytic processes of technological importance and are subject to further exploration, and may potentially lead to novel catalytic processes that capitalize on the unique outcomes of the synergistic plasma-catalyst effects. In spite of the demonstrated advantages, however, plasma catalysis also faces several challenges, both scientific and technological, on the way to widespread practical adaptation of these unconventional catalytic approaches. On the other hand, these challenges create exciting opportunities to further improve our scientific understanding of the fundamental phenomena involved and eventually translate the new knowledge into viable processes and products.

Below we briefly discuss the arising challenges and opportunities for the plasma-catalysis field in the coming years. Without trying to be exhaustive, we will follow the selected areas of this review where the synergistic effects of the plasma and catalytic materials are particularly clear. These areas include (i) plasma-assisted catalytic reforming of natural gas into syngas; (ii) plasma-based large-area graphene synthesis; and (iii) large-scale production of multipurpose inorganic nanowires.

In any area of applications, including the ones mentioned above, using plasmas necessarily implies additional costs due to specialized equipment and energy needed to generate and maintain the plasma. This creates a perception that plasma-based applications are energy-intense and costly, especially upon industry-scale operation.

However, the overwhelming success of the multibillion-dollar semiconductor industry, where capital-intense, low-pressure plasma nanofabrication facilities are used, suggests that the benefits of the creation of value-added products that otherwise are difficult or even impossible to achieve may outweigh the need for the major capital investments in equipment and infrastructure and the associated energy costs.

Let us discuss this issue for the selected focused examples of plasma-assisted catalysis. Generally speaking, these examples show value-added outcomes by using similar or simpler equipment and processes than those in the semiconductor industry. Moreover, additional energy costs associated with the plasma generation may be offset by the benefits offered by the synergistic plasma-catalytic processes. These benefits are expected to be retained at large-scale operation, which, however, introduces specific challenges.

Specifically, in the first example related to plasma-assisted catalytic reforming of natural gas, possible important benefits include operation at reduced temperature, selectivity toward the formation of value-added products, and an extremely fast switch-on time. Operation at reduced temperature leads to reduced coke formation and catalyst poisoning and, therefore, to increased catalyst lifetime. This is a critical parameter in any industrial setting, in part offsetting the capital costs.

Although much research is still needed, plasma-catalytic reforming of natural gas may allow the selective production of syngas, but possibly also other value-added products such as methanol or formaldehyde. This is due to the very nature of the plasma, which in part decomposes and activates the precursor gases, while the catalyst allows for the selective formation of desired products.

The fast plasma switch-on time finally may allow to (partially) cover the imbalance between supply and demand of energy and, hence, the use of intermittent excess energy, e.g., from renewable energy sources, in order to store this excess electrical energy in the form of liquid fuels. There are also many challenges associated with this application. Clearly, large-scale gas conversion requires significant energy input, and hence, the energy efficiency of the process is critical. The major challenge, therefore, is to improve this energy efficiency and reduce the energy cost as much as possible.

A possible way to overcome this challenge is to deposit the appropriate amount of plasma energy in the required energy modes. Specifically, plasma-induced selective pumping of the molecular vibrational levels may provide a means to allow for increased decomposition at the catalyst surface, without wasting energy on heating the process gas.

Achieving this, however, requires a thorough understanding of how the plasma power is coupled into these modes and how these modes in turn give rise to the product intermediates, which are favorable for generating the desired end-product molecules. The advent of combined high-level simulations and dedicated experiments will be of paramount importance in this field.

In the second example related to plasma-based, large-area graphene synthesis, the growth of graphene films is presently possible on much larger substrates than those discussed in section 5.1. For example, few- and single-layer graphene films have recently been synthesized on large-area Cu foil substrates using microwave plasmas.[195,264] The obvious benefits of these processes include amenability for scaled roll-to-roll processing,

DOI: 10.1021/acs.chemrev.5b00362
Chem. Rev. 2015, 115, 13408−13446

substantially reduced (compared to conventional thermal CVD) substrate and gas temperatures, and the possibility to produce good-quality graphene films using low amounts of carbon precursor or even without using carbon-containing gases.

The remaining challenges include the need to further improve graphene film quality and to increase the size of domains with single-layer structure from typically presently achievable ~100 nm in plasma-based processes to micrometers and beyond, reported in conventional thermal CVD yet at much higher temperatures. Important issues including catalyst reuse and reducing the energy consumption needed to maintain plasmas and vacuum operation should also be addressed.

These issues can be overcome by more precise control of the growth and separation of graphene from the metal substrates, which should ideally be reused without losing their catalytic and growth-support functions. The energy efficiency of the plasma-based processes could be improved by more efficient precursor gas handling (e.g., dosing and recycling), using cheap, minimally processed precursors, minimizing the amounts of carbon-bearing and other process gases, and generating plasma discharges featuring time-programmed (e.g., pulsed) energy-delivery functions.

A better understanding of the fundamental mechanisms of the interaction of plasmas with graphene-supporting catalysts is therefore needed, for example, to increase the graphene domain sizes well beyond what is presently possible at low temperatures typical for plasma-based processes. Separation of graphene films from the catalyst in water without etching or damaging the catalyst still remains poorly understood.[265]

A clear explanation of the microscopic effects of the plasma treatment on the catalyst that enables this separation will make it possible to develop reliable strategies for the scaled production of graphene films on reusable metal catalysts. As was explained in section 5.1, synergistic plasma and catalyst effects enable microscopic surface modifications that not only are beneficial for graphene growth but also enable the film separation in water. The obvious challenge is to demonstrate the feasibility of this process at large (e.g., roll-to-roll) processing scale. Combined experimental and numerical modeling efforts are expected to shed more light on these interesting synergistic plasma-catalytic effects.

In the third and final example of large-scale production of multipurpose inorganic nanowires, the benefits of using plasma catalysis include a short reaction time scale, which allows for the large-scale production of nanowires as powders, and similarly short reaction time scales and lower temperatures for growing inorganic nanowire arrays on large areas and substrates such as thin metal foils, flexible plastic, and paper substrates, which moreover are also amenable for large-scale processing.

While the scaling-up is already in progress, various challenges remain. On a practical level, there are still many unknown aspects about equipment design for scale-up. The required design studies, however, are both costly and time-consuming. Similar to plasma-catalytic gas reforming, the capital costs are likely to be significant. On a more fundamental level, the structure, properties, and functionality of catalysts used under plasma activation need to be understood for specific materials of interest. This, in turn, requires better understanding of the elementary processes involved in plasma−catalyst interactions.

In terms of nanowire powder production, the required capital cost may be offset by the possible lowering of the actual production cost, which may be achieved through increasing throughput, potentially by using fluidized-bed reactors and atmospheric plasmas. In the case of nanowire array or film production, the methods need to be optimized for large-scale (e.g., roll-to-roll) processing.

As we have seen from these examples, a substantial research effort is needed to improve both the fundamental understanding of the numerous physicochemical effects involved and the means of translating these effects into practical outcomes. This makes the plasma-catalysis field both exciting and challenging, especially for multidisciplinary collaborations. Finally, we expect more enthusiastic researchers to engage in the coming years and welcome any critical discussions and collaborations.

AUTHOR INFORMATION

Corresponding Author

*E-mail: erik.neyts@uantwerpen.be.

Notes

The authors declare no competing financial interest.

Biographies

Erik C. Neyts is professor at the University of Antwerp, Belgium. He is an expert in the field of atomic-scale modeling and simulation of nanostructures and plasma−surface interactions. He has authored over 90 peer-reviewed papers, including 6 invited papers, and a book chapter on invitation. He has given 25 invited presentations at international conferences and over 20 invited seminars. He served as guest editor for a special issue in *J. Phys. D: Appl. Phys.* (2014) on "Fundamentals of Plasma−Surface Interactions" and for a special issue in *Catal. Today* (2015) on "Plasmas for Catalysis".

DOI: 10.1021/acs.chemrev.5b00362
Chem. Rev. 2015, 115, 13408−13446

Kostya (Ken) Ostrikov is a Science Leader of the Office of Chief Executive with CSIRO, and a Professor with Queensland University of Technology, Australia. His achievements include Pawsey (2008) medal of Australian Academy of Sciences, Walter Boas (2010) medal of Australian Institute of Physics, Building Future Award (2012), NSW Science and Engineering Award (2014), election to the Academy of Europe (2015), 6 prestigious fellowships in 6 countries, several patents, 3 monographs, and 470 journal papers. His research on nanoscale control of energy and matter contributes to the solution of the grand challenge of directing energy and matter at nanoscales, to develop renewable energy and energy-efficient technologies for a sustainable future.

Mahendra K. Sunkara currently directs the Conn Center for Renewable Energy Research and is a Distinguished University Scholar and a Professor of Chemical Engineering at University of Louisville, U.S.A. He is an expert in the field of plasma-based materials processing, large single-crystal growth, and nanowires for Li-ion batteries, solar cells, heterogeneous catalysis, electrocatalysts, and solar fuels. He has published over 120 peer-reviewed publications and a book and has over 15 U.S. patents. He founded a company, Advanced Energy Materials, LLC, which has scaled-up nanowire production for high performance heterogeneous catalyst applications. He received the distinguished faculty award for research from University of Louisville and United Phosphorus Distinguished Speaker Award from the Indian Institute of Chemical Engineers in December 2009.

Annemie Bogaerts is full professor and Francqui Distinguished Research Professor at the University of Antwerp, Belgium. She is a world-leading expert in modeling of reactive plasmas, with special focus on plasma catalysis for CO_2 conversion and plasma medicine applications. She has written over 350 peer-reviewed publications, including 11 invited reviews, as well as 10 invited book chapters. She has given over 100 invited lectures at international conferences and has obtained 20 prestigious awards in various countries. She is currently also editor of *Spectrochimica Acta: Part B* and has often served as guest editor for several journals, including a special issue in *J. Phys. D: Appl. Phys.* (2014) on "Fundamentals of Plasma−Surface Interactions".

ACKNOWLEDGMENTS

ECN and AB gratefully acknowledge financial support from the Fund of Scientific Research Flanders (FWO), Belgium, Grant Number G.0217.14N. KO acknowledges partial support by the Australian Research Council and CSIRO's OCE Science Leaders Program. MKS acknowledges partial support from US National Science Foundation through grants DMS 1125909 and EPSCoR 1355448 and also PhD students Babajide Ajayi, Apolo Nambo and Maria Carreon for their help.

REFERENCES

(1) Ertl, G. Reactions as Surfaces: From Atoms to Complexity (Nobel Lecture). *Angew. Chem., Int. Ed.* **2008**, *47*, 3524−3535.
(2) Bravo-Suárez, J. J.; Chaudhari, R. V.; Subramaniam, B. *Novel Materials for Catalysis and Fuels Processing*; ACS Symposium Series; American Chemical Society: Washington, DC, 2013; Chapter 1.
(3) Mott-Smith, H. M. History of "Plasmas. *Nature* **1971**, *233*, 219.
(4) Bogaerts, A.; Neyts, E.; Gijbels, R.; van der Mullen, J. Gas Discharge Plasmas and their Applications. *Spectrochim. Acta, Part B* **2002**, *57*, 609−658.
(5) Fridman, A. *Plasma Chemistry*; Cambridge University Press: Cambridge, U.K., 2008.
(6) Henis, J. M. Nitrogen oxide decomposition process. U.S. Patent 3983021, 1976.
(7) Van Santen, R. A.; Gelten, R. J. An Introduction to Molecular Heterogeneous Catalysis. In *New Trends in Materials Chemistry*; Catlow, C. R. A., Cheetham, A., Eds.; Kluwer Academic Publishers: Dordrecht, The Netherlands, 1997; pp 345−362.
(8) Nørskov, J. K.; Abild-Pedersen, F.; Studt, F.; Bligaard, T. Density Functional Theory in Surface Chemistry and Catalysis. *Proc. Natl. Acad. Sci. U. S. A.* **2011**, *108*, 937−943.
(9) Nørskov, J. K.; Bligaard, T.; Rossmeisl, J.; Christensen, C. H. Towards the computational design of solid catalysts. *Nat. Chem.* **2009**, *1*, 37−46.
(10) Ruban, A.; Hammer, B.; Stoltze, P.; Skriver, H. L.; Nørskov, J. K. Surface Electronic Structure and Reactivity of Transition and Noble Metals. *J. Mol. Catal. A: Chem.* **1997**, *115*, 421−429.
(11) Hammer, B.; Nørskov, J. K. Theoretical Surface Science and Catalysis − Calculations and Concepts. *Adv. Catal.* **2000**, *45*, 71−129.
(12) Hammer, B. Reactivity of a Stepped Surface NO Dissociation on Pd(211). *Faraday Discuss.* **1998**, *110*, 323−333.
(13) Hammer, B.; Nørskov, J. K. Why Gold is the Noblest of all the Elements. *Nature* **1995**, *376*, 238−240.
(14) Fierro, J. L. G. *Metal Oxides: Chemistry and Applications*; CRC Press: Boca Raton, FL, 2006.
(15) Deutschmann, O.; Knözinger, H.; Kochloefl, K.; Turek, T. *Heterogeneous Catalysis and Solid Catalysts*; Wiley-VCH Verlag GmbH: Weinheim, Germany, 2009.
(16) Bañares, M. A.; Wachs, I. E. Molecular Structures of Supported Metal Oxide Catalysts under Different Environments. *J. Raman Spectrosc.* **2002**, *33*, 359−380.
(17) Zhou, W.; Wachs, I. E.; Kiely, C. J. Nanostructural and Chemical Characterization of Supported Metal Oxide Catalysts by Aberration Corrected Analytical Electron Microscopy. *Curr. Opin. Solid State Mater. Sci.* **2012**, *16*, 10−22.
(18) Macht, J.; Iglesia, E. Structure and Function of Oxide Nanostructures: Catalytic Consequences of Size and Composition. *Phys. Chem. Chem. Phys.* **2008**, *10*, 5331−5343.

DOI: 10.1021/acs.chemrev.5b00362
Chem. Rev. 2015, 115, 13408−13446

(19) Greiner, M. T.; Helander, M. G.; Tang, W.-M.; Wang, Z.-B.; Qiu, J.; Lu, Z.-H. Universal Energy-Level Alignment of Molecules on Metal Oxides. *Nat. Mater.* **2012**, *11*, 76−81.
(20) Cordi, E. M.; Falconer, J. L. Oxidation of Volatile Organic Compounds on Al_2O_3, Pd/Al_2O_3, and PdO/Al_2O_3 Catalysts. *J. Catal.* **1996**, *162*, 104−117.
(21) Weitkamp, J. Zeolites and Catalysis. *Solid State Ionics* **2000**, *131*, 175−188.
(22) Zholobenko, V. L.; Lukyanov, D. B.; Dwyer, J.; Smith, W. J. Ferrierite and SUZ-4 Zeolite: Characterization of Acid Sites. *J. Phys. Chem. B* **1998**, *102*, 2715−2721.
(23) Liu, C.-j.; Mallinson, R.; Lobban, L. Comparative Investigations on Plasma Catalytic Methane Conversion to Higher Hydrocarbons over Zeolites. *Appl. Catal., A* **1999**, *178*, 17−27.
(24) Eliasson, B.; Liu, C.-j.; Kogelschatz, U. Direct Conversion of Methane and Carbon Dioxide to Higher Hydrocarbons Using Catalytic Dielectric-Barrier Discharges with Zeolites. *Ind. Eng. Chem. Res.* **2000**, *39*, 1221−1227.
(25) Trinh, Q. H.; Gandhi, M. S.; Mok, Y. S. Adsorption and Plasma-Catalytic Oxidation of Acetone over Zeolite-Supported Silver Catalyst. *Jpn. J. Appl. Phys.* **2015**, *54*, 01AG04−6.
(26) Zhang, K.; Eliasson, B.; Kogelschatz, U. Direct Conversion of Greenhouse Gases to Synthesis Gas and C_4 Hydrocarbons over Zeolite HY Promoted by a Dielectric-Barrier Discharge. *Ind. Eng. Chem. Res.* **2002**, *41*, 1462−1468.
(27) Jwa, E.; Lee, S. B.; Lee, H. W.; Mok, Y. S. Plasma-assisted Catalytic Methanation of CO and CO_2 over Ni-zeolite catalysts. *Fuel Process. Technol.* **2013**, *108*, 89−93.
(28) Csicsery, S. M. Catalysis by Shape Selective Zeolites − Science and Technology. *Pure Appl. Chem.* **1986**, *58*, 841−856.
(29) Holzer, F.; Roland, U.; Kopinke, F.-D. Combination of Non-Thermal Plasma and Heterogeneous Catalysis for Oxidation of Volatile Organic Compounds Part 1: Accessibility of the Intra-Particle Volume. *Appl. Catal., B* **2002**, *38*, 163−181.
(30) Hensel, K.; Martisovits, V.; Machala, Z.; Janda, M.; Lestinsky, M.; Tardiveau, P.; Mizuno, A. Electrical and Optical Properties of AC Microdischarges in Porous Ceramics. *Plasma Processes Polym.* **2007**, *4*, 682−693.
(31) Neyts, E. C.; Ostrikov, K. Nanoscale Thermodynamic Aspects of Plasma Catalysis. *Catal. Today* **2015**, *256*, 23−28.
(32) Gsell, M.; Jakob, P.; Menzel, D. Effect of Substrate Strain on Adsorption. *Science* **1998**, *280*, 717−720.
(33) Lundqvist, B. I.; Gunnarsson, O.; Hjelmberg, H.; Nørskov, J. K. Theoretical Description of Molecule-Metal Interaction and Surface Reactions. *Surf. Sci.* **1979**, *89*, 196−225.
(34) Darling, G. R.; Holloway, S. H_2 Dissociation Dynamics on Metals: Where Do We Stand? In *The Chemical Physics of Solid Surfaces; Vol. 11: Surface Dynamics*; Woodruff, D. P., Ed.; Elsevier: Amsterdam, 2003; Chapter 2, p 29.
(35) Smith, R. R.; Killelea, D. R.; DelSesto, D. F.; Utz, A. L. Preference for Vibrational over Translational Energy in a Gas-Surface Reaction. *Science* **2004**, *304*, 992−995.
(36) Juurlink, L. B. F.; McCabe, P. R.; Smith, R. R.; DiCologero, C. L.; Utz, A. L. Eigenstate-Resolved Studies of Gas-Surface Reactivity: CH_4 (ν_3) Dissociation on Ni(100). *Phys. Rev. Lett.* **1999**, *83*, 868−871.
(37) Crim, F. F. Chemical Dynamics of Vibrationally Excited Molecules: Controlling Reactions in Gases and on Surfaces. *Proc. Natl. Acad. Sci. U. S. A.* **2008**, *105*, 12654−12661.
(38) Murzin, D.; Salmi, T. *Catalysis Kinetics*; Elsevier: Amsterdam, 2005; Chapter 4, p 136.
(39) Evans, J. W.; Trimm, D. L.; Wainwright, M. S. Effect of Coke Formation on the Reactions of Dimethyl Ether on Acidic Oxide Catalysts. *Ind. Eng. Chem. Prod. Res. Dev.* **1983**, *22*, 242−246.
(40) Corma, A.; Hamid, S. B. A; Iborra, S.; Velty, A. Lewis and Brönsted Basic Active Sites on Solid Catalysts and Their Role in the Synthesis of Monoglycerides. *J. Catal.* **2005**, *234*, 340−347.
(41) Roduner, E. Understanding Catalysis. *Chem. Soc. Rev.* **2014**, *43*, 8226−8239.
(42) Parmon, V. N. Thermodynamic Analysis of the Effect of the Nanoparticle Size of the Active Component on the Adsorption Equilibrium and the Rate of Heterogeneous Catalytic Processes. *Dokl. Phys. Chem.* **2007**, *413*, 42−48.
(43) Murzin, D. Yu. Nanokinetics for Nanocatalysis. *Catal. Sci. Technol.* **2011**, *1*, 380−384.
(44) Bell, A. T. The Impact of Nanoscience on Heterogeneous Catalysis. *Science* **2003**, *299*, 1688−1691.
(45) Moshfegh, A. Z. Nanoparticle Catalysts. *J. Phys. D: Appl. Phys.* **2009**, *42*, 233001.
(46) Campbell, C. T.; Sharp, J. C.; Yao, Y. X.; Karp, E. M.; Silbaugh, T. L. Insights into Catalysis by Gold Nanoparticles and their Support Effects through Surface Science Studies of Model Catalysts. *Faraday Discuss.* **2011**, *152*, 227−239.
(47) Campbell, C. T. The Energetics of Supported Metal Nanoparticles: Relationships to Sintering Rates and Catalytic Activity. *Acc. Chem. Res.* **2013**, *46*, 1712−1719.
(48) Yudanov, I. V.; Genest, A.; Schauermann, S.; Freund, H.-J.; Rösch, N. Size Dependence of the Adsorption Energy of CO on Metal Nanoparticles: a DFT Search for the Minimum Value. *Nano Lett.* **2012**, *12*, 2134−2139.
(49) Philippot, K.; Serp, P. Concepts in Nanocatalysis. In *Nanomaterials in Catalysis*; Serp, P., Philippot, K., Eds.; Wiley-VCH Verlag: Weinheim, Germany, 2013; Chapter 1.
(50) Buffat, Ph.; Borel, J.-P. Size Effect on the Melting Temperature of Gold Particles. *Phys. Rev. A: At., Mol., Opt. Phys.* **1976**, *13*, 2287−2298.
(51) Bachels, T.; Güntherodt, H.-J.; Schäfer, R. Melting of Isolated Tin Nanoparticles. *Phys. Rev. Lett.* **2000**, *85*, 1250−1253.
(52) Haberland, H.; Hippler, T.; Donges, J.; Kostko, O.; Schmidt, M.; von Issendorff, B. Melting of Sodium Clusters: Where Do the Magic Numbers Come From? *Phys. Rev. Lett.* **2005**, *94*, 035701−4.
(53) Shibuta, Y.; Suzuki, T. A Molecular Dynamics Study of the Phase Transition in BCC Metal Nanoparticles. *J. Chem. Phys.* **2008**, *129*, 144102−10.
(54) Shibuta, Y.; Suzuki, T. Phase Transition in Substrate-Supported Molebdenum Nanoparticles: a Molecular Dynamics Study. *Phys. Chem. Chem. Phys.* **2010**, *12*, 731−739.
(55) Neyts, E. C.; Bogaerts, A. Numerical Study of the Size-Dependent Melting Mechanisms of Nickel Nanoclusters. *J. Phys. Chem. C* **2009**, *113*, 2771−2776.
(56) Engelmann, Y.; Bogaerts, A.; Neyts, E. C. Thermodynamics at the Nanoscale: Phase Diagrams of Nickel-Carbon Nanoclusters and Equilibrium Constants for Phase Transitions. *Nanoscale* **2014**, *6*, 11981−11987.
(57) Jiang, A.; Awasthi, N.; Kolmogorov, A. N.; Setyawan, W.; Börjesson, A.; Bolton, K.; Harutyunyan, A. R.; Curtarolo, S. Theoretical study of the thermal behavior of free and alumina-supported Fe-C nanoparticles. *Phys. Rev. B: Condens. Matter Mater. Phys.* **2007**, *75*, 205426−12.
(58) Klasovsky, F.; Claus, P. Metal Nanoclusters in Catalysis: Effects of Nanoparticle Size, Shape and Structure. In *Metal Nanoclusters in Catalysis and Materials Science: The Issue of Size Control*; Corain, B., Schmid, G., Toshima, N., Eds.; Elsevier: Amsterdam, 2008; Chapter 8.
(59) Lopez, N.; Janssens, T. V. W.; Clausen, B. S.; Xu, Y.; Mavrikakis, M.; Bligaard, T.; Nørskov, J. K. *J. Catal.* **2004**, *223*, 232−235.
(60) Hvolbaek, B.; Janssens, T. V. W.; Clausen, B. S.; Falsig, H.; Christensen, C. H.; Nørskov, J. K. Catalytic Activity of Au Nanoparticles. *Nano Today* **2007**, *2*, 14−18.
(61) Neyts, E. C. Plasma-Surface Interactions in Plasma Catalysis. *Plasma Chem. Plasma Process.* **2015**, DOI: 10.1007/s11090-015-9662-5.
(62) Meyyappan, M. A Review of Plasma Enhanced Chemical Vapour Deposition of Carbon Nanotubes. *J. Phys. D: Appl. Phys.* **2009**, *42*, 213001−15.

DOI: 10.1021/acs.chemrev.5b00362
Chem. Rev. 2015, 115, 13408−13446

(63) Neyts, E. C. PECVD Growth of Carbon Nanotubes: From Experiment to Simulation. *J. Vac. Sci. Technol. B* **2012**, *30*, 030803−17.
(64) Zhang, G.; Qi, P.; Wang, X.; Lu, Y.; Li, X.; Tu, R.; Bangsaruntip, S.; Mann, D.; Zhang, L.; Dai, H. Selective Etching of Metallic Carbon Nanotubes by Gas-Phase Reaction. *Science* **2006**, *314*, 974−977.
(65) Neyts, E. C.; Ostrikov, K.; Han, Z. J.; Kumar, S.; van Duin, A. C. T.; Bogaerts, A. Defect Healing and Enhanced Nucleation of Carbon Nanotubes by Low-Energy Ion Bombardment. *Phys. Rev. Lett.* **2013**, *110*, 065501−5.
(66) Neyts, E. C.; Bogaerts, A. Ion Irradiation for Improved Graphene Network Formation in Carbon Nanotube Growth. *Carbon* **2014**, *77*, 790−795.
(67) Gohier, A.; Minea, T. M.; Djouadi, A. M.; Granier, A.; Dubosc, M. Limits of the PECVD Process for Single Wall Carbon Nanotubes Growth. *Chem. Phys. Lett.* **2006**, *421*, 242−245.
(68) Gohier, A.; Minea, T. M.; Djouadi, A. M.; Granier, A. Impact of the Etching Gas on Vertically Oriented Single Wall and Few Walled Carbon Nanotubes by Plasma Enhanced Chemical Vapor Deposition. *J. Appl. Phys.* **2007**, *101*, 054317.
(69) Gohier, A.; Minea, T. M.; Point, S.; Mevellec, J.-Y.; Jimenez, J.; Djouadi, M. A.; Granier, A. Early Stages of the Carbon Nanotube Growth by Low Pressure CVD and PE-CVD. *Diamond Relat. Mater.* **2009**, *18*, 61−65.
(70) Kato, T.; Hatakeyama, R. Kinetics of Reactive Ion Etching Upon Single-Walled Carbon Nanotubes. *Appl. Phys. Lett.* **2008**, *92*, 031502.
(71) Yu, S.; Liang, Y.; Sun, S.; Zhang, K.; Zhang, J.; Fang, J. Vehicle Exhaust Gas Clearance by Low Temperature Plasma-Driven Nano-Titanium Dioxide Film Prepared by Radiofrequency Magnetron Sputtering. *PLoS One* **2013**, *8*, e59974:1−8.
(72) Rafiq, M. H.; Jakobsen, H. A.; Hustad, J. E. Modeling and Simulation of Catalytic Partial Oxidation of Methane to Synthesis Gas by Using a Plasma-Assisted Gliding Arc Reactor. *Fuel Process. Technol.* **2012**, *101*, 44−57.
(73) Nozaki, T.; Muto, N.; Kadio, S.; Okazaki, K. Dissociation of Vibrationally Excited Methane on Ni Catalyst Part 2: Process Diagnostics by Emission Spectroscopy. *Catal. Today* **2004**, *89*, 67−74.
(74) Zhang, X.; Lee, C. S.-M.; Mingos, D. M. P.; Hayward, D. O. Oxidative Coupling of Methane Using Microwave Dielectric Heating. *Appl. Catal., A* **2003**, *249*, 151−164.
(75) Amara, H.; Bichara, C.; Ducastelle, F. Understanding the Nucleation Mechanisms of Carbon Nanotubes in Catalytic Chemical Vapor Deposition. *Phys. Rev. Lett.* **2008**, *100*, 056105:1−4.
(76) Diarra, M.; Zappelli, A.; Amara, H.; Ducastelle, F.; Bichara, C. Importance of Carbon Solubility and Wetting Properties of Nickel Nanoparticles for Single Wall Nanotube Growth. *Phys. Rev. Lett.* **2012**, *109*, 185501:1−5.
(77) Shariat, M.; Shokri, B.; Neyts, E. C. On the Low-Temperature Growth Mechanism of Single Walled Carbon Nanotubes in Plasma Enhanced Chemical Vapor Deposition. *Chem. Phys. Lett.* **2013**, *590*, 131−135.
(78) Shariat, M.; Hosseini, S. I.; Shokri, B.; Neyts, E. C. Plasma Enhanced Growth of Single Walled Carbon Nanotubes at Low Temperature: A Reactive Molecular Dynamics Simulation. *Carbon* **2013**, *65*, 269−276.
(79) Shang, S.; Liu, G.; Chai, X.; Tao, X.; Li, X.; Bai, M.; Chu, W.; Dai, X.; Zhao, Y.; Yin, Y. Research on Ni/γ-Al_2O_3 Catalyst for CO_2 Reforming of CH_4 Prepared by Atmospheric Pressure Glow Discharge Plasma Jet. *Catal. Today* **2009**, *148*, 268−274.
(80) Kim, H.-H.; Ogata, A. Nonthermal Plasma Activates Catalyst: From Current Understanding And Future Prospects. *Eur. Phys. J.: Appl. Phys.* **2011**, *55*, 13806:1−11.
(81) Sano, T.; Negishi, N.; Sakai, E.; Matsuzawa, S. Contributions of Photocatalytic/Catalytic Activities of TiO_2 and γ-Al_2O_3 in Nonthermal Plasma on Oxidation of Acetaldehyde and CO. *J. Mol. Catal. A: Chem.* **2006**, *245*, 235−241.
(82) Chen, H. L.; Lee, H. M.; Chen, S. H.; Chao, Y.; Chang, M. B. Review of Plasma Catalysis on Hydrocarbon Reforming for Hydrogen Production − Interaction, Integration, and Prospects. *Appl. Catal., B* **2008**, *85*, 1−9.
(83) Van Durme, J.; Dewulf, J.; Leys, C.; Van Langenhove, H. Combining Non-Thermal Plasma with Heterogeneous Catalysis in Waste Gas Treatment: A Review. *Appl. Catal., B* **2008**, *78*, 324−333.
(84) Neyts, E. C.; Bogaerts, A. Understanding Plasma Catalysis Through Modelling and Simulation − A Review. *J. Phys. D: Appl. Phys.* **2014**, *47*, 224010:1−18.
(85) Vandenbroucke, A. M.; Morent, R.; De Geyter, N.; Leys, C. Non-Thermal Plasmas For Non-Catalytic And Catalytic Volatile Organic Compound Abatement. *J. Hazard. Mater.* **2011**, *195*, 30−54.
(86) Witvrouwen, T.; Paulussen, S.; Sels, B. The Use of Non-Equilibrium Plasmas for the Synthesis of Heterogeneous Catalysts. *Plasma Processes Polym.* **2012**, *9*, 750−760.
(87) Liu, C.-j.; Vissokov, G. P.; Jang, B. W.-L. Catalyst Preparation Using Plasma Technologies. *Catal. Today* **2002**, *72*, 173−184.
(88) Tang, X.; Li, K.; Yi, H.; Ning, P.; Xiang, Y.; Wang, J.; Wang, C. MnO_x Catalysts Modified by Nonthermal Plasma for NO Catalytic Oxidation. *J. Phys. Chem. C* **2012**, *116*, 10017−10028.
(89) Guo, Y.-F.; Ye, D.-Q.; Chen, K.-F.; He, J.-C.; Chen, W.-L. Toluene Decomposition Using a Wire-Plate Dielectric Barrier Discharge Reactor With Manganese Oxide Catalyst In Situ. *J. Mol. Catal. A: Chem.* **2006**, *245*, 93−100.
(90) Gallon, H. J.; Tu, X.; Twigg, M. V.; Whitehead, J. C. Plasma-Assisted Methane Reduction of a NiO Catalyst - Low Temperature Activation of Methane and Formation of Carbon Nanofibres. *Appl. Catal., B* **2011**, *106*, 616−620.
(91) Tu, X.; Gallon, H. J.; Whitehead, J. C. Plasma-Assisted Reduction of a NiO/Al_2O_3 Catalyst in Atmospheric Pressure H_2/Ar Dielectric Barrier Discharge. *Catal. Today* **2013**, *211*, 120−125.
(92) Li, Y.; Wei, Z.; Wang, Y. Ni/Mgo Catalyst Prepared Via Dielectric-Barrier Discharge Plasma With Improved Catalytic Performance for Carbon Dioxide Reforming of Methane. *Front. Chem. Sci. Eng.* **2014**, *8*, 133−140.
(93) Demidyuk, V.; Whitehead, J. C. Influence of Temperature on Gas-Phase Toluene Decomposition in Plasma-Catalytic System. *Plasma Chem. Plasma Process.* **2007**, *27*, 85−94.
(94) Wang, L.; Zhao, Y.; Liu, C.; Gong, W.; Guo, H. Plasma Driven Ammonia Decomposition on a Fe-Catalyst: Eliminating Surface Nitrogen Poisoning. *Chem. Commun.* **2013**, *49*, 3787−3789.
(95) Nozaki, T.; Okazaki, K. Non-Thermal Plasma Catalysis of Methane: Principles, Energy Efficiency, and Applications. *Catal. Today* **2013**, *211*, 29−38.
(96) Takuma, T. Field Behavior at a Triple Junction in Composite Dielectric Arrangements. *IEEE Trans. Electr. Insul.* **1991**, *26*, 500−509.
(97) Ogata, A.; Yamanouchi, K.; Mizuno, K.; Kushiyama, S.; Yamamoto, T. Decomposition of Benzene Using Alumina-Hybrid and Catalyst-Hybrid Plasma Reactors. *IEEE Trans. Ind. Appl.* **1999**, *35*, 1289−1295.
(98) Liang, W.-J.; Ma, L.; Liu, H.; Li, J. Toluene Degradation by Non-Thermal Plasma Combined With a Ferroelectric Catalyst. *Chemosphere* **2013**, *92*, 1390−1395.
(99) Roland, U.; Holzer, F.; Kopinke, F.-D. Improved Oxidation of Air Pollutants in a Non-Thermal Plasma. *Catal. Today* **2002**, *73*, 315−323.
(100) Tu, X.; Whitehead, J. C. Plasma-Catalytic Dry Reforming Of Methane In An Atmospheric Dielectric Barrier Discharge: Understanding The Synergistic Effect At Low Temperature. *Appl. Catal., B* **2012**, *125*, 439−448.
(101) Tu, X.; Gallon, H. J.; Whitehead, J. C. Electrical and Spectroscopic Diagnostics of a Single-Stage Plasma-Catalysis System: Effect of Packing With TiO_2. *J. Phys. D: Appl. Phys.* **2011**, *44*, 482003:1−4.
(102) Hensel, K.; Katsura, S.; Mizuno, A. DC Microdischarges Inside Porous Ceramics. *IEEE Trans. Plasma Sci.* **2005**, *33*, 574−575.

DOI: 10.1021/acs.chemrev.5b00362
Chem. Rev. 2015, 115, 13408−13446

(103) Ertl, G. Dynamics of Reactions at Surfaces. *Adv. Catal.* **2000**, *45*, 1−69.
(104) Kang, M.; Kim, B.-J.; Cho, S. M.; Chung, C.-H.; Kim, B.-W.; Han, G. Y.; Yoon, K. J. Decomposition of Toluene Using an Atmospheric Pressure Plasma/TiO_2 Catalytic System. *J. Mol. Catal. A: Chem.* **2002**, *180*, 125−132.
(105) Lee, B.-Y.; Park, S.-H.; Lee, S.-C.; Kang, M.; Choung, S.-J. *Catal. Today* **2004**, *93*−*95*, 769−776.
(106) Rousseau, A.; Guaitella, O.; Gatilova, L.; Thevenet, F.; Guillard, C.; Röpcke, J.; Stancu, G. D. Photocatalyst Activation In A Pulsed Low Pressure Discharge. *Appl. Phys. Lett.* **2005**, *87*, 221501:1−3.
(107) Thevenet, F.; Guaitella, O.; Puzenat, E.; Herrmann, J.-M.; Rousseau, A.; Guillard, C. Oxidation of Acetylene by Photocatalysis Coulpled With Dielectric Barrier Discharge. *Catal. Today* **2007**, *122*, 186−194.
(108) Beckerle, J. D.; Yang, Q. Y.; Johnson, A. D.; Ceyer, S. T. Collision-Induced Dissociative Chemisorption of Adsorbates: Chemistry With a Hammer. *J. Chem. Phys.* **1987**, *86*, 7236−7237.
(109) Beckerle, J. D.; Johnson, A. D.; Yang, Q. Y.; Ceyer, S. T. Collision Induced Dissociative Chemisorption of CH_4 on Ni(111) by Inert Gas Atoms: The Mechanism for Chemistry With a Hammer. *J. Chem. Phys.* **1989**, *91*, 5756−5777.
(110) Popov, V. N. Carbon nanotubes: properties and application. *Mater. Sci. Eng., R* **2004**, *43*, 61−102.
(111) Fiawoo, M.-F. C.; Bonnot, A.-M.; Amara, H.; Bichara, C.; Thibault-Pénisson, J.; Loiseau, A. Evidence of Correlation between Catalyst Particles and the Single-Wall Carbon Nanotube Diameter: A First Step towards Chirality Control. *Phys. Rev. Lett.* **2012**, *108*, 195503:1−5.
(112) Zhong, G.; Hofmann, S.; Yan, F.; Telg, H.; Warner, J. H.; Eder, D.; Thomsen, C.; Milne, W. I.; Robertson, J. Acetylene: A Key Growth Precursor for Single-Walled Carbon Nanotube Forests. *J. Phys. Chem. C* **2009**, *113*, 17321−17325.
(113) Ziebro, J.; Lukasiewicz, I.; Borowiak-Palen, E.; Michalkiewicz, B. Low Temperature Growth Of Carbon Nanotubes From Methane Catalytic Decomposition Over Nickel Supported On A Zeolite. *Nanotechnology* **2010**, *21*, 145308:1−10.
(114) Kumar, M.; Ando, Y. Chemical Vapor Deposition of Carbon Nanotubes: A Review on Growth Mechanism and Mass Production. *J. Nanosci. Nanotechnol.* **2010**, *10*, 3739−3758.
(115) Wagner, R. S.; Ellis, W. C. Vapor-Liquid-Solid Mechanism of Single Crystal Growth. *Appl. Phys. Lett.* **1964**, *4*, 89−90.
(116) Baker, R. T. K.; Barber, M. A.; Harris, P. S.; Feates, F. S.; Waite, R. J. Nucleation and growth of carbon deposits from the nickel catalyzed decomposition of acetylene. *J. Catal.* **1972**, *26*, 51−62.
(117) Neyts, E. C.; Shibuta, Y.; Bogaerts, A. Bond Switching Regimes in Nickel and Nickel-Carbon Nanoclusters. *Chem. Phys. Lett.* **2010**, *488*, 202−205.
(118) Ostrikov, K. *Plasma Nanoscience: Basic Concepts and Applications of Deterministic Nanofabrication*; Wiley VCH Verlag: Weinheim, Germany, 2008; Chapter 7.
(119) Page, A. J.; Chandrakumar, K. R. S.; Irle, S.; Morokuma, K. SWNT Nucleation from Carbon-Coated SiO_2 Nanoparticles via a Vapor-Solid-Solid Mechanism. *J. Am. Chem. Soc.* **2011**, *133*, 621−628.
(120) Rao, F.; Li, T.; Wang, Y. Growth of "All-Carbon" Single-Walled Carbon Nanotubes From Diamonds and Fullerenes. *Carbon* **2009**, *47*, 3580−3584.
(121) Liu, H.; Takagi, D.; Chiashi, S.; Homma, Y. The Growth of Single-Walled Carbon Nanotubes on a Silica Substate Without Using a Metal Catalyst. *Carbon* **2010**, *48*, 114−122.
(122) Kumar, S.; Mehdipour, H.; Ostrikov, K. Plasma-Enabled Graded Nanotube Biosensing Arrays on a Si Nanodevice Platform: Catalyst-Free Integration and In Situ Detection of Nucleation Events. *Adv. Mater.* **2013**, *25*, 69−74.
(123) Durand, F.; Duby, J. C. Carbon Solubility in Solid and Liquid Silicon − A Review with Reference to Eutectic Equilibrium. *J. Phase Equilib.* **1999**, *20*, 61−63.
(124) Derycke, V.; Martel, R.; Radosavljevic, M.; Ross, F. M.; Avouris, Ph. Catalyst-Free Growth of Ordered Single-Walled Carbon Nanotube Networks. *Nano Lett.* **2002**, *2*, 1043−1046.
(125) Takagi, D.; Hibino, H.; Suzuki, S.; Kobayashi, Y.; Homma, Y. Carbon Nanotube Growth from Semiconductor Nanoparticles. *Nano Lett.* **2007**, *7*, 2272−2275.
(126) Lim, S. H.; Luo, Z.; Shen, Z.; Lin, J. Plasma-Assisted Synthesis of Carbon Nanotubes. *Nanoscale Res. Lett.* **2010**, *5*, 1377−1386.
(127) Ostrikov, K.; Mehdipour, H. Nanoscale Plasma Chemistry Enables Fast, Size-Selective Nanotube Nucleation. *J. Am. Chem. Soc.* **2012**, *134*, 4303−4312.
(128) Ostrikov, K.; Mehdipour, H. Thin Single-Walled Carbon Nanotubes with Narrow Chirality Distribution: Constructive Interplay of Plasma and Gibbs-Thomson Effects. *ACS Nano* **2011**, *5*, 8372−8382.
(129) Luo, Z.; Lim, S.; You, Y.; Miao, J.; Gong, H.; Zhang, J.; Wang, S.; Lin, J.; Shen, Z. Effect of ion bombardment on the synthesis of vertically aligned single-walled carbon nanotubes by plasma-enhanced chemical vapor deposition. *Nanotechnology* **2008**, *19*, 255607.
(130) Neyts, E. C. The Role of Ions in Plasma Catalytic Carbon Nanotube Growth: A Review. *Front. Chem. Sci. Eng.* **2015**, *9*, 154−162.
(131) Yamazaki, Y.; Sakuma, N.; Katagiri, M.; Suzuki, M.; Sakai, T.; Sato, S.; Nihei, M.; Awano, Y. High-Quality Carbon Nanotube Growth at Low Temperature by Pulse-Excited Remote Plasma Chemical Vapor Deposition. *Appl. Phys. Express* **2008**, *1*, 034004:1−3.
(132) Hiramatsu, M.; Nagao, H.; Taniguchi, M.; Amano, H.; Ando, Y.; Hori, M. High-Rate Growth of Films of Dense, Aligned Double-Walled Carbon Nanotubes Using Microwave Plasma-Enhanced Chemical Vapor Deposition. *Jpn. J. Appl. Phys.* **2005**, *44*, L693−L695.
(133) Hofmann, S.; Csányi, G.; Ferrari, A. C.; Payne, M. C.; Robertson, J. Surface Diffusion: The Low Activation Energy Path for Nanotube Growth. *Phys. Rev. Lett.* **2005**, *95*, 036101:1−4.
(134) Denysenko, I.; Ostrikov, K. Ion-Assisted Precursor Dissociation and Surface Diffusion: Enabling Rapid, Low-Temperature Growth of Carbon Nanofibers. *Appl. Phys. Lett.* **2007**, *90*, 251501:1−3.
(135) Hofmann, S.; Ducati, C.; Robertson, J.; Kleinsorge, B. Low-Temperature Growth of Carbon Nanotubes by Plasma-Enhanced Chemical Vapor Deposition. *Appl. Phys. Lett.* **2003**, *83*, 135−137.
(136) Ducati, C.; Alexandrou, I.; Chhowalla, M.; Amaratunga, G. A. J.; Robertson, J. Temperature Selective Growth of Carbon Nanotubes by Chemical Vapor Deposition. *J. Appl. Phys.* **2002**, *92*, 3299−3303.
(137) Kato, T.; Hatakeyama, R. Formation of Freestanding Single-Walled Carbon Nanotubes by Plasma-Enhanced CVD. *Chem. Vap. Deposition* **2006**, *12*, 345−352.
(138) Neyts, E. C.; van Duin, A. C. T.; Bogaerts, A. Insights in the Plasma-Assisted Growth of Carbon Nanotubes through Atomic Scale Simulations: Effect of Electric Field. *J. Am. Chem. Soc.* **2012**, *134*, 1256−1260.
(139) Kato, T.; Kuroda, S.; Hatakeyama, R. Diameter Tuning of Single-Welled Carbon Nanotubes by Diffusion Plasma CVD. *J. Nanomater.* **2011**, *2011*, 490529:1−7.
(140) Kato, T.; Jeong, G.-H.; Hirata, T.; Hatakeyama, R.; Tohji, K. Freestanding Individual Single-walled Carbon Nanotube Synthesis Based on Plasma Sheath Effects. *Jpn. J. Appl. Phys.* **2004**, *43*, L1278−L1280.
(141) Ghorannevis, Z.; Kato, T.; Kaneko, T.; Hatakeyama, R. Narrow-Chirality Distributed Single-Walled Carbon Nanotube Growth from Nonmagnetic Catalyst. *J. Am. Chem. Soc.* **2010**, *132*, 9570−9572.

DOI: 10.1021/acs.chemrev.5b00362
Chem. Rev. 2015, 115, 13408−13446

(142) Choi, Y. C.; Shin, Y. M.; Lee, Y. H.; Lee, B. S.; Park, G.-S.; Choi, W. B.; Lee, N. S.; Kim, J. M. Controlling The Diameter, Growth Rate, And Density Of Vertically Aligned Carbon Nanotubes Synthesized By Microwave Plasma-Enhanced Chemical Vapor Deposition. *Appl. Phys. Lett.* **2000**, *76*, 2367−2369.
(143) Kato, T.; Hatakeyama, R. Direct Growth of Short Single-Walled Carbon Nanotubes with Narrow-Chirality Distribution by Time-Programmed Plasma Chemical Vapor Deposition. *ACS Nano* **2010**, *4*, 7395−7400.
(144) Handuja, S.; Srivastava, P.; Vankar, V. D. On The Growth And Microstructure Of Carbon Nanotubes Grown By Thermal Chemical Vapor Deposition. *Nanoscale Res. Lett.* **2010**, *5*, 1211−1216.
(145) Xu, M.; Futaba, D. N.; Yumura, M.; Hata, K. Alignment Control Of Carbon Nanotube Forest From Random To Nearly Perfectly Aligned By Utilizing The Crowding Effect. *ACS Nano* **2012**, *6*, 5837−5844.
(146) Lunsford, J. H. Catalytic Conversion of Methane to More Useful Chemicals and Fuels: A Challenge for the 21st Century. *Catal. Today* **2000**, *63*, 165−174.
(147) Mikkelsen, M.; Jørgensen, M.; Krebs, F. C. The Teraton Challenge. A Review of Fixation and Transformation of Carbon Dioxide. *Energy Environ. Sci.* **2010**, *3*, 43−81.
(148) McDonough, W.; Braungart, M. *Cradle 2 Cradle: Remaking the Way We Make Things*; North Point Press: New York, 2002.
(149) Wagman, D. D.; Kilpatrick, J. E.; Taylor, W. J.; Pitzer, K. S.; Rossini, F. D. Heats, Free Energies and Equilibrium Constants of some Reactions Involving O_2, H_2, H_2O, C, CO, CO_2 and CH_4. *J. Res. Natl. Bur. Stand.* **1945**, *34*, 143−161.
(150) Rayne, S. Carbon dioxide splitting: A summary of the peer-reviewed scientific literature. *Nature Precedings* **2008**, DOI: 10.1038/npre.2008.1741.2.
(151) Nigara, Y.; Cales, B. Production of Carbon Monoxide by Direct Thermal Splitting of Carbon Dioxide at High Temperature. *Bull. Chem. Soc. Jpn.* **1986**, *59*, 1997−2002.
(152) Itoh, N.; Sanchez, M. A.; Xu, W.-C.; Haraya, K.; Hongo, M. Application of a membrane reactor system to thermal decomposition of CO_2. *J. Membr. Sci.* **1993**, *77*, 245−253.
(153) Fan, M.-S.; Abdullah, A. Z.; Bhatia, S. Utilization of Greenhouse Gases through Dry Reforming: Screening of Nickel-Based Bimetallic Catalysts and Kinetic Studies. *ChemSusChem* **2011**, *4*, 1643−1653.
(154) Zhang, J.; Wang, H.; Dalai, A. K. Development of Stable Bimetallic Catalysts for Carbon Dioxide Reforming of Methane. *J. Catal.* **2007**, *249*, 300−310.
(155) Wang, S.; Lu, G. Q.; Millar, G. J. Carbon Dioxide Reforming of Methane To Produce Synthesis Gas over Metal-Supported Catalysts: State of the Art. *Energy Fuels* **1996**, *10*, 896−904.
(156) Paulussen, S.; Verheyde, B.; Tu, X.; De Bie, C.; Martens, T.; Petrovic, D.; Bogaerts, A.; Sels, B. Conversion Of Carbon Dioxide To Value-Added Chemicals In Atmospheric Pressure Dielectric Barrier Discharges. *Plasma Sources Sci. Technol.* **2010**, *19*, 034015.
(157) Pinhao, N. R.; Janeco, A.; Branco, J. B. Influence Of He On The Conversion Of Methane And CO_2 In A Dielectric Barrier Discharge. *Plasma Chem. Plasma Process.* **2011**, *31*, 427−439.
(158) Lindon, M. A.; Scime, E. E. CO_2 Dissociation Using the Versatile Atmospheric Dielectric Barrier Discharge Experiment (VADER). *Front. Phys.* **2014**, *2*, 55:1−13.
(159) Silva, T.; Britun, N.; Godfroid, T.; Snyders, R. Optical Characterization of a MW Pulsed Discharge Used For Dissociation Of CO_2. *Plasma Sources Sci. Technol.* **2014**, *23*, 025009.
(160) Gutsol, A.; Rabinovich, A.; Fridman, A. Combustion-Assisted Plasma In Fuel Conversion. *J. Phys. D: Appl. Phys.* **2011**, *44*, 274001.
(161) Nunnally, T.; Gutsol, K.; Rabinovich, A.; Fridman, A.; Gutsol, A.; Kemoun, A. Dissociation Of CO_2 In A Low Current Gliding Arc Plasmatron. *J. Phys. D: Appl. Phys.* **2011**, *44*, 274009.
(162) Tu, X.; Whitehead, J. C. Plasma Dry Reforming Of Methane In Atmospheric Pressure Alternative Current Gliding Arc Discharge: Co-Generation Of Syngas And Carbon Nanomaterials. *Int. J. Hydrogen Energy* **2014**, *39*, 9658−9669.
(163) Kozak, T.; Bogaerts, A. Splitting Of CO_2 By Vibrational Excitation In Non-Equilibrium Plasmas: A Reaction Kinetics Model. *Plasma Sources Sci. Technol.* **2014**, *23*, 045004.
(164) Snoeckx, R.; Aerts, R.; Tu, X.; Bogaerts, A. Plasma-Based Dry Reforming: A Computational Study Ranging From Nanoseconds To Seconds Timescale. *J. Phys. Chem. C* **2013**, *117*, 4957−4970.
(165) Aerts, R.; Somers, W.; Bogaerts, A. CO_2 Splitting In A Dielectric Barrier Discharge Plasma: A Combined Experimental And Computational Study. *ChemSusChem* **2015**, *8*, 702−716.
(166) Scarduelli, G.; Guella, G.; Ascenzi, D.; Tosi, P. Synthesis Of Liquid Organic Compounds From CH_4 And CO_2 In A Dielectric Barrier Discharge Operating At Atmospheric Pressure. *Plasma Processes Polym.* **2011**, *8*, 25−31.
(167) Kraus, M.; Eliasson, B.; Kogelschatz, U.; Wokaun, A. CO_2 Reforming Of Methane By The Combination Of Dielectric Barrier Discharges And Catalysis. *Phys. Chem. Chem. Phys.* **2001**, *3*, 294−300.
(168) Mei, E.; Zhu, X.; He, Y.; Yan, J. D.; Tu, X. Plasma-Assisted Conversion Of CO_2 In A Dielectric Barrier Discharge Reactor: Understanding The Effect Of Packing Materials. *Plasma Sources Sci. Technol.* **2015**, *24*, 015011.
(169) Yu, Q.; Kong, M.; Liu, T.; Fei, J.; Zheng, X. Characteristics Of The Decomposition Of CO_2 In A Dielectric Packed-Bed Plasma Reactor. *Plasma Chem. Plasma Process.* **2012**, *32*, 153−163.
(170) Scapinello, M.; Martini, L. M.; Tosi, P. CO_2 Hydrogenation by CH_4 in a Dielectric Barrier Discharge: Catalytic Effect Of Ni And Cu. *Plasma Processes Polym.* **2014**, *11*, 624−628.
(171) Brock, S. B.; Marquez, M.; Suib, S.; Hayashi, Y.; Matsumoto, H. Plasma Decomposition of CO_2 in Presence of Metal Catalysts. *J. Catal.* **1998**, *180*, 225−233.
(172) Krawczyk, K.; Mlotek, M.; Ulejczyk, B.; Schmidt-Szalowski, K. Methane Conversion With CO_2 In Plasma-Catalytic System. *Fuel* **2014**, *117*, 608−617.
(173) Zhang, X.; Zhu, A.; Li, X.; Gong, W. Oxidative Dehydrogenation of Ethane With CO_2 Over Catalyst Under Pulse Corona Plasma. *Catal. Today* **2004**, *89*, 97−102.
(174) Amouroux, J.; Cavadias, S.; Doubla, A. CO_2 Reduction by Non-Equilibrium Electrocatalysis Plasma Reactor. *IOP Conf. Ser.: Mater. Sci. Eng.* **2011**, *19*, 012005.
(175) Wang, Q.; Cheng, Y.; Jin, Y. Dry Reforming Of Methane In An Atm Pressure Plasma Fluidized Bed With Ni/γ-Al_2O_3 Catalyst. *Catal. Today* **2009**, *148*, 275−282.
(176) Wang, Q.; Yan, B.-H.; Jin, Y.; Cheng, Y. Dry Reforming Of Methane In A Dielectric Barrier Discharge Reactor With Ni/Al_2O_3 Catalyst: Interaction Of Catalyst And Plasma. *Energy Fuels* **2009**, *23*, 4196−4201.
(177) Eliasson, B.; Kogelschatz, U.; Xue, B.; Zhou, L.-M. Hydrogenation Of Carbon Dioxide To Methanol With A Discharge-Activated Catalyst. *Ind. Eng. Chem. Res.* **1998**, *37*, 3350−3357.
(178) Zhang, A.-J.; Zhu, A.-M.; Guo, J.; Xu, Y.; Shi, C. Conversion of Greenhouse Gases Into Syngas Via Combined Effects of Discharge Activation and Catalysis. *Chem. Eng. J.* **2010**, *156*, 601−606.
(179) Tu, X.; Gallon, H. J.; Twigg, M. V.; Gorry, P. A.; Whitehead, J. C. Dry Reforming of Methane Over a Ni/Al_2O_3 Catalyst in a Coaxial Dielectric Barrier Discharge Reactor. *J. Phys. D: Appl. Phys.* **2011**, *44*, 274007.
(180) Sentek, J.; Krawczyk, K.; Mlotek, M.; Kalczewska, M.; Kroker, T.; Kolb, T.; Schenk, A.; Gericke, K.-H.; Schmidt-Szalowski, K. Plasma-Catalytic Methane Conversion With Carbon Dioxide In Dielectric Barrier Discharges. *Appl. Catal., B* **2010**, *94*, 19−26.
(181) Spencer, L. F.; Gallimore, A. D. CO_2 Dissociation In An Atmospheric Pressure Plasma/Catalyst System: A Study Of Efficiency. *Plasma Sources Sci. Technol.* **2013**, *22*, 015019.

DOI: 10.1021/acs.chemrev.5b00362
Chem. Rev. 2015, 115, 13408−13446

(182) Lee, H.; Sekiguchi, H. Plasma-Catalytic Hybrid System Using Spouted Bed With A Gliding Arc Discharge: CH_4 Reforming As A Model Reaction. *J. Phys. D: Appl. Phys.* **2011**, *44*, 274008.
(183) Rueangjitt, N.; Sreethawong, T.; Chavadej, S.; Sekiguchi, H. Plasma-Catalytic Reforming Of Methane In AC Microsized Gliding Arc Discharge: Effects Of Input Power, Reactor Thickness, And Catalyst Existence. *Chem. Eng. J.* **2009**, *155*, 874−880.
(184) Allah, Z. A.; Whitehead, J. C. Plasma-Catalytic Dry Reforming Of Methane In An Atmospheric Pressure AC Gliding Arc Discharge. *Catal. Today* **2015**, *256*, 76.
(185) Kato, T.; Hatakeyama, R. Site- and Alignment-Controlled Growth of Graphene Nanoribbons from Nickel Nanobars. *Nat. Nanotechnol.* **2012**, *7*, 651−656.
(186) Kato, T.; Hatakeyama, R. Direct Growth of Doping-Density-Controlled Hexagonal Graphene on SiO_2 Substrate by Rapid-Heating Plasma CVD. *ACS Nano* **2012**, *6*, 8508−8515.
(187) Elliott, J. A.; Shibuta, Y.; Amara, H.; Bichara, C.; Neyts, E. C. Atomistic Modelling of CVD Synthesis of Carbon Nanotubes and Graphene. *Nanoscale* **2013**, *5*, 6662−6676.
(188) Li, X.; Cai, W.; An, J.; Kim, S.; Nah, J.; Yang, D.; Piner, R.; Velamakanni, A.; Jung, I.; Tutuc, E.; Banerjee, S. K.; Colombo, L.; Ruoff, R. S. Large-Area Synthesis of High-Quality and Uniform Graphene Films on Copper Foils. *Science* **2009**, *324*, 1312−1314.
(189) Bae, S.; Kim, H.; Lee, Y.; Xu, X.; Park, J.-S.; Zheng, Y.; Balakrishnan, J.; Lei, T.; Kim, H. R.; Song, Y. I.; et al. Roll-To-Roll Production of 30-Inch Graphene Films for Transparent Electrodes. *Nat. Nanotechnol.* **2010**, *5*, 574−578.
(190) Kobayashi, T.; Bando, M.; Kimura, N.; Shimizu, K.; Kadono, K.; Umezu, N.; Miyahara, K.; Hayazaki, S.; Nagai, S.; Mizuguchi, Y.; et al. Production Of A 100-M-Long High-Quality Graphene Transparent Conductive Film By Roll-To-Roll Chemical Vapor Deposition And Transfer Process. *Appl. Phys. Lett.* **2013**, *102*, 023112.
(191) Mehdipour, H.; Ostrikov, K. Kinetics of Low-Pressure, Low-Temperature Graphene Growth: Toward Single-Layer, Single-Crystalline Structure. *ACS Nano* **2012**, *6*, 10276−10286.
(192) Ostrikov, K.; Neyts, E. C.; Meyyappan, M. Plasma Nanoscience: From Nano-Solids in Plasmas to Nano-Plasmas in Solids. *Adv. Phys.* **2013**, *62*, 113−224.
(193) Yamada, T.; Ishihara, M.; Kim, J.; Hasegawa, M.; Iijima, S. A Roll-To-Roll Microwave Plasma Chemical Vapor Deposition Process For The Production Of 294 mm Width Graphene Films At Low Temperature. *Carbon* **2012**, *50*, 2615−2619.
(194) Kumar, S.; van der Laan, T.; Rider, A. E.; Randeniya, L.; Ostrikov, K. Multifunctional Three-Dimensional T-Junction Graphene Micro-Wells: Energy-Efficient, Plasma-Enabled Growth and Instant Water-Based Transfer for Flexible Device Applications. *Adv. Funct. Mater.* **2014**, *24*, 6114−6122.
(195) Kato, R.; Tsugawa, K.; Okigawa, Y.; Ishihara, M.; Yamada, T.; Hasegawa, M. Bilayer Graphene Synthesis by Plasma Treatment of Copper Foils Without Using a Carbon-Containing Gas. *Carbon* **2014**, *77*, 823−828.
(196) Schmidt, V.; Senz, S.; Gösele, U. Diameter-Dependent Growth Direction of Epitaxial Silicon Nanowires. *Nano Lett.* **2005**, *5*, 931−935.
(197) Cui, Y.; Lauhon, L. J.; Gudiksen, M. S.; Wang, J.; Lieber, C. M. Diameter-Controlled Synthesis of Single Crystal Silicon Nanowires. *Appl. Phys. Lett.* **2001**, *78*, 2214−2216.
(198) Westwater, J.; Gosain, D. P.; Tomiya, S.; Usui, S.; Ruda, H. Growth of silicon nanowires via gold/silane vapor−liquid−solid reaction. *J. Vac. Sci. Technol., B: Microelectron. Process. Phenom.* **1997**, *15*, 554−557.
(199) Wong, Y.; Yahaya, M.; Mat Salleh, M.; Yeop Majlis, B. Controlled Growth Of Silicon Nanowires Synthesized Via Solid−Liquid−Solid Mechanism. *Sci. Technol. Adv. Mater.* **2005**, *6*, 330−334.
(200) Ma, Z.; McDowell, D.; Panaitescu, E.; Davydov, A. V.; Upmanyu, M.; Menon, L. Vapor−Liquid−Solid Growth Of Serrated Gan Nanowires: Shape Selection Driven By Kinetic Frustration. *J. Mater. Chem. C* **2013**, *1*, 7294−7302.
(201) Purushothaman, V.; Jeganathan, K. Investigations on the role of Ni-catalyst for the VLS growth of quasi-aligned GaN nanowires by chemical vapor deposition. *J. Nanopart. Res.* **2013**, *15*, 1−12.
(202) Zhou, G.; Yang, J. C.; Xu, F.; Barnard, J. A.; Zhang, Z. Quantitative VLS Growth Model and Experiments of Fe Catalyzed Si Nanowire Formation. In *MRS Proceedings*; Cambridge University Press: Cambridge, U.K., 2002; p F6.3.
(203) Arbiol, J.; Kalache, B.; Roca i Cabarrocas, P.; Morante, J. R.; Fontcuberta i Morral, A. Influence Of Cu As A Catalyst On The Properties Of Silicon Nanowires Synthesized By The Vapour−Solid−Solid Mechanism. *Nanotechnology* **2007**, *18*, 305606.
(204) Wittemann, J. V.; Münchgesang, W.; Senz, S.; Schmidt, V. Silver Catalyzed Ultrathin Silicon Nanowires Grown By Low-Temperature Chemical-Vapor-Deposition. *J. Appl. Phys.* **2010**, *107*, 096105.
(205) Chen, C.-C.; Yeh, C.-C.; Chen, C.-H.; Yu, M.-Y.; Liu, H.-L.; Wu, J.-J.; Chen, K.-H.; Chen, L.-C.; Peng, J.-Y.; Chen, Y.-F. Catalytic Growth And Characterization Of Gallium Nitride Nanowires. *J. Am. Chem. Soc.* **2001**, *123*, 2791−2798.
(206) Hou, W.-C.; Chen, L.-Y.; Hong, F. C.-N. Fabrication Of Gallium Nitride Nanowires By Nitrogen Plasma. *Diamond Relat. Mater.* **2008**, *17*, 1780−1784.
(207) Wang, B.; Zheng, K.; Shao, R.; Wang, Y.; Wang, R.; Yan, Y. Structure And Electrical Property Of Gallium Nitride Nanowires Synthesized In Plasma-Enhanced Hot Filament Chemical Vapor Deposition System. *J. Phys. Chem. Solids* **2013**, *74*, 862−866.
(208) Hou, W. C.; Hong, F. C.-N. Controlled Surface Diffusion In Plasma-Enhanced Chemical Vapor Deposition Of GaN Nanowires. *Nanotechnology* **2009**, *20*, 055606.
(209) Lari, L.; Murray, R.; Bullough, T.; Chalker, P.; Gass, M.; Cheze, C.; Geelhaar, L.; Riechert, H. Nanoscale Compositional Analysis Of Ni-Based Seed Crystallites Associated With Gan Nanowire Growth. *Phys. E* **2008**, *40*, 2457−2461.
(210) Hofmann, S.; Ducati, C.; Neill, R.; Piscanec, S.; Ferrari, A.; Geng, J.; Dunin-Borkowski, R.; Robertson, J. Gold Catalyzed Growth Of Silicon Nanowires By Plasma Enhanced Chemical Vapor Deposition. *J. Appl. Phys.* **2003**, *94*, 6005−6012.
(211) Ostrikov, K.; Seo, D. H.; Mehdipour, H.; Cheng, Q.; Kumar, S. Plasma Effects In Semiconducting Nanowire Growth. *Nanoscale* **2012**, *4*, 1497−1508.
(212) Mehdipour, H.; Ostrikov, K.; Rider, A. E.; Furman, S. A. Minimizing the Gibbs-Thomson Effect in the Low-Temperature Plasma Synthesis of Thin Si Nanowires. *Nanotechnology* **2011**, *22*, 315707:1−14.
(213) Colli, A.; Hofmann, S.; Fasoli, A.; Ferrari, A. C.; Ducati, C.; Dunin-Borkowski, R. E.; Robertson, J. Synthesis and Optical Properties of Silicon Nanowires Grown by Different Methods. *Appl. Phys. A: Mater. Sci. Process.* **2006**, *85*, 247−253.
(214) Szabó, D. V.; Schlabach, S. Microwave Plasma Synthesis of Materials—From Physics and Chemistry to Nanoparticles: A Materials Scientist's Viewpoint. *Inorganics* **2014**, *2*, 468−507.
(215) Kortshagen, U. Nonthermal Plasma Synthesis Of Semiconductor Nanocrystals. *J. Phys. D: Appl. Phys.* **2009**, *42*, 113001.
(216) Tang, W.-C.; Hong, F. C.-N. Growths Of Indium Gallium Nitride Nanowires By Plasma-Assisted Chemical Vapor Deposition. *Thin Solid Films* **2014**, *570*, 315−320.
(217) Zheng, J.; Song, X.; Li, X.; Pu, Y. Large-Scale Production Of Amorphous Silicon Oxynitride Nanowires By Nickel-Catalyzed Transformation Of Silicon Wafers In NH_3 Plasma. *J. Phys. Chem. C* **2008**, *112*, 27−34.
(218) Sharma, S.; Sunkara, M. Direct Synthesis Of Single-Crystalline Silicon Nanowires Using Molten Gallium And Silane Plasma. *Nanotechnology* **2004**, *15*, 130−134.
(219) Sunkara, M. K.; Sharma, S.; Miranda, R.; Lian, G.; Dickey, E. Bulk Synthesis Of Silicon Nanowires Using A Low-Temperature Vapor−Liquid−Solid Method. *Appl. Phys. Lett.* **2001**, *79*, 1546−1548.

DOI: 10.1021/acs.chemrev.5b00362
Chem. Rev. 2015, 115, 13408−13446

(220) Chandrasekaran, H.; Sumanasekara, G. U.; Sunkara, M. K. Rationalization Of Nanowire Synthesis Using Low-Melting Point Metals. *J. Phys. Chem. B* **2006**, *110*, 18351−18357.
(221) Sharma, S.; Sunkara, M. K. Direct Synthesis Of Gallium Oxide Tubes, Nanowires, And Nanopaintbrushes. *J. Am. Chem. Soc.* **2002**, *124*, 12288−12293.
(222) Landré, O.; Songmuang, R.; Renard, J.; Bellet-Amalric, E.; Renevier, H.; Daudin, B. Plasma-Assisted Molecular Beam Epitaxy Growth Of Gan Nanowires Using Indium-Enhanced Diffusion. *Appl. Phys. Lett.* **2008**, *93*, 183109.
(223) Jeon, M.; Tomitsuka, Y.; Kamisako, K. Synthesis Of Gallium-Catalyzed Silicon Nanowires By Hydrogen Radical-Assisted Deposition Method. *J. Ind. Eng. Chem.* **2008**, *14*, 836−840.
(224) Carreon, M. L.; Jasinski, J.; Sunkara, M. Low Temperature Synthesis Of Silicon Nanowire Arrays. *Mater. Res. Express* **2014**, *1*, 045006.
(225) Novikov, S.; Foxon, C. Plasma-Assisted Electroepitaxy Of Gan Layers From The Liquid Ga Melt. *J. Cryst. Growth* **2012**, *354*, 44−48.
(226) Meyyappan, M.; Sunkara, M. K. In *Inorganic Nanowires: Applications, Properties, and Characterization*; CRC Press: Boca Raton, FL, 2009; Chapter 9.
(227) Ostrikov, K.; Levchenko, I.; Cvelbar, U.; Sunkara, M.; Mozetic, M. From Nucleation To Nanowires: A Single-Step Process In Reactive Plasmas. *Nanoscale* **2010**, *2*, 2012−2027.
(228) Mozetič, M.; Cvelbar, U.; Sunkara, M. K.; Vaddiraju, S. A Method For The Rapid Synthesis Of Large Quantities Of Metal Oxide Nanowires At Low Temperatures. *Adv. Mater.* **2005**, *17*, 2138−2142.
(229) Cvelbar, U.; Chen, Z.; Sunkara, M. K.; Mozetič, M. Spontaneous Growth Of Superstructure A-Fe_2O_3 Nanowire And Nanobelt Arrays In Reactive Oxygen Plasma. *Small* **2008**, *4*, 1610−1614.
(230) Cvelbar, U.; Ostrikov, K.; Levchenko, I.; Mozetic, M.; Sunkara, M. K. Control Of Morphology And Nucleation Density Of Iron Oxide Nanostructures By Electric Conditions On Iron Surfaces Exposed To Reactive Oxygen Plasmas. *Appl. Phys. Lett.* **2009**, *94*, 211502.
(231) Kumar, V.; Kim, J. H.; Jasinski, J. B.; Clark, E. L.; Sunkara, M. K. Alkali-Assisted, Atmospheric Plasma Production Of Titania Nanowire Powders And Arrays. *Cryst. Growth Des.* **2011**, *11*, 2913−2919.
(232) Cvelbar, U. Towards Large-Scale Plasma-Assisted Synthesis Of Nanowires. *J. Phys. D: Appl. Phys.* **2011**, *44*, 174014.
(233) Harling, A. M.; Demidyuk, V.; Fischer, S. J.; Whitehead, J. C. Plasma-Catalysis Destruction Of Aromatics For Environmental Clean-Up: Effect Of Temperature And Configuration. *Appl. Catal., B* **2008**, *82*, 180−189.
(234) Whitehead, J. C. Plasma Catalysis: A Solution For Environmental Problems. *Pure Appl. Chem.* **2010**, *82*, 1329−1336.
(235) Chen, H. L.; Lee, H. M.; Chen, S. H.; Chang, M. B. Review Of Packed-Bed Plasma Reactor For Ozone Generation And Air Pollution Control. *Ind. Eng. Chem. Res.* **2008**, *47*, 2122−2130.
(236) Chen, H. L.; Lee, H. M.; Chen, S. H.; Chang, M. B.; Yu, S. J.; Li, S. N. Removal Of Volatile Organic Compounds By Single-Stage And Two-Stage Plasma Catalysis Systems: A Review Of The Performance Enhancement Mechanisms, Current Status And Suitable Applications. *Environ. Sci. Technol.* **2009**, *43*, 2216−2227.
(237) Demeestere, K.; Dewulf, J.; Ohno, T.; Salgado, P. H.; Van Langenhove, H. Visible Light Mediated Photocatalytic Degradation Of Gaseous Trichloroethylene And Dimethyl Sulfide On Modified Titanium Dioxide. *Appl. Catal., B* **2005**, *61*, 140−149.
(238) Guaitella, O.; Thevenet, F.; Puzenat, E.; Guillard, C.; Rousseau, A. C_2H_2 Oxidation By Plasma/TiO_2 Combination: Influence Of The Porosity And Photocatalytic Mechanisms Under Plasma Exposure. *Appl. Catal., B* **2008**, *80*, 296−305.
(239) Wallis, A. E.; Whitehead, J. C.; Zhang, K. Plasma-Assisted Catalysis For The Destruction Of CFC-12 In Atmospheric Pressure Gas Streams Using TiO_2. *Catal. Lett.* **2007**, *113*, 29−33.
(240) Kim, H.-H.; Kim, J.-H.; Ogata, A. Microscopic Observation Of Discharge Plasma On The Surface Of Zeolites Supported Metal Nanoparticles. *J. Phys. D: Appl. Phys.* **2009**, *42*, 135210.
(241) Das, D.; Veziroğlu, T. N. Hydrogen Production By Biological Processes: A Survey Of Literature. *Int. J. Hydrogen Energy* **2001**, *26*, 13−28.
(242) Bromberg, L.; Cohn, D. R.; Rabinovich, A.; Alexeev, N. Plasma Catalytic Reforming of Methane. *Int. J. Hydrogen Energy* **1999**, *24*, 1131−1137.
(243) Sugasawa, M.; Terasawa, T.; Futamura, S. Effects Of Initial Water Content On Steam Reforming Of Aliphatic Hydrocarbons With Nonthermal Plasma. *J. Electrost.* **2010**, *68*, 212−217.
(244) Futamura, S.; Kabashima, H.; Annadurai, G. Roles of CO_2 and H_2O as Oxidants in the Plasma Reforming of Aliphatic Hydrocarbons. *Catal. Today* **2006**, *115*, 211−216.
(245) Nozaki, T.; Muto, N.; Kado, S.; Okazaki, K. Dissociation Of Vibrationally Excited Methane On Ni Catalyst. Part 1. Application to Methane Steam Reforming. *Catal. Today* **2004**, *89*, 57−65.
(246) Halonen, L.; Bernasek, S. L.; Nesbitt, D. J. Reactivity of vibrationally excited methane on nickel surfaces. *J. Chem. Phys.* **2001**, *115*, 5611−5619.
(247) Nozaki, T.; Okazaki, K. Innovative Methane Conversion Technology Using Atmospheric Pressure Non-Thermal Plasma. *J. Jpn. Pet. Inst.* **2011**, *54*, 146−158.
(248) Pietruszka, B.; Heintze, M. Methane Conversion At Low Temperature: The Combined Application Of Catalysis And Non-Equilibrium Plasma. *Catal. Today* **2004**, *90*, 151−158.
(249) Corbo, P.; Migliardini, F. Hydrogen Production By Catalytic Partial Oxidation Of Methane And Propane On Ni And Pt Catalysts. *Int. J. Hydrogen Energy* **2007**, *32*, 55−66.
(250) Chao, Y.; Huang, C.-T.; Lee, H.-M.; Chang, M.-B. Hydrogen Production Via Partial Oxidation Of Methane With Plasma-Assisted Catalysis. *Int. J. Hydrogen Energy* **2008**, *33*, 664−671.
(251) Rico, V. J.; Hueso, J. L.; Cotrino, J.; Gallardo, V.; Sarmiento, B.; Brey, J. J.; Gonzalez-Elipe, A. R. Hybrid Catalytic-DBD Plasma Reactor For The Production Of Hydrogen And Preferential CO Oxidation (CO-PROX) At Reduced Temperatures. *Chem. Commun.* **2009**, 6192−6194.
(252) Kandemir, T.; Schuster, M. E.; Senyshyn, A.; Behrens, M.; Schlögl, R. The Haber-Bosch Process Revisited: On The Real Structure And Stability Of "Ammonia Iron" Under Working Conditions. *Angew. Chem., Int. Ed.* **2013**, *52*, 12723−12726.
(253) Giddey, S.; Badwal, S. P. S.; Kulkarni, A. Review of Electrochemical Ammonia Production Technologies and Materials. *Int. J. Hydrogen Energy* **2013**, *38*, 14576−14594.
(254) Hellman, A.; Baerends, E. J.; Biczysko, M.; Bligaard, T.; Christensen, C. H.; Clary, D. C.; Dahl, S.; van Harrevelt, R.; Honkala, K.; Jonsson, H.; et al. Predicting Catalysis: Understanding Ammonia Synthesis from First-Principles Calculations. *J. Phys. Chem. B* **2006**, *110*, 17719−17735.
(255) Hessel, V.; Anastasopoulou, A.; Wang, Q.; Kolb, G.; Lang, J. Energy, Catalyst And Reactor Considerations For (Near)-Industrial Plasma Processing And Learning For Nitrogen-Fixation Reactions. *Catal. Today* **2013**, *211*, 9−28.
(256) Mizushima, T.; Matsumoto, K.; Sugoh, J.-i.; Ohkita, H.; Kakuta, N. Tubular Membrane-Like Catalyst For Reactor With Dielectric-Barrier-Discharge Plasma And Its Performance In Ammonia Synthesis. *Appl. Catal., A* **2004**, *265*, 53−59.
(257) Bai, M.; Zhang, Z.; Baik, H. K.; Bai, M.; Ning, W. Plasma Synthesis Of Ammonia With A Microgap Dielectric Barrier Discharge At Ambient Pressure. *IEEE Trans. Plasma Sci.* **2003**, *31*, 1285−1291.
(258) Nakajima, J.; Sekiguchi, H. Synthesis of Ammonia Using Microwave Discharge at Atmospheric Pressure. *Thin Solid Films* **2008**, *516*, 4446−4451.
(259) Kiyooka, H.; Matsumoto, O. Reaction Scheme Of Ammonia Synthesis In The ECR Plasmas. *Plasma Chem. Plasma Process.* **1996**, *16*, 547−562.

DOI: 10.1021/acs.chemrev.5b00362
Chem. Rev. 2015, 115, 13408−13446

(260) Uyama, H.; Nakamura, T.; Tanaka, S.; Matsumoto, O. Catalytic Effect Of Iron Wires On The Syntheses Of Ammonia And Hydrazine In A Radio-Frequency Discharge. *Plasma Chem. Plasma Process.* **1993**, *13*, 117−131.
(261) Tanaka, S.; Uyama, H.; Matsumoto, O. Synergistic Effects Of Catalysts And Plasmas On The Synthesis Of Ammonia And Hydrazine. *Plasma Chem. Plasma Process.* **1994**, *14*, 491−504.
(262) Van Helden, J. H.; Wagemans, W.; Yagci, G.; Zijlmans, R. A. B.; Schram, D. C.; Engeln, R.; Lombardi, G.; Stancu, G. D.; Röpcke, J. Detailed Study Of The Plasma-Activated Catalytic Generation Of Ammonia In N2-H2 Plasmas. *J. Appl. Phys.* **2007**, *101*, 043305.
(263) Mizushima, T.; Matsumoto, K.; Ohkita, H.; Kakuta, N. Catalytic Effects Of Metal-Loaded Membrane-Like Alumina Tubes On Ammonia Synthesis In Atmospheric Pressure Plasma By Dielectric Barrier Discharge. *Plasma Chem. Plasma Process.* **2007**, *27*, 1−11.
(264) Okigawa, Y.; Kato, R.; Yamada, T.; Ishihara, M.; Hasegawa, M. Electrical Properties and Domain Sizes of Graphene Films Synthesized by Microwave Plasma Treatment Under a Low Carbon Concentration. *Carbon* **2015**, *82*, 60−66.
(265) van der Laan, T.; Kumar, S.; Ostrikov, K. Water-mediated and instantaneous transfer of graphene grown at 220 °C enabled by a plasma. *Nanoscale* **2015**, DOI: 10.1039/C5NR06365E.

DOI: 10.1021/acs.chemrev.5b00362
Chem. Rev. 2015, 115, 13408−13446